Herstellung und Untersuchung schaltbarer Polymerschichten mit hydrophobem/ hydrophilem Charakter

(Fabrication and Study of Switchable Polymer Layers with Hydrophobic/Hydrophilic Behavior)

D I S S E R T A T I O N

zur Erlangung des akademischen Grades

Doktor rerum naturalium
(Dr. rer. nat.)

vorgelegt

am Fachbereich Chemie
der Fakultät Mathematik und Naturwissenschaften
der Technischen Universität Dresden

von

Mikhail Motornov

geboren am 20 April 1974 in Klimovsk, Russland

Gutachter: Prof. Dr. S. Minko

Prof. Dr. M. Stamm

Prof. Dr. T. Wolff

Eingereicht am: 18.02.2004

Tag der Verteidigung: 24.06.2004

Contents

Chapter 1
Introduction. 1

Chapter 2
Theoretical Background and Experimental Considerations 4
2.1. Modification of Polymer Surface Behavior 4
2.1.1. Introduction 4
2.1.2 Modification of Polymer Surface Behavior by Chemical/Physical Treatment 4
2.2. Polymer Brushes 9
2.2.1 Introduction 9
2.2.2 Theoretical and Experimental Studies of Homopolymer Brushes 11
2.2.3 Theoretical and Experimental Studies of Mixed Polymer Brushes 14
2.2.4. Responsive/Switching/Adaptive Behavior 16
2.2.5. Synthesis of Mixed Brushes 18
2.2.6 Methods to Study Responsive Behavior 22

Chapter 3
Experimental Techniques 24
3.1 Introduction 24
3.2. Ellipsometry 24
3.3. Atomic Force Microscopy (AFM) 28
3.4. Determination of Surface Tension 31
3.4.1. Surface Tension Component Approach 32
3.4.2. Equation of State Approach 34
3.4.3. Contact Angles on Heterogeneous Surfaces 34
3.4.4. Contact Angle Measurement Techniques 37
3.5. X-Ray Photoelectron Spectroscopy (XPS) 38
3.6. Infrared Spectroscopy 41

Chapter 4
Mixed Polymer Brushes on Polyamide Substrates 43
4.1. Introduction 43
4.2. Materials 45
4.3. Surface modification of PA substrates 47
4.4. Preparation of the binary brushes via *grafting from* approach 47
4.4.1. Attachment of azo-initiator 47
4.4.2 Grafting procedure 48
4.5. Preparation of the binary brushes via *grafting to* approach 48
4.6. Sample Characterization 49
4.6.1 Ellipsometry 49
4.6.2 FTIR-ATR 49
4.6.3 XPS 50
4.6.4 AFM 51
4.6.5 Contact angle measurements 51
4.6.6 Biological tests of PA materials with grafted binary polymer brushes 51
4.7. Results and Discussion 52
4.7.1 Plasma treatment 52

4.7.2 Synthesis of the Binary Brushes via *Grafting From* Approach 55
4.7.3 Grafting of the Mixed Brushes 55
4.7.4 Synthesis of the Binary Brushes via G*rafting To* Approach 56
4.7.5 Characterization of the Grafted Brushes 57
4.7.6. Switching/Adaptive Properties 62
4.7.7. The Estimation of Biological Efficiency of the Grafted Polymer Layers to PA Textiles 67
4.8. Conclusions 68

Chapter 5
Block-Copolymer Responsive Brushes 70
5.1 Introduction 70
5.2. Materials 72
5.3. Preparation of the Mixed Brushes on Silica Wafers 72
5.4. Preparation of the Mixed Brushes on Silica Nanoparticles 73
5.5. Sample Characterization 73
5.5.1 Ellipsometry 73
5.5.2. FTIR 74
5.5.3. AFM 74
5.5.4. Scanning Electron Microscopy (SEM) 74
5.5.5 Contact angles 74
5.6. Results and Discussion 74
5.6.1 Grafting of BUDTMS 74
5.6.2. Grafting of the Block Copolymers 75
5.6.3. Switching/Adaptive Properties 76
5.6.4. Block Copolymer Brushes on Silica Nanoparticles 78
5.6.5. Switching/Adaptive Properties of Block Copolymer Brushes on Silica Nanoparticles 82
5.7. Conclusions 84

Chapter 6
Hierarchically Structured Self-Adaptive Surfaces on PTFE Substrates 85
6.1. Introduction 85
6.2. Materials 87
6.3. Plasma treatment of PTFE substrates 88
6.4. Preparation of the binary brushes 89
6.5. Sample characterization 89
6.5.1. Ellipsometry 89
6.5.2. SEM 89
6.5.3. AFM 90
6.5.4. XPS 91
6.5.5. Contact Angle Measurements 91
6.5.6. FTIR-ATR 92
6.6. Results and discussion 92
6.7. Conclusions 103

Summary and Outlook 104

References 107

List of Abbreviations 113

Publications and Contributions to Conferences 117

Chapter 1

Introduction.

There is a currently growing interest in improving and regulation of surface characteristics of polymer materials due to many potential applications in the field of nanotechnology, medicine, and biomaterials.

There is a general agreement that the ultimate performance of materials in many traditional and modern applications depends not only on their bulk properties, but also heavily relies on their surface microstructure and interfacial behavior because of inventible involvement of such phenomena as friction, shearing, lubrication, abrasion, wetting, adhesion, adsorption, and indentation phenomena [Tsu97, Bhu98, Bhu97, Pok02]. This importance is becoming paramount in the age of eve shrinking operational dimensions in micro- and nanodevices and demand on materials with extreme properties [Gra00, Tsu01, Laf03]. In many studies, a special attention is devoted to the fine design of the topmost surface layer incorporating all necessary elements controlling a predictable surface response or a variable surface response under different conditions [Cre03, Tsu00, Tsu98, San93, Bir00, Bli98]. For this reason, structure and characteristics of the phase boundaries are of the utmost importance for the understanding of the material properties in processing and use. Moreover, further advances in materials science impose requirements for the surface properties that are frequently in a conflict: a given material, depending on the conditions under which it is utilized, has to be hydrophobic or hydrophilic, acidic or basic, conductive or nonconductive, adhesive or repellent, release or absorb some species. With the increasing demand for more sophisticated surfaces, one of the current targets is the fabrication and understanding of materials with interfacial properties capable of consistent reversible changes in their characteristics according to external conditions or stimuli.

An intensive study in the filed of the adaptive/responsive surfaces began several decades ago from attempts to understand relationships between bulk properties/composition of pristine polymeric materials and their surface characteristics. With time, the focus of researches has moved to the design of materials with “smart” or “intelligent” surface behavior. A number of approaches has been employed to reach the goal, which includes but not limited to (a) synthesis of functional polymers with specific composition and architecture; (b) blending of a virgin polymer material with small amounts of (macro)molecular additive; and (c) surface modification by various chemical/physical treatment [Nak99, You99, Cre99, Lai92].

Modification of polymer surfaces via grafting of polymers is a very well known and widely used approach of modern material science, for example, to regulate friction, adsorption, adhesion, and wettability as well.

Controlling the wettability of solid surfaces is of abiding importance for many processes in living organisms (e.g. ultra-water repellent materials are found in self cleaning surfaces of plants and insects [Bar97,] and for numerous industrial applications [Oga93, Tad97, Nak99, Vee97, You99, Cou00, Cre99, Lai92, Sin97, Zha00c]. Advantages of ultrahydrophobic surfaces, however, can turn into disadvantages: the self cleaning properties of a surface may result in static electric charges, of poor adhesion, or dyeability. The ability to reversible switch the properties of the same material from water-repellent to hydrophilic would allow for a diverse range of applications. In general, however, polymer surfaces have fixed properties. Design of switchable coatings is a formidable challenge.

Resent investigations have shown that a combination of two different polymers in the same thin polymer coating for the surface modification results in new properties of the materials resembling somehow responsive properties in nature [Min01]. The latter work was done with mixed polymer brushes when two incompatible polymers were randomly grafted by end groups to/from the surface of Si wafers [Sid99a, Min02a]. The mixed polymer brushes represent a polymer system with remarkable responsive properties. In contrast to homopolymer brushes, consisting of one kind of homopolymer, they can amplify the response due to the combination of conformational changes with the *microphase* separation (Figure1.1 b). If the mixed brush constituted of both hydrophilic and hydrophobic homopolymers is exposed to a hydrophilic solvent, the hydrophilic component preferentially segregates to the top of the film and the surface becomes hydrophilic (Figure1.1 a).

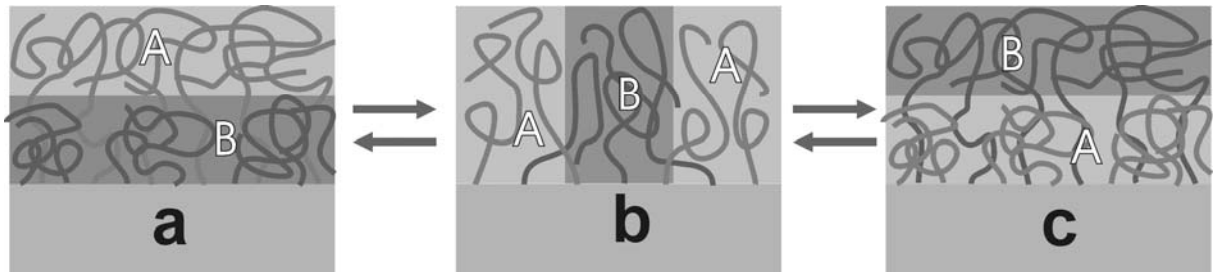

Figure 1.1. Switchable mixed A/B polymer brush in selective solvent for chains(a, c) and non-selective solvent (b).

Exposing the same brush to the hydrophobic solvent reversibly switches the surface from hydrophilic to hydrophobic state (Figure1.1 c). This adaptive behavior is very promising for engineering of smart surfaces for biomedical applications and micro- and/or nanodevices.

This thesis is focused on the fabrication of switchable surfaces consisting of mixed polymer brushes with a wide range of switching properties on both flat and rough substrates exploiting for different approaches of the modification of the substrates and grafting techniques.

These techniques include grafting of mixed polymer brushes after the plasma modification of polymer substrates. The switchable surfaces are obtained using grafting of different homo-, co-, and blockcopolymers.

In addition to the study of surface modification and grafting approaches, the work contains comparing different approaches and some optimization of the process of the fabrication of the switchable surfaces.

Chapter 2

Theoretical Background and Experimental Considerations

2.1. Modification of Polymer Surface Behavior

2.1.0. Abstract.

In this chapter basic principles of polymer surface modification approaches as well as theoretical and experimental considerations of polymer brushes are described. A short introduction to modified polymer materials is given. More comprehensive and detailed descriptions of the reviewed techniques can be found in the references quoted.

2.1.1. Introduction

Many polymers have excellent bulk properties, low cost, and are well suited for some particular applications. For these reasons, various surface modification techniques that could transform these pristine, inexpensive materials into sophisticated elements of the complex adaptive/responsive systems are under development in various laboratories. Modification strategies, which are supposed not to affect the bulk properties significantly, involve either blending of a virgin material with small amounts of (macro)molecular additive or/and the surface modification by chemical/physical treatment to alter the surface properties.

Over many years, polymer surface modification have been studied in various fields of industrial applications, using different innovative techniques including chemical and physical processes. Physical processes take advantages of surface segregation, radiation, electromagnetic waves, and oxidation with gases, while chemical modification use wet treatment, blending, coating, and metallization.

2.1.2 Modification of Polymer Surface Behavior by Chemical/Physical Treatment

Surface modification of polymeric materials with chemical or physical treatments has been accomplished by a variety of procedures. [Chan93, Ber94, Ber98]. Flame, corona, and plasma treatments were generally applicable methods which serve to introduce various oxygen, nitrogen, and other functionalities. Plasma polymerization process has been also used to tailor the polymer surface. As a result, thin modifying surface films, which are usually highly cross-linked can be obtained on a polymeric surface. Solution oxidation using reactive

oxidants have successfully produced oxygenated and sulfonated surfaces. Ion-beam treatment, photon and γ-radiation also have been utilized to modify polymer surfaces [Chan93, Ber94, Ber98]. Once functionalized, often the second stage such as an attachment of some functional molecules and/or polymer grafting is required to produce a surface with necessary properties. Some of aforesaid modification methods are confirmed to be capable to convert an inert polymer substrate into a material with the adaptive/responsive surface behavior.

To this end, Whitesides et al. [Hol87, Whi90] studied reconstruction of the interface of oxidatively functionalized polyethylene and derivatives on heating. Oxidation of low-density polyethylene (PE) film with chromic acid resulted in the material (PE-CO_2H) bearing hydrophilic carboxylic acid and ketone groups in a thin oxidatively functionalized surface. This interface was indefinitely stable at room temperature. Functionalized hydrophilic interfaces of oxidized PE film became hydrophobic and similar in the wettability to the non-functionalized PE film upon heating under vacuum. This demonstrates the surface reconstruction after modification. The progression of water contact angle from the initial value of 55° to the final value of 103° indicates that the polar functional groups disappear from the interface by diffusion. The migration of functional groups away from the interface was driven by the minimization of the interfacial free energy and by the dilution of the interfacial functional group in the polymer interior. The rate of the surface reconstruction decreased with increasing size of the functional groups deposited on the surface. Functional groups, which migrated into the bulk polymer, were still available to reagents in aqueous solutions in contact with the film even when the wetting properties had become similar to those of unmodified PE film. Samples that previously reconstructed by the heating could, to a limited extend, be made to become hydrophilic again by heating in water.

The next paper examined the surface wetting by water of functionalized PE [Hol88]. It was determined that the wettability of the PE-CO_2H surface depends on pH: at pH ≤ 4, the carboxylic acid groups are protonated and the surface is less hydrophilic (advancing contact angle is ~ 55°); at pH ≥ 10 the carboxylic acid groups are present as the more hydrophilic carboxilate ions, and the contact angle drops down to 20°. Wilson and Whitesides [Wil88] reported that anthranilate amide of the PE-CO_2H surface showed an exceptionally large change with pH in its wettability by water. Indeed, the advancing contact angle of the PE-anthranilate decreased from 110° at pH 1 to 33° at pH 12. Comparison of these values with those for corresponding amides of m- and p-aminobenzoic acid and aniline suggested that both the conformational mobility of the polar functional group at the solid-water interface and the surface roughness contributed to the large change in wettability with pH.

Generally, enthalpic forces (e.g., hydrogen bonding, Lewis acid-base interactions, and van der Waals forces) between a polymer and any contacting phase determine the relative concentrations of polar and nonpolar groups in the outermost portion of the polymer material with modified/functionalized surface. Nevertheless, when Bergbeiter and Kabza studied annealing and the surface reorganization of sulfonated PE (in order to produce surface-modified films of varying hydrophilicity), some unanticipated surface response was found. [Ber91] The sulfonation of PE surfaces resulted in relatively hydrophilic films whose hydrophilicity, however, was increased upon thermal annealing. This behavior was in a contradiction to that seen for the PE-CO_2H and its derivatives. The extent to which such surfaces did not reorganize to a less hydrophilic surface was affected by the presence of alkylammonium salts. Films with long chain alkylammonium salts at their surface reorganized thermally to less hydrophilic surfaces while films with short chain alkylammonium salts had contact angles which decreased on heating instead. According to the authors, the reason for the unanticipated behavior might be due to a change in the uniformity distribution of sulfonic acid groups during the annealing.

In different developments, in a series of papers Ferguson et al. reported on a responsive polymer material with a chemically modified surface for which entropy plays a central role in determining the composition of the polymer surface when it is in contact with water or a polar substrate [Car96, Car00, Kho01, Kho02]. The authors studied the surface/interfacial behavior of syndiotactic 1,2-polybutadiene (PBD) modified by the oxidation of the surface with aqueous $KMnO_4/K_2CO_3$. When heated against water, the surface of PBD-ox became more hydrophobic, a result apparently contrary to that expected based on the tendency of systems to minimize interfacial free energy. The advancing contact angle of water for this system, in fact, increased with increasing temperature of the water against which it was equilibrated. Initially, the hydrophilicity of the surface varied reversibly as a function of temperature, reflecting reversible changes in the relative concentrations of hydrophilic and hydrophobic groups at the interface. Eventually, however, the surface remained hydrophilic against water, independently on temperature. The temperature dependence of this phenomenon suggested the importance of entropy in determining the state of minimum interfacial free energy in this system.

This entropic effect was attributed to rubber elasticity arising from crystallinity in the polymer, and its loss was associated with a change in the amount and type of crystallinity. The authors suggested that in lightly cross-linked elastomers, the rubber elasticity might compete with the tendency to minimize the interfacial free energy and perhaps dominate the

interfacial behavior at high temperatures. As a result, the migration of functional groups attached to the mobile segments could require the extension of chains out of their relaxed, random-coil conformations. When the temperature is increased, however, the polymer chains recoil, pulling these polar groups away from the interface. This hypothesis is analogous to the thermodynamic changes that accompany small extensions of an elastomer: while stretching of an elastomer can be enthalpically favorable, an entropic restoring force determines the equilibrium extent of the extension.

Khongtong and Ferguson have employed the observed surface behavior of the PBD-ox for designing smart adhesive systems in which the surface adhesion itself is responsive to changes in environmental conditions. Specifically, the strength of adhesion in laminated PBD-ox/Al samples that have been equilibrated at room temperature and at elevated temperature was examined. In fact, the PBD-ox/Al interface displayed temperature-dependent adhesion. It was proposed that the temperature dependence in this system arised from the rubber elasticity of the polymer and reflected the interfacial behavior of the same polymer against water. The interface produced a strong adhesive joint at room temperature due to enthalpically favorable chemical interactions between the added functional groups and the surface of the metal substrate. However, the migration of these functional groups into the contact with the aluminum (oxide) required the extension of the polymer chains out of their random coil conformations, thus reducing the entropy in that region of the polymer. At high temperature, in turn, these functional groups were pulled away from the interface by the elastic restoring force induced by the entropic loss in the extended polymer chains. As a result, adhesion at the oxidized-1,4-PBD interface decreased dramatically when temperature increased. The change in the adhesion at the PBD-ox/Al interface was reversible; the interfacial adhesion slowly recovered and reached its initial steady-state level within about 40 h. This reversibility extended through several cycles of heating up to 80° C and cooling to room temperature.

Another example of a very different polymer material demonstrating the responsive surface behavior are cross-linked polymers in their rubbery state with chemically modified surface. The material can be easily stretched/contracted causing significant increase/decrease in the surface area. Thus, the surface concentration of the functional groups introduced on the polymer surface can be varied by the extension/retraction of the elastomer. Genzer and Efimenko have used this change in surface area for the generation of hydrophobic polymer surfaces that can change the hydrophobicity level when the rubbery material is stretched or

relaxed [Gen00]. At the first step, they oxidized the surface of the stretched PDMS film by ultraviolet/ozone (UVO) treatment to introduce –OH functionalities. Next, perfluoroalkanes possessing low surface energy were deposited on the surface from vapor, and hydrophobic self-assembled monolayer was formed on the rubbery substrate. When the modified PDMS samples were relaxed, water contact angle with significantly increased. The values of the contact angle were strongly dependent on the degree of stretching of the PDMS substrate before the UVO treatment. The approach proposed by Genzer and Efimenko is very attractive, since any external force or stimulus, (e.g. heat or solvent exposure), that causes the elastomer to deform, changes the wetting characteristics of the surface and can be used to tailor its wetting properties in a predictable manner.

Lampitt et al. reported another mechanism of switching of liquid repellent surfaces through generation of polyelectrolyte-surfactant complexes on a substrate surface [Lam00]. They employed plasma polymerization of maleic anhydride as a direct and interfacially specific approach to the functionalization. The plasma polymer layer was deposited by pulsing the electrical discharge on the submicrosecond time scale in order to achieve a high structural retention of the anhydride groups. Next, a complex between the plasma polymer and cationic fluorinated surfactant was obtained. The fluorocontaining surfactant-plasma polymer layer was found to repel oil but allow the spreading of water. Thus, the cationic fluorosurfactants complexed to maleic anhydride polymer layers readily underwent the surface reconstruction in a response to their local liquid environment. It was shown that this ability to switch between oleophobicity and hydrophilicity could be repeated at least 20 times.

Actually, in the aforesaid work by Lampitt et al., glass slides were used as model substrates for the plasma polymer deposition to obtain the material with responsive/adaptive surface. However, the proposed method can be readily applied to a polymer boundary, since the deposition of a functional layer on a polymer surface by plasma polymerization has been successfully used for the treatment of polymeric materials. In fact, once stimuli-responsive (macro)molecular system is identified and its behavior understood, the modification approach frequently could be translated to other polymers and any inorganic substrates of interest. Then, the problem to create materials with the smart surface can be viewed from another point and more general questions can be formulated. What are the optimum structure, composition, and properties of the stimuli-responsive layer grafted to a surface that can bring adaptive/responsive behavior to any non-polymer (e.g., metals, semiconductors) material? How this layer should be attached to the underlying surface to perform its function in the best

way? How the substrate nature and morphology will affect the polymer layer responsiveness? For that reason, significant efforts have been made to prepare, characterize, and understand the functional surface layers. The next sections of the present review are devoted to the analysis of the progress in this area.

2.2. Polymer Brushes

2.2.1 Introduction

Polymer brushes (or tethered polymers) attracted attention in 1950s when it was found that grafting of polymer molecules to colloidal particles was a very effective way to prevent flocculation [Waa50, Waa51, Mac51, Mac52, Mil89, Cla66b]. In other words, one can attach polymer chains with which prefer the suspension solvent to the colloidal particle surface; the brushes of two approaching particles resist overlapping and colloidal stabilization is achieved. It was found that polymer brushes can be useful in other applications such as new adhesive materials, [Rap92, Jih93] protein resistant biosurfaces, [Ami93] chromatographic devices, [Zan94] lubricants, [Joa92] polymer surfactants, [Tke94] and polymer compatibilizers [Ito97].

In terms of polymer chemical compositions, polymer brushes tethered to a solid substrate surface can be derived into *homopolymer brushes* (Figure 2.1a), *mixed homopolymer brushes* (Figure 2.1b), *random copolymer brushes* (Figure 2.1c) *and block copolymer brushes* (Figure 2.1d) [Zha00b] Homopolymer brushes refer to an assembly of tethered polymer chains consisting of one type of repeat units. Mixed homopolymer brushes are composed of two or more types of homopolymer chains [Sog96]. Random copolymer brushes refer to polymer chains consisting of two different repeat units, which are randomly distributed along the polymer chain [Man97]. Block copolymer brushes refer to an assembly of tethered polymer chains consisting of two or more homopolymer chains covalently connected to each other at one end [Zha99]. Homopolymer brushes can be further divided into neutral polymer brushes and charged polymer brushes (Figure 2.1e). They may also be classified in flexible polymer brush, semiflexible polymer brushes and liquid crystalline polymer brushes (Figure 2.1f).

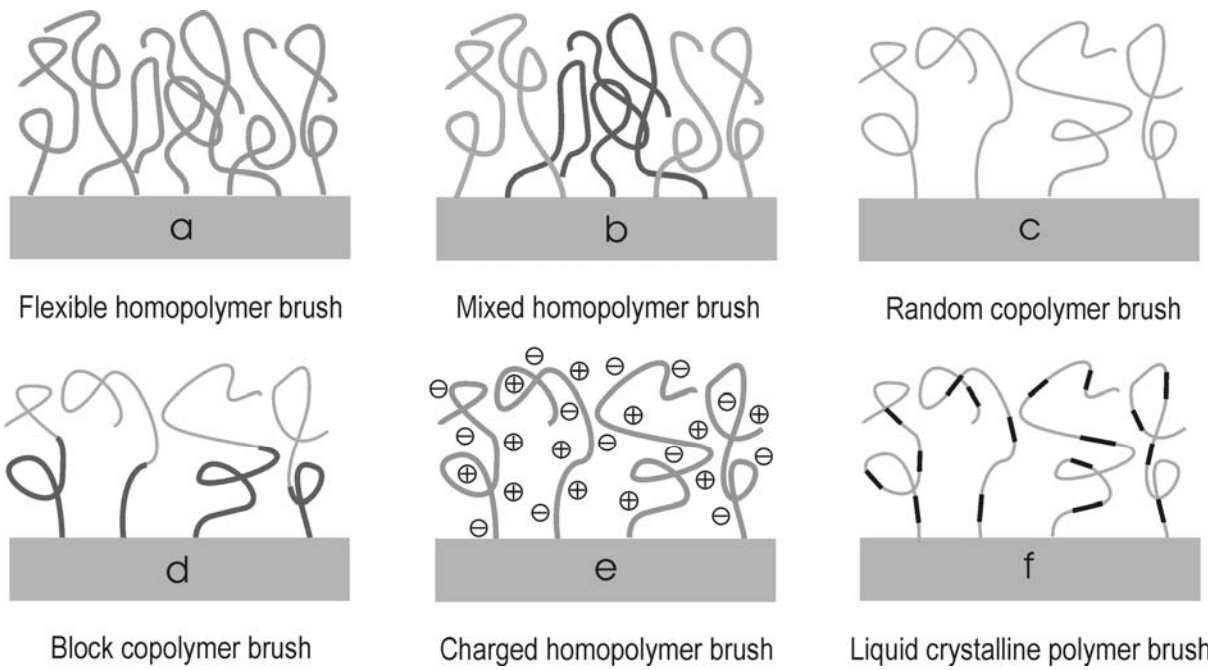

Figure 2.1. Classification of linear polymer brushes.

Polymer brushes refer to an assembly of polymer chains, which are tethered by one end to a surface or an interface [Mil91, Hal92, Szl96]. Tethering is sufficiently dense so that the polymer chains are crowded and forced stretch away from the surface or interface to avoid overlapping, sometimes much further than the typical unstretched size of chain. These stretched configurations are found under equilibrium conditions; neither a confining geometry nor an external field is required. This situation, in which polymer chains stretch along the direction normal to the grafting surface, is quite different from the typical behavior of flexible polymer chains in solution where chains adopt a random-walk configuration [Zha00b]. Series of discovers show that the deformation of densely tethered chains affects many aspects of their behavior and results in many novel properties of polymer brushes [Hal92].

Polymer brushes are a central model for many practical polymer systems such as polymer micelles; block copolymers at fluid-fluid interfaces (e.g. microemulsions and vesicles), grafted polymers on solid surfaces, adsorbed diblock copolymers and graft copolymers at fluid-fluid interfaces. All of these systems have a common feature: the polymer chains exhibit deformed configurations. Solvent can be either present or absent in polymer brushes. In the presence of the good solvent, the polymer chains try to avoid contact with each other to maximize contact with solvent molecules. With solvent absence (melt conditions) polymer chains must stretch away from the interface to avoid overfilling incompressible space [Zha00].

2.2.2 Theoretical and Experimental Studies of Homopolymer Brushes.

Alexander [Ale77] was one of the first scientists who noted the distinctive properties of polymer brushes through theoretical analysis concerning the end-adsorption of terminally fictionalized polymers on a flat surface. Further elaboration by the Gennes [Gen76, Gen80] and by Cantor [Can81] stressed the utility of tethered chains to the description of self-assembled block copolymers. The internal structure of polymer brushes was illustrated by numerical and analytical self-consisted field (SCF) calculations, and by computer simulations.

The configurational space of the polymer chains is limited by the presence of the interface. The deformation of densely tethered polymer chains reflects a balance between interaction and free elastic energies. Dense tethering of polymer chains on an interface enforces a strong overlap among the under formed coils, increases the monomer-monomer unit contact and the corresponding interaction energy. The polymer chains are forced to stretch away along the direction normal to the grafting sites, thereby lowering the monomer concentration in the layer and increasing the layer thickness, L. Stretching lowers the interaction energy per chain, F_{int}, by the price of a high elastic free energy, F_{el}. The interplay of these two terms determines the equilibrium thickness of the layer.

The Alexanders model considers a flat, nonadsorbing surface to which monodisperce polymer chains are tethered. The polymer chains consist of N statistical segments of diameter a, the average distance between the tethering points is d, which is much smaller than the radius of gyration of a free, underformed chain. The free energy chain includes two terms:

$$F = F_{int} + F_{el} \tag{2.1}$$

F_{int} refers to the interaction energy between two statistical segments and F_{el} refers to the elastic free energy. Two assumptions are made to enable simple expressions for these two terms. The first one is that the depth profile of statistical segments is step-like. The concentration of statistical segments is a constant within brushes, $\varphi = Na^3/d^2L$. The second is that all free ends of tethered polymer chains are located in the single plane at a distance L from the tethering surface.

The "Flory approximation" [Flo81] is used to obtain the explicit expression for free energy. This argument estimates the reduction in configurational entropy from results for an ideal random walk chain constrained to travel a distance L from the grafting surface to the outer edge of polymer brush. The corresponding free energy per chain can bee expressed in the following equation:

$$F/kT \approx \nu\varphi^2 d^2 L/a^3 + L^2/R_0^2 \tag{2.2}$$

where ν is a dimensionless excluded volume parameter and R_0 is the radius of an unperturbed,

ideal coil. The first term represents the interaction energy between statistical segments and the second represents the elasticity of Gaussian chains. A "scaling argument" approach gives a similar result. The equilibrium thickness is obtained by minimization of F with respect to L and is shown in the following equation:

$$L/a \approx N\,(a/d)^{2/3} \tag{2.3}$$

The most important and distinctive characteristic of polymer brushes expressed in Equation (2.3) is that the equilibrium thickness varies linearly with the degree of polymerization. This is in contrast with free polymer chains in a good solvent, where the dimension of polymer chain varies with N in a relationship of $R \sim N^{3/5}$

Theoretical considerations demonstrate that the densely tethered polymer chains are deformed. The relationship between the equilibrium thickness and degree of polymerization of polymer chains is linear. This is the origin of the novel behavior of tethered polymer brushes.

The idea of the balance of interaction energy and elastic free energy, the essential features in the Alexander model, can be applied to other situations involving polymer brushes in a theta solvent or a poor solvent [Hal88] In a theta solvent, the interaction between statistical segments disappears. The free energy per chain is expressed in the following equation:

$$F/kT = \omega\varphi^3 d^2 L/a^3 + L^2/Na^2 \tag{2.4}$$

Where ω is a dimensionless third viral coefficient. The relationship between the equilibrium thickness and N can be obtained by minimization of free energy with respect to L:

$$L/a \approx N(a/d) \tag{2.5}$$

It is interesting to note that the linearity of L with N is maintained with the solvent and poor solvents. Compared to Equation (2.3), the chains have shrunk by a factor of $(a/d)^{1/3}$, but polymer chains are still distorted at the theta point. This is remarkably different from the behavior of free polymer chains in theta solvent, where the relationship between chain dimension and N is $R_0 \sim N^{1/2}$.

For a brush without solvent (melt brush), the relationship between the thickness of polymer brushes and degree of polymerization can be obtained by a similar approach. It was found that the relationship can be described in the following equation:

$$L \sim N^{2/3} \tag{2.6}$$

As indicated in Equation (2.6), the tethered polymer chains in the melt state are deformed as compared with the behavior of free polymer chains in melt state, where the relationship is $R_0 \sim N^{1/2}$.

In conclusion, no matter in the presence of a good solvent, a theta solvent, a poor solvent, or in the absence of solvent (melt conditions), the polymer chains in tethered polymer brushes exhibit deformed configurations. The degree of deformation of polymer chains depends on environment conditions to which the tethered polymer is exposed.

The Alexander approach is a simple free energy balance argument. It does not attempt to examine of the details of the conformation of polymer chains or the density profile of chain units at a distance from the grafting surface. This simple model can be used to describe the hydrodynamic properties of polymer brushes and other properties, which depend on perturbing the balance between chain stretching and chain-chain repulsion. Such properties are the hydrodynamic thickness, permeability of a brush and the force per area required to compress a brush (either vertically or laterally). The lubrication forces that arise if two brushes are brought into near contact are related to the hydrodynamic properties.

However, the following question on brush structures are not well represented by the Alexander model. These questions include: the shape of the chain unit density function, the location of the free ends of polymer chains, how the polymer chains segregate or mix in a mixed polymer brush of either different chain lengths or different chemical compositions, and how the polymer chains interpenetrate each other.

Relatively simple theoretical results have been obtained for a wide variety of brush properties and situations under the conditions of strong stretching. A simple hypothesis about free chain ends from the interface is made: free chain ends may be located at any distance from the interface [Mil91, Sem75, Mil88, Mil89]

Experimental research has been carried out to elucidate polymer brush structure and explore their novel properties. For end adsorbed polymer brushes, optical probes such as evanescent waves [All81], ellipsometry [Sau89], infrared spectroscopy [Kaw88], and multiple-reflection interferometry [Mun90a, Mun90b] give information equivalent to the total amount of polymer adsorbed. Many scattering experiments have been performed to investigate the structure of end-grafted polymer systems [Cos90, Cos87]. Parsonage and co-workers [Per87] studied the adsorption of the diblock copolymer polystyrene-*b*-poly(4-vinylpyridine) (PS-*b*-PVP) from toluene solution onto mica and used radiolabeling techniques to measure the coverage for various PS-*b*-PVP copolymers on mica. Patel and al. [Pat87] studied a series of adsorbed block copolymers where a block strongly interacts with the surface and the other block adsorbs weakly. The work of Auroy et al. [Aur91] gave strong support of linearity of polymer brush height with respect to the degree of polymerisation of tethered polymer chains.

2.2.3 Theoretical and Experimental Studies of Mixed Polymer Brushes

Theoretical study of mixed brushes started in early 90-th by Marko and Witten, who demonstrated for the first time that the system of anchored polymer chains of two chemically distinct types undergoes the microphase separation, if incompatibility of the chains is sufficiently high. This result has been obtained in frames of the mean-field strong stretching theory, which has been earlier successfully applied to homopolymer brushes. Since then, the mixed brushes have been explored with a number of powerful theoretical tools of polymer physics.

The basic assumption of the mean-field strong stretching theory is the strong stretching limit (SSL). The analytical theory, based on the SSL, was proved to be very useful for analysis of brushes, consisting of chemically equivalent chains. In 1991, Marko and Witten [Mar91] extended it to the case of binary brushes. They considered the case of the brush under melt conditions, composed of two species of incompatible molecules (called usually *A* and *B* molecules). Chemical difference of the unlike molecules gives rise to a mixing free energy per chain which is a function of the monomer concentrations:

$$\frac{E}{nkT} = \Lambda \int \frac{d^3 r}{\Omega\sigma} \phi_A(\vec{r})\phi_B(\vec{r}) \tag{2.7}$$

where $n = \Omega\sigma$ is the total number of molecules in the layer, Ω is the surface of the layer. The coupling constant Λ has units of inverse volume and related to the Flory-Huggins parameter χ via $\chi = \Lambda V / N$, where N is the polymerization index. The incompressibility condition expressed by $\phi_A = 1 - \phi_B$. The positive value of the coupling constant Λ implies that the system will tend to phase separation of the *A* and *B* monomers. This separation is opposed by the loss of entropy. The equilibrium configuration is the result of the balance of the mixing energy and the entropic cost.

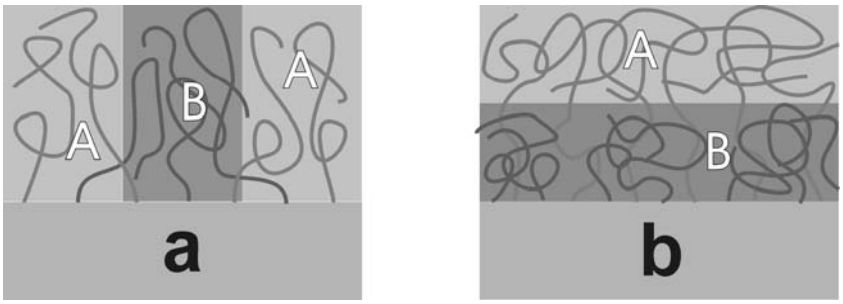

Figure 2.2. Schematic representation of phase segregation of a mixed polymer brush.

There are basically two possibilities of the phase separation. In case of *perpendicular segregation* (Figure 2.2b), a layer enriched by the *A* component lies below the layer enriched

by the *B*-component, or vice versa. Then the lost of entropy is that of the distribution of the free ends of the chains. In case of *lateral segregation* (Figure 2.2a), homogeneity in the lateral direction is broken and the chains can form ripples, clusters etc. This behavior of the mixed brushes is qualitatively similar to the behavior of free block-copolymer melts, but the self-assembled structures are periodic in two dimensions and have a brush-like structure perpendicular to the grafting surface. The entropy cost is then due to subtle changes of the chain conformations traveling through different regions of the layer. Further progress can be made if one assumes that the mixing energy is much smaller than the stretching energy of the chains. Then the pressure inside the brush is dominated by the excluded volume interactions and can be described by the formula (2.1). Using the Green function formalism, Marko and Witten have shown that the brush undergoes the second order phase transition to the ripple laterally segregated structure as the incompatibility Λ increases: the monomer density difference behaves as

$$\phi_A - \phi_B \approx \left(\Lambda - \Lambda^*\right)^{1/2} \cos(kx) \tag{2.8}$$

where the wavelength of the ripples is approximately two times larger than the average end-to-end distance R_E of unconstrained chains in the θ-solvent, $\lambda = 2\pi/k = 1.97R_E$. The theory predicts, that the transition to the ripple morphology occurs at smaller values of incompatibility, than the transition to the layered phase. In other words, the ripping transition pre-empts the layering transition.

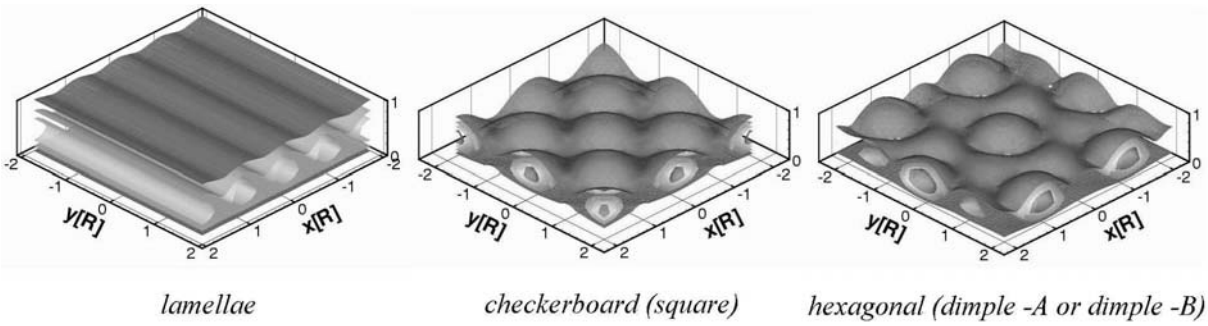

Figure 2.3. Morphologies of a binary mixed polymer brush with symmetric composition.

Although the theory, developed by Milner, Witten, Marko and Cates, do predicts the major phenomena, which take place in the binary brushes, it is constrained to the case of very high grafting densities and/or long chains. A more general method, based on the self-consistent field theory has been developed recently by Müller [Muel02]. The calculation technique was designed initially by Matsen and Schick [Mat94] for calculation of the phase diagram of block-copolymers with the use of Fourier representation of the monomer densities and effective fields. This technique allows to analyze the stability of different lateral

morphologies, such as lamellar, check board and hexagonal "dimple" phases (Figure 2.3). The first-order phase transitions between the different morphologies depend on the number of parameters, which characterize the brush and the solvent. The phase diagrams of the mixed brushes were calculated for varying incompatibility (Flory-Huggins parameter), difference of the solvent quality for the brush components, total grafting density and the relative grafting density of the *A* and the *B*-species. It was shown, that the morphology of the mixed brush is the result of the delicate interplay between the lateral and the perpendicular phase segregation [Min02a].

Using two-dimensional SCF calculations, Zhulina et al. [Zhul96] have studied diblock copolymer brushes. They have found that under the poor solvent conditions and sparse grafting density the brush self-organizes in an ordered array of micelles, which have “onion” or “garlic-like” structures. The spacing between the micelles can be manipulated by the molecular weight of the chains and fraction of the species. They also suggested that mixed brushes find applications as coatings of colloids and enable some fine-tuning of their interaction.

2.2.4. Responsive/Switching/Adaptive Behaviour

Sidorenko et. al. [Sid99a] for the first time reported on the responsive behaviour of the mixed PS/P2VP brush. XPS and contact angle experiments have shown that the surface composition of the brush and the surface wetting behavior switched upon exposure to different selective solvents. Recently, it was proven for various mixed binary brushes that they are capable of switching their structure in response to solvent quality, temperature, pH, and confining wall signals [Min 03b, Uso02].

The origin for the responsive behavior is in the reversible microphase segregation of the components in the mixed brush [Min02a]. The phase diagram for symmetrical mixed brush as a function of the solvent selectivity ζ is presented in Figure2.4. In a non-selective solvent, $\zeta=0$, a transition from laterally homogeneous phase to a ripple phase was observed upon increasing the incompatibility of A and B species. As solvent quality for the A-component ($\zeta<0$) decreased, the ripple phase transformed to a dimple structure, where the A component segregated into clusters. Similarly, a dimple structure with a collapsed B polymer was observed when solvent was poor for the B component ($\zeta>0$). At higher incompatibility (or poorer solvent quality) only dimple structures were stable. Experimentally, this mechanism was proved by applying the combination of X-ray photoemission electron

microscopy (XPEEM), contact angle, and AFM techniques for the binary mixed brush [Lem03b, Lem03c].

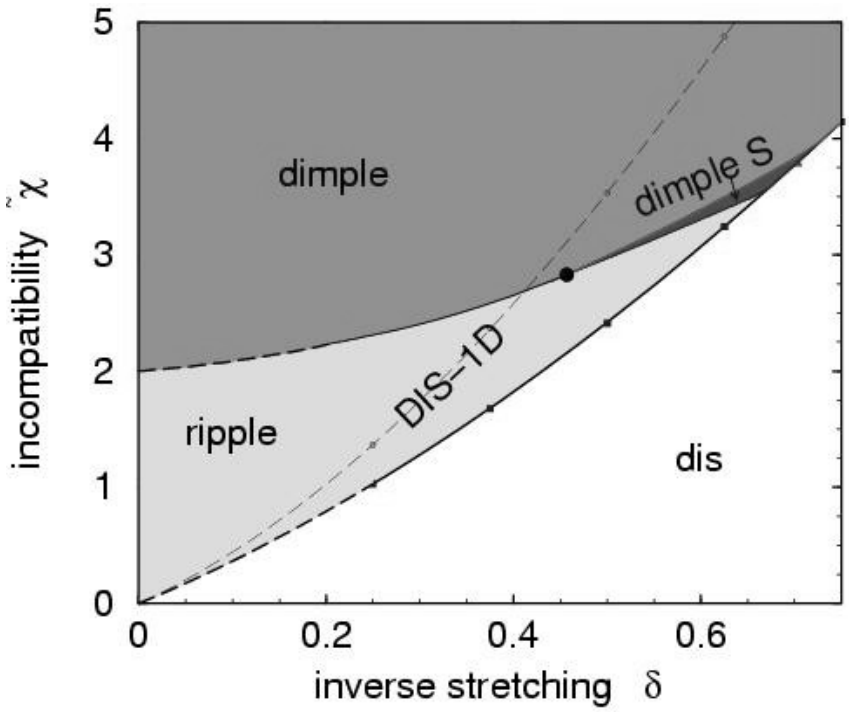

Figure 2.4. Phase diagram for a symmetric binary polymer brush as a function of incompatibility χ' and inverse stretching δ'.

Lemieux at.al [Lem03a] have proved the mechanism of structural reorganization by studying nanomechanical properties of the mixed binary brush prepared from two polymers with very different mechanical behavior of PSF and polymethylacrylate (PMA). This was demonstrated for corresponding homobrushes. [Lem03b] The lateral and vertical reordering of the mixed brush was observed to be relatively quick (on the order of a few minutes), and reversibility between good and bad solvent states for each component. Since PSF and PMA are mechanically dissimilar (glassy and rubbery, respectively) at room temperature, AFM phase imaging was used to verify the resulting laterally segregated structures. To determine the vertical segregation in addition to the lateral ordering, surface nanomechanical mapping was conducted to directly determine the surface distribution of the elastic modulus and adhesive forces. Results show a clear bimodal response of the mechanically heterogeneous surface, with elastic modulus and adhesion contributions very different for the “glassy state” and the “rubbery state”. Furthermore, depth profiling of the elastic modulus was exploited to understand the vertical segregation in the mixed brush and verify partial vertical segregation of dissimilar components. Results of this study quantified the elastic properties of PSF and PMA, demonstrated the dramatic mechanical contrast of the surface as a function of solvent

conditions, and decisively revealed the lateral and layered modes of the phase segregation in a binary polymer brush.

2.2.5. Synthesis of Mixed Brushes

Two well established approaches are usually used to synthesize mixed brushes: “grafting from“ (Figure 2.5) and “grafting to“ (Figure 2.6) methods. The “*Grafting from*” method refers to the approach when the initiator is attached to the solid substrate and polymerization is done in situ on the solid surface.

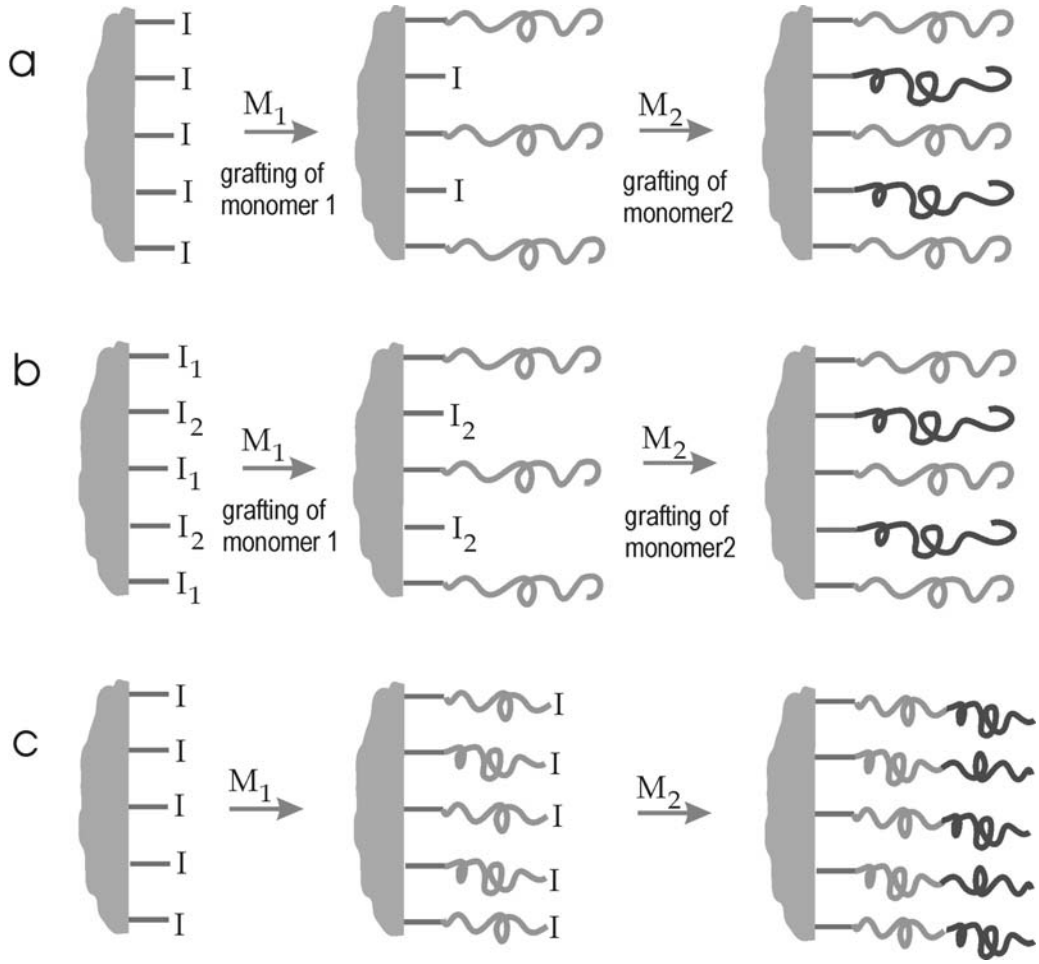

Figure 2.5. Scheme of synthesis of binary polymer brushes via “grafting from” approach: (a) two-step polymerization with a slow rate of surface-initiation, the same initiator is used for the both steps; (b) two-step polymerization with different surface-immobilized initiators used for two grafting steps; (c) end-grafting of di- (or tri-) block copolymer brushes via living (controlled) polymerization from one kind of surface-immobilized initiator.

For instance, Sidorenko et.al. [Sid99b] applied the approach suggested by Tsubokawa et. al. [Tsu90] to introduce the initiator on the solid substrate. First, ω-epoxysilane was used to introduce epoxy functional groups on the surface of silicon wafers.

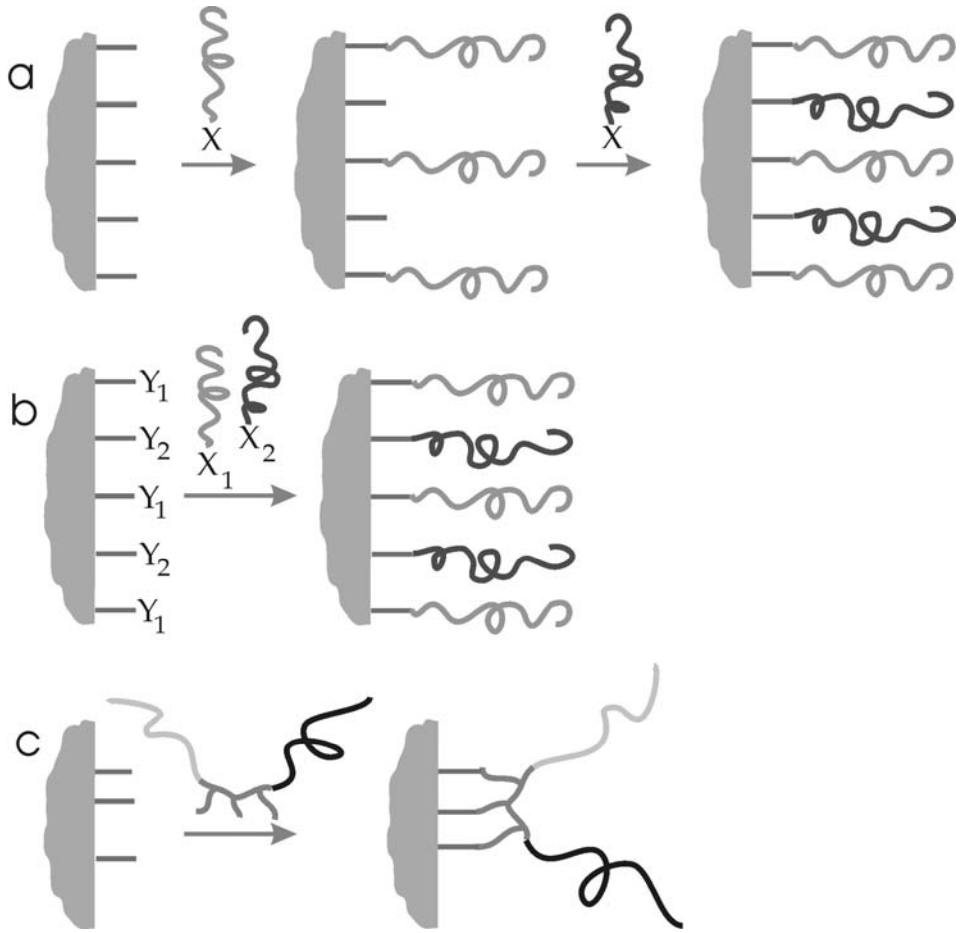

Figure 2.6 Scheme of synthesis of binary polymer brushes via "Grafting to" approach: (a) two-step anchoring of two different end-functionalized homopolymers to one kind of surface reactive groups; (b) simultaneous anchoring of two end-functional homopolymers via different mechanisms to complementary functionalities on the substrate; (c) immobilization on surface of triblock copolymers via the middle anchoring block.

Afterward, 4,4´-azobis(4-cyanopentanoic acid) (ACPA) was anchored using the catalytic reaction of the epoxy groups on the surface with carboxyl groups of the azoinitiator. Another approach [Min00] was based on the method of Boven et.al [Bov90] where the ω-aminosilane was grafted on the silicon wafer and then the chloride derivative of ACPA (Cl-ACPA) was bonded to the substrate. Both methods were found to have disadvantages. In the first case, the reaction of epoxy groups with ACPA was not very well controlled. Moreover, during chemisorption a large fraction of epoxy rings is lost by a catalytic effect of the surface and

adsorbed water. In the second case, due to the high reactivity of amino groups, the chemisroption of ω-aminosilane was not well-controlled process.

Recently, Usov et al. [Uso02] suggested a solution of the problem when, in the first step, 3-glycidoxypropyl trimethoxysilane (GPS) was used to modify the surface of Si-wafers resulting in the chemisorbed layer with epoxide and hydroxyl groups. A high density monolayer can be formed with epoxy groups [Tsu99, Luz00a]. In the second step, the epoxy-terminated silicon wafer was treated with ethylene diamine to transform epoxy groups into more reactive amino groups. Finally, Cl-ACPA was attached by the reaction with amino and hydroxyl groups on the surface in the presence of a catalytic amount of thriethylamine to bind released HCl . The latter method demonstrated very good reproducibility

A novel method to introduce epoxide and hydroxyl groups on the surface of different substrates by the deposition of a thin (1-2 nm) film of poly(glycidylmethacrylate) (PGMA) has been reported in literature [Luz03, Swa03]. Upon heating, this film was cross-linked and formed a stable smooth polymer “carpet” with a high density of hydroxyl and epoxy group on the surface. This method is universal and can be applied for the modification of different substrates because the cross-linked PGMA forms the stable surface film due to the multi-point interactions between backbones and the surface even in the case of the participation of weak van der Waals attractive interactions between PGMA monomer units with the substrate.

Once the initiator was attached to the solid substrate, the two-step radical polymerization procedure was performed to graft two different polymers. The first polymerization step was done for the controlled periods of time to use only a fraction of the initiator. Afterwards, the obtained monobrush was thoroughly rinsed to remove the non-grafted polymer after the first reaction. Then the second grafting polymerization was performed using the residual initiator on the surface.

The alternative strategy for synthesis of mixed polymer brushes consists of the combination of atom transfer radical polymerization (ATRP) and nitroxide-mediated radical polymerization (NMRP) [Eja03, Zha03]. These two controlled radical polymerization techniques depend upon different mechanisms and can be performed at very different temperatures. A nitroxide-terminated and ATRP- initiator terminated organotrichlor- or triethoxy silanes were used to graft the initiators to the solid substrate. Then two-step polymerization procedure is applied to fabricate mixed brushes.

On the contrary, the “*grafting to*” method employs end functionalized homopolymers or random copolymers, or functionalized block-copolymers with functional groups located near the point connecting different blocks. The polymers are grafted onto the substrate via

chemical reaction of the polymer functional precursor groups and complimentary functional groups on the surface.

Grafting density of polymer brushes prepared with the “grafting to” method usually is relatively low because of the kinetic limitations resulting from the very low diffusion rate of polymer chains penetrating through the already grafted brush layer. In the framework of this approach, the largest grafting density was obtained for the grafting performed from concentrated solutions or polymer melts when the concentration of the polymer segments with the functional groups have approached the maximal possible level. Under these grafting conditions, two incompatible polymers segregate macroscopically when one of polymers preferentially occupies the substrate surface. One of the problems with this approach is that, upon heating, the film can dewet the substrate and the grafting may result in a very inhomogeneous polymer film. Thus, the two step grafting procedure avoiding the phase segregation during grafting was developed. For example, the mixed brush from carboxyl terminated homopolymers PS and P2VP was prepared with the two-step procedure. First, PS was grafted to the GPS modified silicon wafer. The PS film on the wafer surface was prepared by spin coating. The grafting was performed upon heating above the glass transition temperature for controlled period of time to assure that the first grafting step was terminated at the grafting density less than the plateau value. Then, the non-grafted polymer was removed and the same procedure was repeated to graft carboxyl terminated P2VP. This routine was also successfully used to graft PS/PtBA mixed brush and, after hydrolysis, PS/PAA binary brushes. [Jul03a]. These mixed brushes showed clearly pronounced switchable behavior with dramatic rearrangements of surface morphology upon exposure to different solvents. The authors observed that not only the surface wettability changed significantly, but also surface nanomechanical properties were altered by this reorganization.

This procedure was the most successful if a less polar polymer (PS) was grafted first. It gives an additional driving force for the second polymer to penetrate the layer of the first grafted polymer. With “grafting to” approach, the mixed brushes with the grafting densities ranging from 0.01 to 0.2 nm^{-2} and molecular mass from 4Kg/mol to 100 Kg/mol were synthesized.

Recently, the synthesis of the PS/PBA mixed brush by the combination of the "grafting to" and "grafting from" methods was reported in literature. [Kle03] The Si-wafer substrate was modified with the PGMA thin layer. Then, the sample was treated with a vapor of 2-bromoisobutiric acid, which can serve as an initiator for ATRP. In the first step, the carboxyl terminated poly(tert-butylacrylate) was grafted to the silicon wafer via “grafting to”

method involving the reaction of the end carboxyl groups with the epoxy groups of the PGMA modified substrate. In the second step, ATRP of styrene was carried out. The high-density brushes were synthesized with this approach. The advantage of this method refers to the possibility to substantially extend the range of polymers, which can be exploited for the fabrication of mixed brushes.

It is worth to note that mixed brushes prepared by different grafting methods show very similar surface behavior. The general tendency reveals that the higher grafting density results in the larger range of switching until the limiting state (e.g., complete switching between properties of polymers A and B) is approached. In other words, the increase of the grafting density within the practical experimental region of the grafting densities enhances the tendency to both vertical and lateral phase segregation of dissimilar components.

To approach the maximal switching range controlled by the phase transition mechanism, the mixed brush should be randomly grafted. However, the microphase segregation even before or during grafting tends to deviate from random grafting. Modifications of grafting procedures aim to overcome this inhomogeneous grafting affected by the microphase segregation.

2.2.6 Methods to Study Responsive Behavior.

The main problem in studying the phase transition and responsive properties of the mixed brushes is affected by the high sensitivity of the polymer chain conformation to a change of environment. On top of this, the simultaneous segregation in lateral and vertical directions makes the problem to be much more difficult. It implies that *in situ* study of the morphology of the brushes should be performed with methods sensitive to the brush profile with a lateral resolution at the molecular dimension scale. There are only few methods, known for investigations of thin polymer films, which can in principal fit the requirements: AFM with direct scanning under solvent (in a liquid cell) and neutron reflectivity from solid-liquid interfaces. Only two reports are published in the literature about the investigation of the mixed brush morphology performed with AFM *in situ* in a selective solvent and demonstrating reversible switching of surface morphology [Lem03c, Mel03]. So far to our knowledge, there were no attempts to the present time to employ neutron reflectivity for study of mixed brushes in situ.

The task of studying of mixed brushes is much easier if we make an assumption that the original brush morphology is frozen in dry state due to the rapid evaporation of solvent. Indeed, during drying the brush undergoes collapse mainly in Z direction, so that the lateral

morphology should remain almost unchanged. The profile in Z direction is strongly modified because of solvent evaporation. However, the relative distribution of the polymers A and B in Z direction still reflects the layered or vertical segregation. Practically, it means that after the rapid evaporation of solvent one can measure the surface composition of the dry mixed brush with an appropriate lateral resolution and then reconstruct the morphology of the brush, which corresponds to that in solvent. That assumption is quite reasonable because the solvent evaporation time from the brush layer is much smaller than the characteristic time of polymer diffusion in a swollen state.

In fact, it is commonly used practice to freeze the morphology of multicomponent polymer materials by rapid drying or cooling. There are also several experimental evidences supporting the assumption: 1) the morphology of the dry brush reversibly switches upon exposure to different solvents; 2) the morphologies after the treatment by a particular solvent are reproducible and can be repeated many times; 3) the AFM scanning under solvents proved that the lateral structures in dry film and under solvent are similar, but sizes in a swollen state somewhat larger, that is quite reasonable for a good solvent; 4) the surface structures observed for dry mixed brushes are in good agreement with theoretical predictions made for the brushes in solvent [Min01, Min02a, Zha00a, Zha00b]. Based on that, the brush morphology was studied for the dry mixed brushes of different compositions with AFM and XPEEM and considered to be relevant to actual morphology of brushes in different solvents. [Jul03b]. The integral chemical composition of the top layer of the mixed brushes is evaluated with contact angle, nanomechanical probing, ζ-potential, and XPS methods. Adsorption of colloidal particles and adhesion tests were used to probe the surface composition of mixed brushes [Zha00a, Zha00c].

Chapter 3

Experimental Techniques.

3.1 Introduction

The field of polymer and materials research creates the need of specific analytical techniques for the investigation and determination of chemical composition (UV-vis, FT-IR spectroscopy, X-ray diffraction (XRD), X-ray photoelectron spectroscopy (XPS)), end groups (MALDI-TOF-MS, NMR spectroscopy), polymerization kinetics (GC), molecular weights and polydispersity (gel permeation chromatography (GPC)), Tm and Tg, morphology (atomic force microscopy (AFM), scanning electron microscopy (SEM), transmission electron microscopy (TEM)) and solution properties, such as viscosity.

During recent years, many surface sensitive techniques have been developed to analyze polymer surfaces. However, the surface investigated by one technique may be the bulk if studied by another. An appropriate definition of a surface, e.g., the sampling depth observed, is therefore very important. These techniques provide compositional information for different depth below the surface. When structural information (surface topology, lateral heterogeneity) is required, various types of microscopic techniques are appropriate, such as scanning electron microscopy (SEM), transmission electron microscopy (TEM) and more recently atomic force microscopy (AFM).

The choice of a suitable analytical surface technique involves the consideration of what kind of surface information is needed. Contact angle data, which are extremely surface sensitive, are important for the determination of surface tensions of the solid surface. However, these data do not provide direct information about the chemical composition of the surface. In this respect XPS, SIMS have to be used. The combination of several techniques can provide complementary surface information and can result in a more detailed view on the chemical composition and the component distribution, particularly in relation to a better understanding of the phenomena of wetting and adhesion.

3.2. Ellipsometry.

Ellipsometry is an optical technique that uses polarised light to probe the dielectric properties of a sample. The most common application of ellipsometry is the analysis of very thin films. Through the analysis of the state of polarisation of the light that is reflected from

the sample, ellipsometry can yield information about layers that are thinner than the wavelength of the light itself, down to a single atomic layer or less. Depending on what is already known about the sample, the technique can probe a range of properties including the layer thickness, morphology, or chemical composition.

The name "ellipsometry" stems from the fact that the most general state of polarization is elliptic. The technique has been known for almost a century, and today has many standard applications. It is mainly used in semiconductor research and fabrication to determine properties of layer stacks of thin films and the interfaces between the layers.

An illustration of the transmitted, reflected, and incident beams is shown in Figure 3.1. A beam of light is incident on a sample at some arbitrary angle of incidence θ_i, the angle of incidence is defined as the angle between the input beam direction and the direction normal to the sample surface. At the boundary of the medium, part of the light will be reflected at angle θ_γ while the other part will be transmitted through the sample at angle θ_t. Snell's law requires that all three beams be in the plane of incidence. The plane of incidence is defined as a plane which contains the incident beam, the reflected beam.

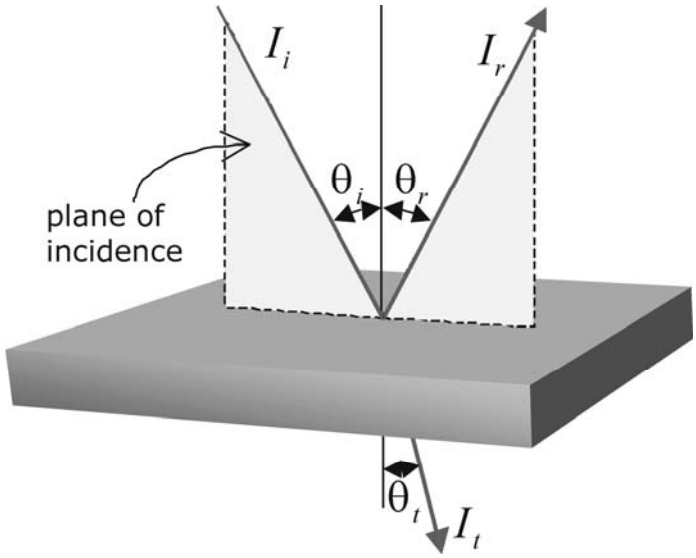

Figure 3.1 Schematic showing the incident, reflected, and transmitted light.

The transmission and reflection measurements acquire the intensity ratios, T and R respectively, over a given range of wavelengths. T and R are defined as the ratio of the light intensity being transmitted I_t or reflected I_r over the incident light intensity I_i on the sample, as shown in Equations (3.1) and (3.2)

$$T = I_t / I_i \tag{3.1}$$

$$R = I_\gamma / I_i \tag{3.2}$$

Ellipsometry measures the change in polarization state of light reflected from the surface of a sample. The measured values are expressed as Ψ and Δ. These values are related to the ratio of Fresnel reflection coefficients, R_p and R_s for p and s-polarized light, respectively.

$$\tan(\Psi)e^{i\Delta} = \frac{R_p}{R_s} \tag{3.3}$$

Because ellipsometry measures the ratio of two values, it can be highly accurate and very reproducible. From Equation (3.3) the ratio is seen to be a complex number, thus it contains "phase" information contained in Δ, which makes the measurement very sensitive. In the Figure 3.2, a linearly polarized incident beam is converted to an elliptically polarized reflected beam. For any angle of incidence in the range between 0° and 90°, p-polarized light and s-polarized will be reflected differently.

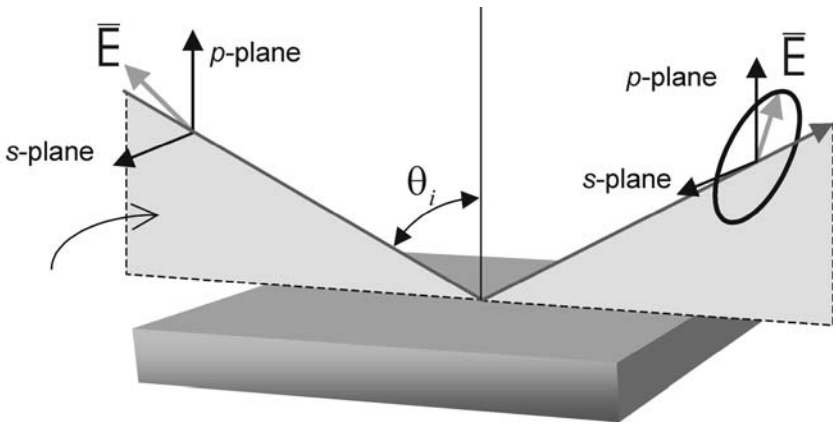

Figure 3.2 Scheme of an ellipsometry experiment.

The coordinate system used to describe the ellipse of polarization is the p-s coordinate system. The s-direction is taken to be perpendicular to the direction of propagation and parallel to the sample surface. The p-direction is taken to be perpendicular to the direction of propagation and contained in the plane of incidence.

The optical constants define how light interacts with a material. The complex refractive index is a representation of the optical constants of a material, it is represented by

$$\tilde{n} = n + ik \tag{3.4}$$

The real part or index of refraction, n, defines the light propagation velocity of light in material:

$$v = \frac{c}{n} \tag{3.5}$$

where v is the speed of light in the material and c is the speed of light in vacuum. The imaginary part or extinction coefficient, k, determines how fast the amplitude of the wave decreases. The extinction coefficient is directly related to the absorption of a material and is related to the absorption coefficient by:

$$\alpha = \frac{4\pi k}{\lambda} \tag{3.6}$$

were α is the absorption coefficient and λ is the wavelength of light.

The Equation (3.3) is the basic equation of ellipsometry [Azz79]: The values Ψ and Δ are the ellipsometric angles, which are directly obtained from an ellipsometric experiment. The thickness of a thin film and its refractive index are calculated from the Ψ and Δ using an appropriate physical model:

There are different methods for determination of the Ψ and Δ parameters [Azz79] . We used null-ellipsometry [Mots91] in this work. The principal setup is depicted in Figure 3.3.

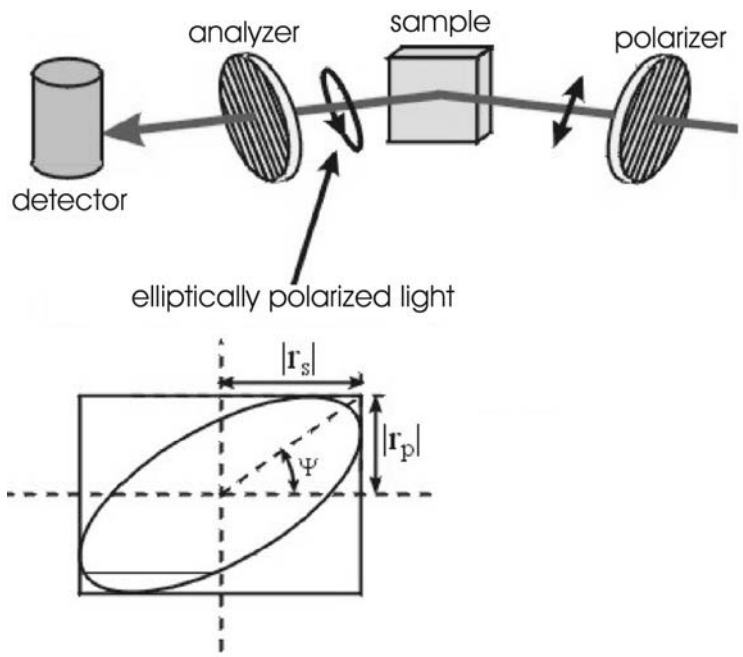

Figure 3.3. Ellipsometr set-up.

The light source is a He-Ne laser producing monochromatic red light (λ = 632.8 nm). The beam passing through the polarizer and the compensator adopts an elliptical polarization. It is incident at 70° to the sample (optimal for Si substrates with natural SiO_2 layer). The polarization state of the incident beam is chosen so (rotating the polarizer, the compensator position is fixed) that the reflected beam is linearly polarized and can be fully cancelled by the analyzer. The intensity of the beam passed through the analyzer is measured with the 4-

section photodiode. The Ψ and Δ values are derived from positions of the polarizer (P) and analyzer (A), which lead to zero intensity of the beam at the detector [Azz79, Mots91]:

$$\Psi=A,\ \Delta=2P+90^{o} \qquad (3.7).$$

Glan-Thompson prisms made of calcite $CaCO_3$ were used as the polarizer and the analyzer. The prism splits a propagating beam into two beams of mutual perpendicular polarization: the extraordinary and the ordinary beam [Mots91a]. The prism is designed in a way that the extraordinary beam is totally reflected whereas the ordinary beam is transmitted. The compensator was made of a properly cut quartz plate with two distinct orthogonal directions: the slow and the fast axis [Mots91a]. For an arbitrary orientation of the electric field vector of a propagated beam, the electric field vector is decomposed in its two components parallel to the fast and the slow axis. Since the refractive indices do not match a phase shift occurs. The thickness of the quartz plate is chosen so that the produced phase shift equals $\pi/2$. The compensator converts linearly polarized light into elliptically polarized light.

For the thin layers of few nanometers thick the change of the Ψ and Δ relative to the bare substrate is small, what makes impossible parallel determination of the refractive index and the thickness of the film [Zhan96]. In such cases the refractive index is measured in an independent experiment on a thick film of the same material or is taken from literature.

3.3. Atomic Force Microscopy (AFM).

The Atomic Force Microscope (AFM) is being used to solve processing and materials problems in a wide range of technologies The materials being investigating include thin and thick film coatings, ceramics, composites, glasses, synthetic and biological membranes, metals, polymers, and semiconductors. AFM investigates properties of a top layer of materials through measuring interaction forces between a probe and the sample surface. Van der Waals, friction, electrostatic, and magnetic forces are the examples of the interaction kinds, which can be probed with AFM [Han88].

The principle scheme of AFM is very simple (Figure 3.4). A very sharp tip is scanned over a surface with feedback mechanisms that enable the piezo-electric scanners to maintain the tip at a constant force (to obtain topography information), or height (to obtain force information) above the sample surface. Tips are typically made from Si_3N_4 or Si. The nanoscope AFM head employs an optical detection system in which the tip is attached to the underside of a reflective cantilever.

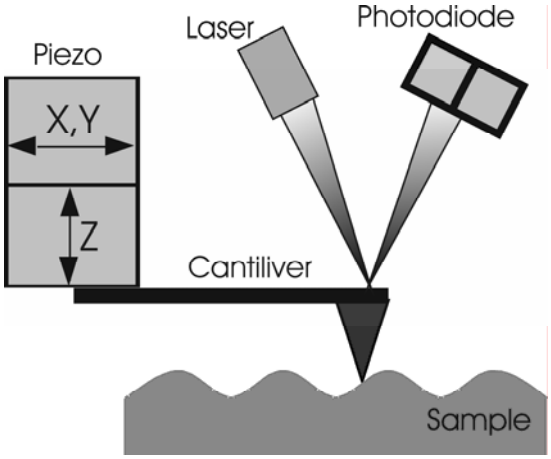

Figure 3.4. Scheme of an AFM microscope

A diode laser is focused onto the back of a reflective cantilever. As the tip scans the surface of the sample, moving up and down with the contour of the surface, the laser beam is deflected off the attached cantilever into a dual element photodiode. The photo detector measures the difference in light intensities between the upper and lower photo detectors, and then converts to voltage. Feedback from the photodiode difference signal, through computer control, enables the tip to maintain either a constant force or constant height above the sample. In the constant force mode the piezo-electric transducer monitors real time height deviation. In the constant height mode the cantilever deflection force caused by the interaction with the sample is recorded.

Three imaging modes, contact mode, non-contact mode, and intermittent contact or tapping mode can be used to produce topographic images of sample surfaces. In contact mode, the probe is essentially dragged across the sample surface. (Figure 3.5) During scanning, a constant bend in the cantilever is maintained. A bend in the cantilever corresponds to a displacement of the probe tip, z_t, relative to an undeflected cantilever, and the applied normal force, $P = kz_t$, where k is the cantilever spring constant. As the topography of the sample changes, the z-scanner must move the relative position of the tip with respect to the sample to maintain this constant deflection. Using this feedback mechanism, the topography of the sample is thus mapped during scanning by assuming that the motion of the z-scanner directly corresponds to the sample topography. To minimize the value of the applied force used to scan the sample, low spring constant ($k < 1$ N/m) probes are normally used. [DI99]. In the tapping mode, an external periodic force is applied to the probe. That causes the cantilever to oscillate perpendicular to the sample surface with a typical amplitude 20-100 nm. The tapping mode was developed [Zho93, Qui94] for investigation of soft materials. When the oscillating cantilever approaches the surface and the tip starts to interact with it, the amplitude

of oscillation linearly decreases (Figure 3.6c) and is maintained constant at a certain value (amplitude set-point) by the feedback loop of the microscope.

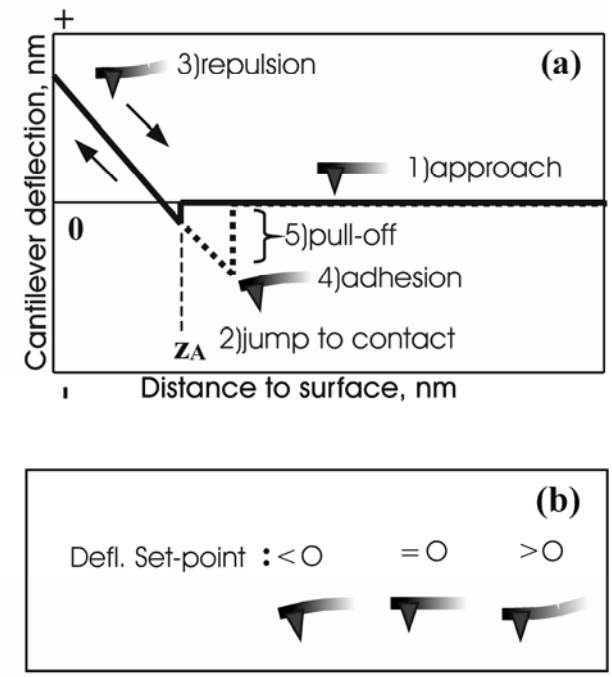

Figure 3.5. Contact mode. (a) Force distance diagram, solid line-approach, dot line-withdraw of the tip. (b) Maintaining the interaction force at the constant level.

The lower is the set-point (or the amplitude set-point ratio A/A_0, where A_0 is the amplitude of free oscillations), the closer the tip can come to the sample. Changes in the vertical coordinate (z) of the sample (or the cantilever) upon scanning the surface needed to keep a constant amplitude of oscillation are monitored and displayed as a topography signal. The typical amplitude while imaging in air allows the tip to contact the sample surface through an adsorbed liquid layer without getting stuck. Time of the contact of the tip with the surface and the friction energy are from one to two orders smaller in the tapping mode than in the contact mode [Tam96]. The contact time increases upon decreasing the amplitude set-point ratio.

The non-contact mode differs from the tapping mode by smaller amplitude of cantilever oscillations which is <10 nm. The tip does not have enough energy to strike the sample but oscillates in the range of the attractive forces [DI99]. Application of the non-contact mode is limited by materials where the adsorbed liquid layer is thin, otherwise the tip becomes trapped by it and scrapes the sample.

3.4. Determination of Surface Tension.

Surface tensions of solid-vapor interfaces and solid-liquid interfaces are important parameters in many areas of applied science and technology. These interfacial tensions are responsible for the behavior and properties of commonly used materials such as paints, adhesives, detergents and lubricants.

The combined use of the first and the second law of thermodynamics give the variation of the internal energy U of a macroscopically homogeneous bulk phase:

$$dU = TdS - pdV + \sum \mu_i dn_i \tag{3.8}$$

where S is entropy, V volume, and μ chemical potential. The index i refer to the type of molecules. For a thermodynamic description of bulk properties this equation is adequate but considering surfaces it has to be extended since the boundary of the system is the locus of some excess energy. This excess term is proportional to the change in surface area A and the associated intensive variable is the surface tension γ so that Equation (3.8) is modified:

$$dU = TdS - pdV + \sum_i \mu_i dn_i + \gamma dA \tag{3.9}$$

The surface tension γ, is the most important quantity that characterizes a surface. Thermodynamically, the surface tension of a solid material in contact with vapor γ_{SV} is thus defined as the change in energy (U) of the whole system with change of surface area (A) at constant entropy (S), volume (V) and number of moles of the components involved (n). It can be shown that γ is also equal to the change in Gibbs energy (G) at constant temperature (T), pressure (p) and number of moles (n), *i.e.* [Zan88]

$$\gamma_{SV} = \left(\frac{dU}{dA}\right)_{S,V,n} = \left(\frac{dG}{dA}\right)_{T,p,n} \tag{3.10}$$

For liquids there are several direct methods, *e.g.* Wilhelmy plate, capillary rise and pendant drop, for direct determination of the surface tension. However, it is impossible to measure directly the surface tension of a solid, such as a polymer. Therefore, indirect methods have to be used similar to the liquid homologue method, the polymer melt method and contact angle measurements. The last method is perhaps the simplest and most widely used techniques for the evaluation of surface tension. Various approaches have been developed to calculate surface tension of solids from contact angle measurements. They all are based on the Young's equation in which the relation is given between the surface tension γ and contact angle Θ for a (pure) solid in contact with a (pure) liquid. When a droplet of a wetting liquid comes into the contact with the solid surface (Figure 3.7), the balance between the forces along the three phase boundaries is defined by the Young's equation:

$$\gamma_{lv} \cos\Theta = \gamma_{sv} - \gamma_{sl} \tag{3.11}$$

where γ_{lv}, γ_{sv}, and γ_{sl} denote the interfacial tension of the liquid-vapor, the solid-vapor and the solid-liquid interfaces, respectively. The terms on the left hand side are readily obtained experimentally leaving γ_{sv} and γ_{sl} as unknown. While only the value of γ_{sv} -γ_{lv} can be obtained from contact angle measurements, the value of γ_{sl} is needed for the evaluation of γ_{sv}. Numerous approximate models have been developed to determine the surface tension of solids from contact angle measurements. There are, for instance, the critical surface tension concept of Zisman [Zis64], the surface tension components approach of Fowkes [Wus82], and the equation of state approach of Neumann [Kwo99]. The last two methods will be discussed here in brief. In spite of the extensive studies, a definite theoretical framework has yet not been established and all models are more or less subject to arguments.

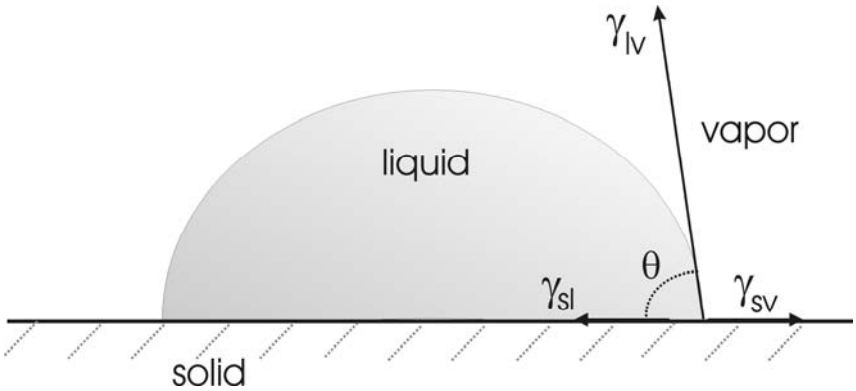

Figure 3.7. Balance of interfacial tensions between a solid, a liquid and a vapor.

3.4.1. Surface Tension Component Approach

Fowkes pioneered the approach of surface tension components. He assumed that the total surface tension γ is composed of different surface tension components, each of which arises from specific intermolecular or inter-atomic forces at the interface. Then the surface tension can be written as:

$$\gamma = \gamma^d + \gamma^p + \gamma^h + \gamma^i + \gamma^m + ... \tag{3.12}$$

where γ^d, γ^p, γ^h, γ^I, γ^m. are the contribution due to London dispersive forces, Keesom permanent dipole-dipole forces, hydrogen bonds, Debye induction forces, and metallic interactions, respectively. For a two phase system, in which only dispersive forces are operative $(\gamma = \gamma^d)$ across the interface γ_{12} can be written (using a geometric mean approach) as:

$$\gamma_{12} = \gamma_1 + \gamma_2 - 2(\gamma_1\gamma_2)^{1/2} = \gamma_1^d + \gamma_2^d - 2(\gamma_1^d\gamma_2^d)^{1/2} \tag{3.13}$$

where subscript 1 and 2 represent phase 1 and 2, respectively. For a solid-liquid interface, Equation. (3.13) results in:

$$\gamma_{sl}^{d} = \gamma_{sv}^{d} + \gamma_{lv}^{d} - 2(\gamma_{sv}^{d}\gamma_{lv}^{d})^{1/2} \tag{3.14}$$

Owens, Wendt and Kaelble [Owe69] extended this concept by considering both dispersive and polar forces. Using the geometrical mean approach in combination with the Young's equation they proposed:

$$\gamma_{lv}(1+\cos\Theta) = 2(\gamma_{sv}^{d}\gamma_{lv}^{d})^{1/2} + 2(\gamma_{sv}^{p}\gamma_{lv}^{p})^{1/2} \tag{3.15}$$

The surface tension γ_{sv}. of the solid surface and its components. and γ^{d}_{sv} and γ^{d}_{sv} can be determined according to Equation (3.15) by using two different liquids with known dispersive γ^{d}_{lv} and polar components γ^{p}_{lv} of their surface tensions.

Wu [Wus82] suggested another empirical approximation in which the "harmonic-mean" instead of a geometric mean approach was used for the interfacial tension. Substitution in the Young's equation leads to:

$$\gamma_{lv}(1+\cos\Theta) = 4\left(\frac{\gamma_{lv}^{d}\gamma_{sv}^{d}}{\gamma_{lv}^{d}+\gamma_{sv}^{d}} + \frac{\gamma_{lv}^{p}\gamma_{sv}^{p}}{\gamma_{lv}^{p}+\gamma_{sv}^{p}}\right) \tag{3.16}$$

Similar to the geometric-mean approach, two relationships are obtained after substituting the contact angles of two wetting liquids into Equation (3.16), with γ^{d}_{sv} and γ^{p}_{sv} as unknown parameters. Solution of these equations results in the dispersive and polar contribution of the surface tension of the solid substrate. Although there is no theoretical background for the use of the harmonic-mean approach, Wu claimed that surface tensions of a number of polymers, obtained by the harmonic-mean method, are comparable to those obtained by the polymer melt method. Both Equations (3.15) and (3.16) have been used extensively to determine the wettability of polymer surfaces. An analogous approach was used by Van Oss and coworkers[Goo92, Oss88]. According to them, the surface tension of a solid can be divided into two parts:

$$\gamma = \gamma^{LW} + \gamma^{AB} \tag{3.17}$$

where γ^{LW}. denotes the non-covalent long range Lifshitz-Van der Waals interactions and γ^{AB} the short-range Lewis acid-base interactions. The long-range interactions are a summation of:

$$\gamma^{LW} = \gamma^{d} + \gamma^{i} + \gamma^{p} \tag{3.18}$$

Moreover, the short-range interactions can be expressed as a function of the geometric mean of the electron-acceptor γ^{+} and the electron-donor γ^{-} parts:

$$\gamma_{sv}^{AB} = 2\sqrt{(\gamma_{sv}^{+}\gamma_{sv}^{-})} \tag{3.19}$$

Taking the geometric mean of the Lifshitz-Van der Waals component and the electron acceptor and the electron donor part and combining this with Young's equations, the following equation can be obtained:

$$\gamma_{lv}(1+\cos\Theta) = 2\sqrt{\gamma_{lv}^{LW}\gamma_{sv}^{LW})} + 2\sqrt{(\gamma_{lv}^{+}\gamma_{sv}^{-})} + 2\sqrt{(\gamma_{lv}^{-}\gamma_{sv}^{+})} \tag{3.20}$$

To determine the three parameters for the solid surface (γ_{sv}^{LW}, γ_{sv}^{+} γ_{sv}^{-}), three independent equations are obtained by measuring the contact angles of three liquids (two of which must be polar) with known values of γ_{sv}^{LW}, γ_{sv}^{+} and γ_{sv} on the solid surface.

3.4.2. Equation of State Approach

On phenomenological grounds, Neumann *et al* [Kwo99] have proposed an equation of state approach for solid-liquid interfacial tensions interaction:

$$\gamma_{sl} = \gamma_{lv} + \gamma_{sv} - 2\sqrt{\gamma_{lv}\gamma_{sv}}e^{-\beta(\gamma_{lv}-\gamma_{sv})^2} \tag{3.21}$$

where β is a constant which was found to be 0.0001247 $(m^2/mJ)^2$. The combination of this equation with Young's relation results in an equation of state approach, where the relation between $\cos\Theta$ and γ_{lv} is given by:

$$1+\cos\Theta = 2\sqrt{\frac{\gamma_{sv}}{\gamma_{lv}}}e^{-\beta(\gamma_{lv}-\gamma_{sv})^2} \tag{3.22}$$

When the liquid surface tension γ_{lv} is known and the contact angle Θ is measured, γ_{sv} can easily be calculated.

Although there are still some controversies between both methods, the surface tension components approach and the equation of state of approach are both used in literature. In our case the Lifshitz-Van der Waals/Acid-Base method is used to determine the surface tensions of solids.

3.4.3. Contact Angles on Heterogeneous Surfaces.

Wenzel proposed an approach to characterize the influence of the surface roughness on the wettability of a solid [Wen49]. The contact angle Θ^* on a rough surface can be evaluated by considering a little displacement dx of the contact line parallel to the surface (Figure 3.8).

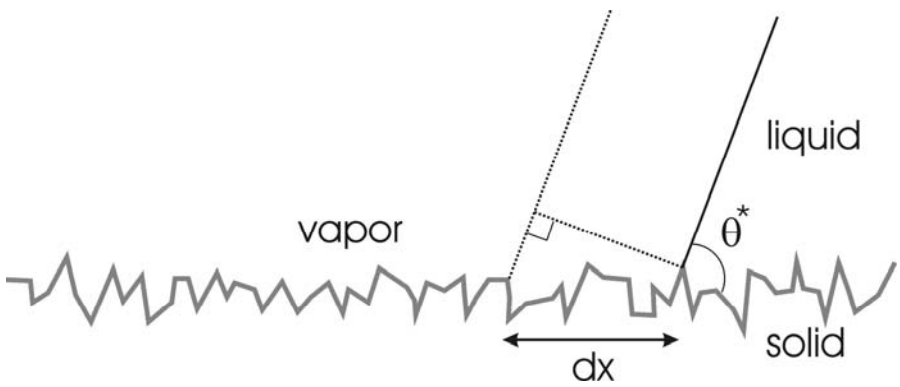

Figure 3.8. Infinitesimal spreading of a liquid wedge on a rough surface.

Then, the surface energies (written per unit length of the contact line) are modified of a quantity dF given by:

$$dF = r(\gamma_{sl} - \gamma_{sv})dx + \gamma dx \cos\Theta^* \tag{3.23}$$

where r is surface roughness, defined as the ratio between the real surface and the projected one. The equilibrium is given by the minimum of F, from which we get the *Wenzel's equation*

$$\cos \Theta^* = r \cos \Theta \tag{3.24}$$

This simple model shows that the effect of surface roughness is to amplify the wetting. Since we always have $r > 1$, the wetting gets better in hydrophilic situations ($\Theta^* < \Theta$ for $\Theta < \pi/2$) and worse in hydrophobic ones ($\Theta^* > \Theta$ for $\Theta > \pi/2$).

For $\Theta > \pi/2$, the surface energy of the dry solid is lower than the surface energy of the wet solid ($\gamma_{sv} < \gamma_{lv}$) and thus it is expected that the contact line does not follow the accidents of the solid surface, as supposed for establishing Equation (3.24). In this case, the drop is rather laid on a composite surface, patchwork of solid and air, as shown directly by Barthlott and Neinhuis [Bar97] who took photomicrographs of drops on a hydrophobic leaf. We can evaluate how the existence of these air pockets modifies the contact angle. The simplest way to treat this problem is to consider a crenellated surface (or equivalently full of holes), as in Figure 3.9a.

Then, displacing the contact line of a quantity dx parallel to the surface implies a change in surface energy dF equal to:

$$dF = \varphi_s(\gamma_{sl} - \gamma_{sv})dx + (1 - \varphi_s)\gamma dx + \gamma dx \cos\Theta^* \tag{3.25}$$

where φ_s is the solid fraction of the surface. The thin lines in Figure 3.9a are the liquid/vapor interfaces (occupying a surface fraction 1 - φ_s) below the liquid drop. Since the drop is much larger than the air pockets and because of the condition of a constant Laplace pressure inside the drop, these interfaces can be drawn with a straight line. Furthermore, all these interfaces

are pinned on the corners of the crenellations, the condition of pinning of a contact line on such corners being precisely a contact angle larger than $\pi/2$ [Oli77].

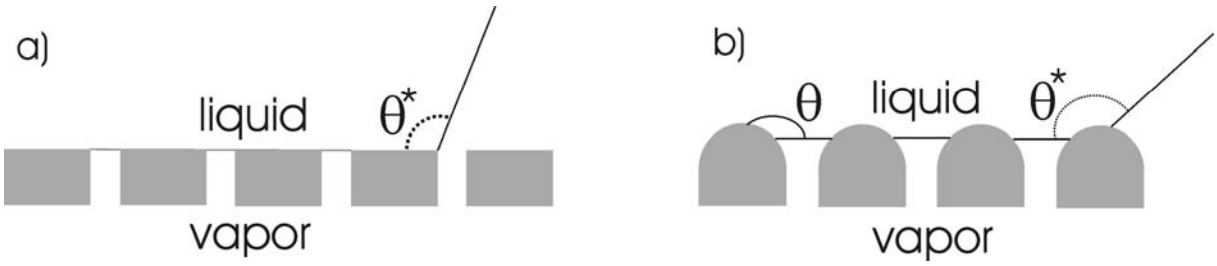

Figure 3.9. Liquid deposited on a model surface with holes (a) crenellated surface; (b) hemispherical bumps: for contact angles larger than $\pi/2$, air is trapped below the liquid, inducing a composite interface between the solid and the drop.

At equilibrium, F is minimum and we get (using Young's equation):

$$\cos \Theta^* = -1 + \phi_s(\cos \Theta + 1) \tag{3.26}$$

Equation (3.26) is a particular form of the Cassie-Baxter equation which gives the contact angle for a drop deposited on a composite surface: the cosine of this angle is the average of the cosines of the different contact angles, weighed by the respective surface fractions of the heterogeneities [Cas44]. It is plotted in full line in Figure 3.10 for $\Theta > \pi/2$, while keeping the Wenzel equation on the hydrophilic side ($\Theta < \pi/2$).

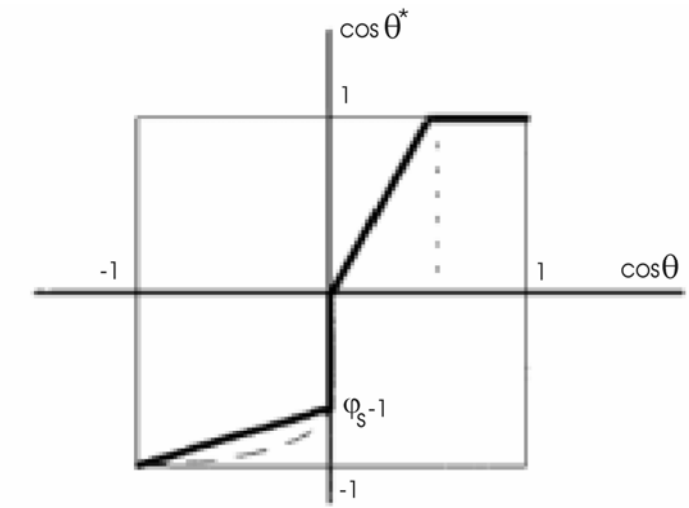

Figure 3.10. Cosine of the effective contact angle Θ^* of a drop on a rough model surface as a function of cosine of the Young contact angle Θ. r is the surface roughness and φ_s is the surface solid fraction. On the hydrophobic side ($\cos\Theta < 0$), the solid line is Equation (3.26) and the dot line is Equation (3.27).

Of course, taking crenellations for modeling the surface is an approximation. On a given rough surface, the fraction φ_s itself is a function of the contact angle Θ. Let us suppose for example that the solid fraction is not flat but ends with hemispherical bumps (Figure 3.9b). Then, the liquid/vapor interfaces (still in thin line) are located where the Young

condition is fulfilled: the surface of solid in contact with the liquid is all the larger since the contact angle is low.

Finally, we can calculate the way φ_s depends on Θ and the effective contact angle Θ^* of a drop, via Equation (3.26). Elementary trigonometry gives

$$\cos \Theta^* = -1 + \varphi_b (\cos\Theta + 1)^2 \qquad (3.27)$$

where φ_b is the ratio of the surfaces of the spike bases over the total solid surface. Equation (3.27) is the parabolic dotted line in Figure 3.10 and turns out to have the same qualitative features as Equation (3.26). In both cases, the contact angle has a discontinuity when q becomes smaller than $\pi/2$, a major difference with Wenzel's equation. As soon as the contact angle is above this value, air is trapped below the drop, which basically modifies the wetting. The limit of a surface which would be one single hole ($\varphi_s = \varphi_b = 0$) is of course $\Theta = \pi$. a static drop in the air is spherical. Another difference with Wenzel's law is the fact that an π-angle is only asymptotic, which is physically reasonable.

3.4.4. Contact Angle Measurement Techniques.

Advancing contact angles were obtained by means of the Contact Angle Measuring Systems ADSA-P (Axisymmetric Drop Shape Analysis Profile) and ADSA-CD (Contact Diameter) [institute-made] (Figure 3.11) and the sessile drop method, using a Krüss set-up (Figure 3.11)

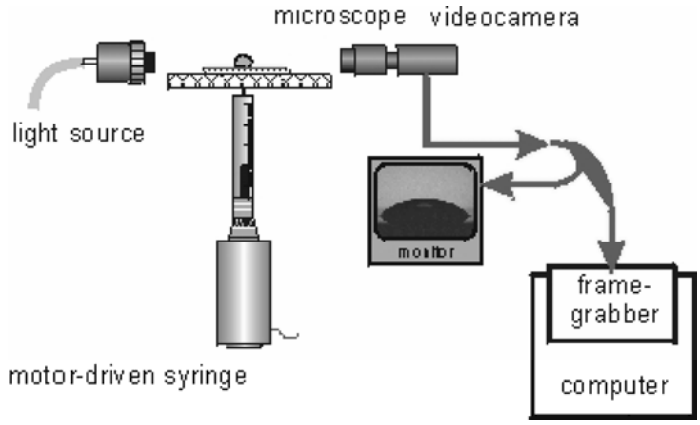

Figure 3.11 Set-up of ADSA technique.

During the measurements of the advancing contact angle the needle remains inside of the drop. The droplet is monitored by a CCD-camera and analyzed by Drop Shape Analysis software (DSA Version 1.0, Krüss). The complete profile of the sessile droplet is to be fitted by the tangent method to a general conic section equation. The derivative of this equation at the baseline gives the slope at the three-phase contact point and thus the contact angle. In this

way angles are determined both at the right and the left side. Reproducibility is within 0.5°, depends on the range.

3.5. X-Ray Photoelectron Spectroscopy (XPS)

X-ray photoelectron spectroscopy (XPS) is one of the most popular spectroscopic techniques available for surface analysis of polymers, including surface modification, polymer chain mobility, degradation, chemical reactions, and biocompatibility [Bri77, Bri82].

X-ray photoelectron spectroscopy, also known as electron spectroscopy for chemical analysis (ESCA), is probably the most widely used technique to study the chemical composition of polymer surfaces. The technique is based on the photoelectrical effect, which provides information on elemental and functional group composition, and oxidation state. In an XPS experiment the surface is irradiated with X-rays. The energy of the incident X-ray photons is that high that electrons can be ejected from electron shells. These ejected electrons are referred to as photoelectrons. A schematic representation of the XPS process is given in Figure 3.12.

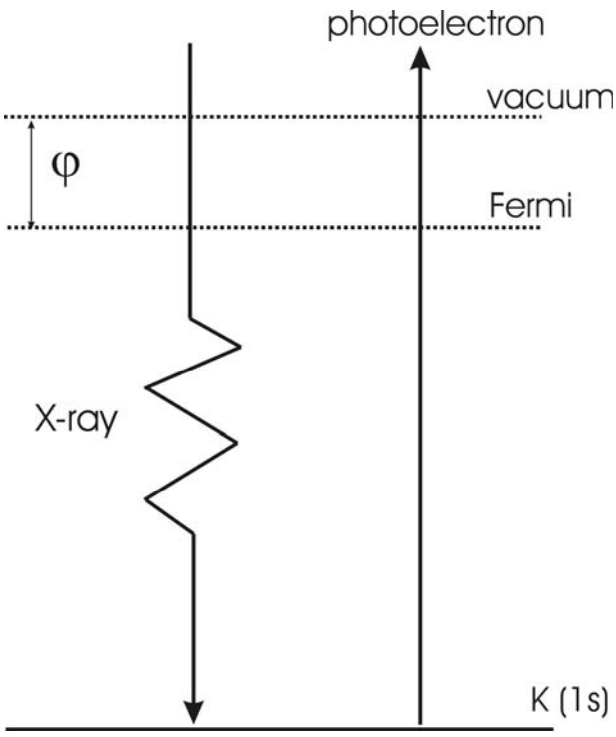

Figure 3.12 Schematic depiction of the XPS process.

From the difference between the known energy of the X-ray photons and the measured kinetic energy of the photoelectrons, the binding energy can be calculated according to: [Nie95] $E_b = h\nu - E_k - \varphi$, where E_b denotes the binding energy of the photoelectrons in the excited electron shell, E_k the kinetic energy of the photoelectrons, h Planck's constant, ν the frequency of the X-ray, and φ the work function of the spectrometer. Elements can be

recognized by their binding energy, which depends slightly on the oxidation state and chemical environment. Some experimental problems can occur in XPS. First, insulating samples (polymers) may become positively charged during the measurement, because photoelectrons leave the sample. Due to the positive charge on the samples, all XPS peaks in the spectrum shift by the same amount to apparently higher binding energies. Calibration is therefore necessary and, in the case of organic polymers, the $-CH_2-$ peak at 284.5 eV is often used. Secondly, organic polymers are damaged during XPS by the impact of photoelectrons and secondary electrons generated from them [Gra93, Bea98]. This gives rise to the generation of free radicals, which react to give various products like crosslinked structures. In order to minimize this polymer degradation, the acquisition time must be limited [Bri98]. The surface sensitivity of XPS is not related to the penetration depth of the incident X-rays, which is many micrometers, but to the probability of the generated photoelectrons being able to leave the surface. Generally, it is accepted that 95% of the signal of the photoelectron originates from 3 times inelastic mean free path λ [Tan94] If an electron is emitted from a deeper layer, it will almost certainly lose its information due to energy loss due to collisions within the solid material and will only contribute to the XPS background. Therefore, the sampling depth d (from which 95% of the emitted electrons originates) in XPS is usually defined as [Bri98].: $d = 3\lambda\cos\theta$, *where* θ represents the angle between the surface normal and the electron detector. This means that measurements can be made more sensitive to the outer surface region by increasing θ, and thus decreasing the actual probing depth (angle dependent XPS, see Figure 3.13). In this way depth profiles of chemical composition are obtained in a non-destructive way.

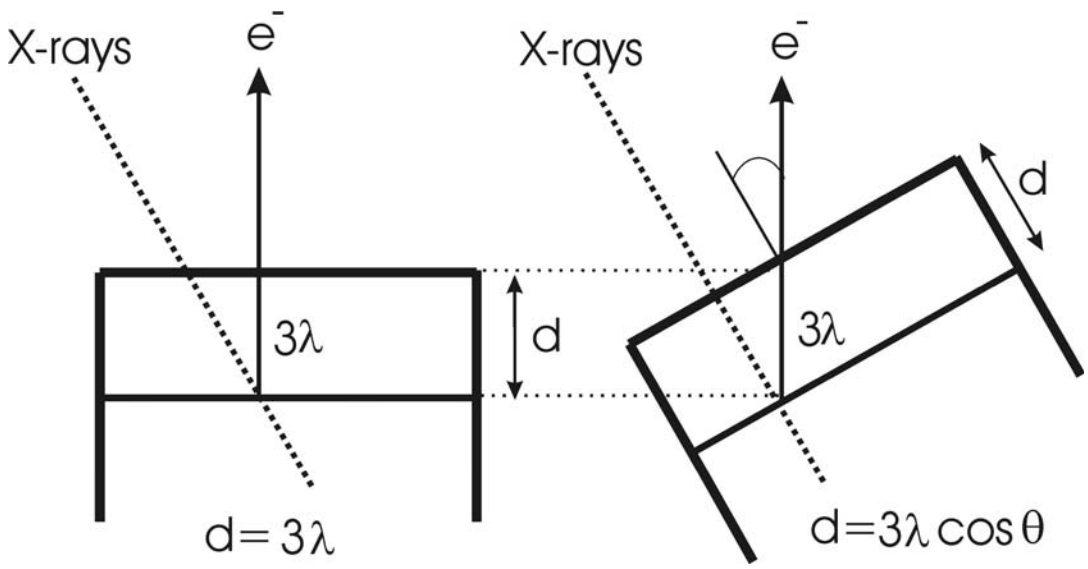

Figure 3.13 Schematic representation of an angle-dependent XPS.

Quantitative surface analyses by XPS have been reviewed extensively by many authors [Bri77]. Usually, a uniform distribution of atoms is assumed with depth. The quantification of the surface composition for XPS can be obtained from the peak areas after correction for the background. Several methods are available for background correction. The most widely used are a linear background subtraction, the Shirley method, and the Tougaard method [Pow90]. The simple linear approach has been recommended for the analysis of polymers over the Shirley method. The Tougaard method is not a proven method for polymers and hence has not been applied. After correction of the background, the atomic concentration *Ci* of an element *i* can be calculated from: $C_i = \frac{A_i / S_i}{\sum_j^m A_j / S_j}$,where *m* is the number of elements in the sample, and *Ai* and *Si* are the peak area and the relative sensitivity factor for element *i*, respectively. These relative sensitivity factors parameters are defined as the ratio of the XPS intensity divided by the number of atoms of the element per unit volume, taking one elemental peak as standard. It is important to note that relative sensitivity factors have to be determined by calibration as they depend on the spectrometer used. Another important point is that the sampling depth, defined as the layer thickness that contributes to the XPS signal, varies from element to element.

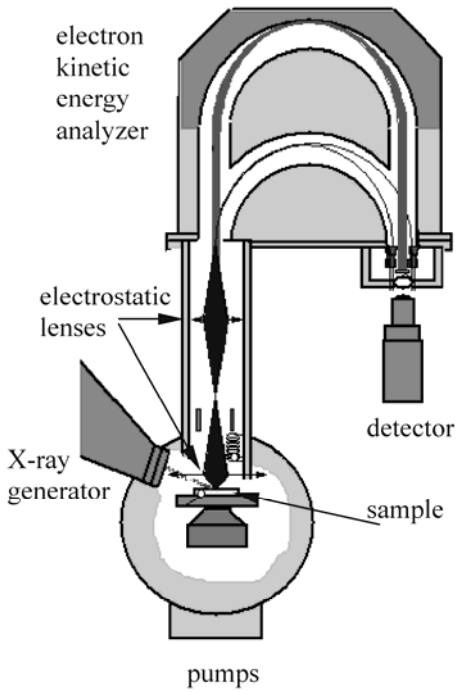

Figure 3.14 Schematic representation of XPS experimental set-up (AXIS ULTRA)

A direct comparison of atomic concentrations as 'determined by XPS' is therefore not possible when dealing with non-homogeneous samples. Therefore, when dealing with organic polymers the best procedure to evaluate the surface composition from XPS data is by curve

fitting the C1s region. In this case the emitted photoelectrons originate from the same sampling depth. [Zhu96].

XPS instrument, schematically presented in Figure 3.14, consists of an X-ray source, an energy analyser for the photoelectrons, and an electron detector.

The analysis and detection of photoelectrons requires the sample to be placed in an Ultra High Vacuum (UHV) chamber. UHV conditions are generally regarded as being in the region below 10^{-7} Pa. The number of gas in a UHV chamber is 1/1,000,000,000,000 that of air per unit volume. UHV is needed to prevent the interaction between photoelectrons and gas molecules. Due to the interaction, the photoelectrons will loose part of their kinetic energy.

The energy of the photoelectrons leaving the sample is determined using a Concentric Hemispherical Analyzer (CHA). The counted photoelectrons, which passed the analyser via the slit plate, are collected by a set of canneltrons. The number of the counted photoelectrons per time (count rate) in dependence on their kinetic or binding energy gives a spectrum with a series of photoelectron and Auger peaks. The peak areas can be used to determine the composition of the material surface. The shape of each peak and the binding energy can be slightly altered by the chemical state of the emitting atoms. Hence, XPS can provide chemical bonding information as well.

3.6. Infrared Spectroscopy.

The spectral range for infrared (IR) spectra used by most chemists is approximately 4000 – 400 cm^{-1}. This range is now called the mid-IR and, because it contains the fundamental vibrational modes, is most useful for qualitative purposes. Also, it is used for quantitative analysis. For some years now, mid-IR spectrometers are based on an interferometer that produces an interferogram of the sample from which the absorbance spectra can be calculated. These spectrometers are known as Fourier Transform Infrared (FTIR) spectrometers. The FTIR approach has a number of advantages in terms of speed, accuracy, reproducibility and sensitivity. Attenuated Total Reflection (ATR) spectroscopy, whose surface analytical potential was initially explored by Harrick [Har67] and further developed by Fringeli [[Fri81] to address biological membrane and liquid crystalline systems quantitatively and *in-situ*, is a powerful analytical tool for the molecular detection of processes at the solid/liquid or solid/air interface.

A scheme of the ATR-IR principle is given in Figure 3.14. If IR light insides from the optical denser medium (e.g. Si) under a certain angle θ, which exceeds the angle of total reflectance, an evanescent wave penetrating in and interacting with the less dense medium, which is material deposited on the internal reflection element (IRE), is established.

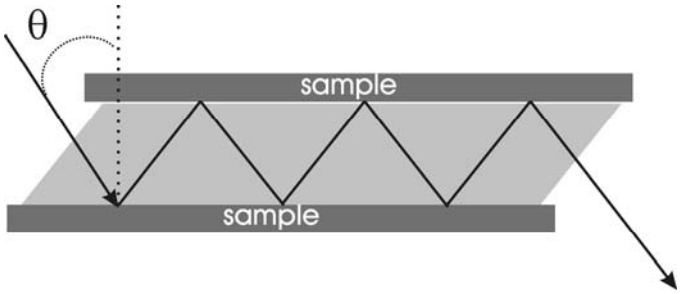

Figure 3.14. The scheme of an ATR IR experiment

Generally, ATR-FTIR spectroscopy enables *in-situ* detection of surface sorbed species of different molecular sizes (gases, water, ions, surfactants, drugs, reactive polymers, polyelectrolytes, lattices, proteins, cells), whereby the sorbates can be *molecularly* identified by their diagnostic IR bands. Conveniently, trapezoidal IREs are used, which are incorporated in *in-situ* cells dividing the ATR plate in an O-ring sealed upper (sample) and lower half (reference), which are alternately and repeatedly shuttled in a fixed IR beam (Single Beam Sample Reference-(SBSR)-concept). Thereby, the reproducibility of the ATR technique, the spectral compensation of the strong water absorptions and the spectral baseline could be significantly improved.

The FTIR techniques and calculation approaches will be described in the experimental part of this thesis (Chapters 4-6).

Chapter 4

Mixed Polymer Brushes on Polyamide Substrates

4.0 Abstract.

This chapter focuses on the development of the route to fabricate the mixed brush-like layers on polyamide substrates (PA-6, PA-6I, PA-66) by "grafting from" and "grafting to" approaches. PA substrates were functionalized by NH_3-plasma and the azo-initiator of radical polymerization was covalently bond to the functionalized PA surface. Two-step grafting procedure was applied to graft polystyrene in the first step and poly(2-vinylpyridine) in the second step. We found remarkable differences between grafting on Si-wafers and PA-substrates. Grafting from the PA surface results in a dramatic increase of the surface roughness of the film which can be explained by grafting in a swollen surface layer of PA. Due to this effect we found the substantial amount of grafted polymers even on not functionalized PA substrates, which was explained by grafting via chain transfer reaction. The mixed polymer brushes (two different incompatible homopolymers randomly grafted to Si-wafer by end groups) were shown to form responsive coatings, which switch their morphology due to the interplay between lateral and vertical phase segregation upon exposure to selective solvent. The switching of morphology affects the change of the surface composition of the brushes and their surface energetic state. The same grafting procedures were performed on the surface of PA fabric. In this case the switching behavior was amplified by a texture of the material: Wettability of the fabric with the mixed brush was switched from complete wetting to highly hydrophobic state (150° water contact angle)

4.1. Introduction

Grafting of polymers is a widely used method for the modification of solid surfaces. A number of grafting points per polymer chain can be different and affects properties of the grafted chains [Gon98]. A thin film with polymer chains grafted to the solid substrate by only one end is a very suitable subject for theoretical analysis and experimental study, because its behavior can be easily modeled and interpreted [Sze96]. If the distance between grafted chains is smaller than an average end-to-end distance of the polymer chain, the layer of the

grafted chains is in the regime of the polymer brush. In this regime, grafted chains are forced to stretch in the direction normal to the plane of grafting and the conformation is determined by the energy balance between the elastic free energy of the stretched chain and the energy of the interaction between statistical segments [Ale91]. Such an arrangement offers many interesting applications of the brush-like layers [Hal92] that have stimulated great interest in synthesis and investigation of polymer brushes [Tha00]. The questions of the regulation of thin polymer film stability [Zer94], wettability [Man97], adhesion [Rap92, Rut00], reactivity and cell protein interaction [Aks96, Phe98], micro/nanopatterning [Niu98, Hus00], swelling [Hab99], friction [Kle94, Berm98], stabilization of colloids [Pin91], core-shell structures [Guo99], and so forth were addressed with respect to the employment of polymer brushes.

Polyamides as semicrystalline thermoplastics have found numerous applications, particular for the fabrication of excellent fibers due to their good thermal stability, flexibility, and mechanical properties. Surface modification of PA is a widely used approach to regulate properties of fiber-reinforced materials, textiles, etc. [Pol96]. Responsive properties of PA surface would extend the application of PA, particularly for bio-medical materials.

The aim of this study is to fabricate PA-based materials, which change surface characteristics in response to environmental conditions. One of the possible routes to approach this goal comprises the grafting of mixed polymer brushes from PA surface, which can introduce adaptive and switching behavior in different surrounding media.

This chapter describes the synthesis of the mixed polymer brushes of two different polymers by both *"grafting from"* and *"grafting to"* (Scheme 4.1) to the PA substrate. The PA surfaces were treated with a low-pressure ammonia plasma, which introduces N-containing functionalities such as amino ($-NH_2$), imino (-CH=NH), cyano (-C≡N), and other functional groups and in addition oxygen-containing groups such as amido ($-CONH_2$) and hydroxyl groups due to the post discharge atmospheric oxidation. We used those functional groups for further surface modification via grafting of mixed polymer brushes. Each step of the surface modification was controlled with ellipsometry, X-ray photoelectron spectroscopy (XPS), atomic force microscopy (AFM), Fourier-transform infrared spectroscopy in attenuated total reflection (FTIR-ATR), and contact angle measurements.

In this chapter a biotest of binary polymer brushes on PA textiles will be presented as well.

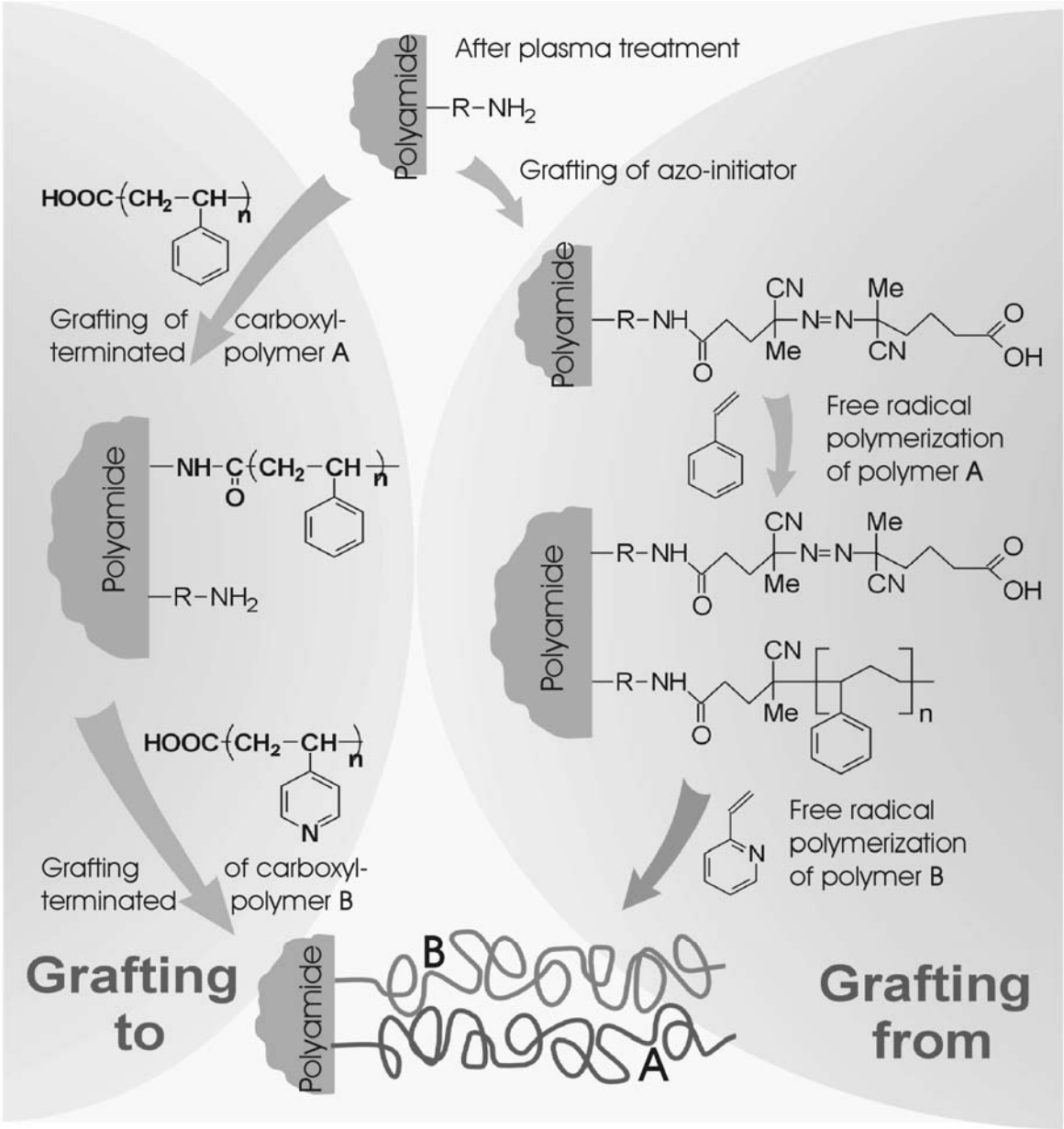

Scheme4.1 Schematic representation of grafting of PS/PVP binary polymer brushes to PA surfaces.

4.2. Materials

PA-6 (Durethan® B) and PA-6I (Durethan® T) were obtained from Bayer AG. Samples of textile made from PA-6 and PA- 6.6 were supplied by Bekleidungphysiologisches Institut Hohenstein (Germany).

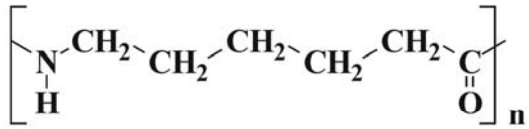

PA-6 Durethan® B

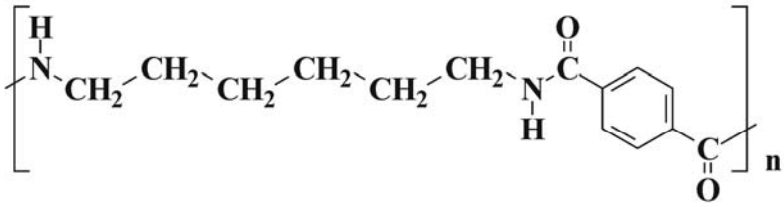

PA-6I Durethan® T

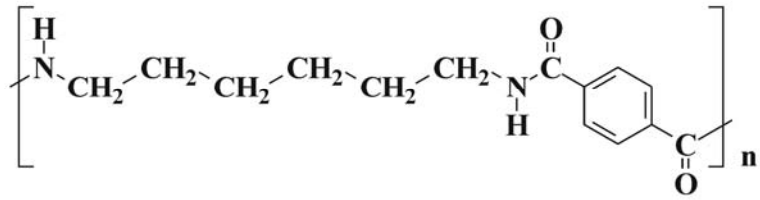

PA-6.6

Styrene and 2-Vinylpyridine (Aldrich) were distilled under reduced pressure of argon. Toluene, tetrahydrofurane (THF) and hexane (Aldrich) were dried over sodium and distilled. Methanol, ethanol and p-chlorophenol (Aldrich) were used as received. Dichloromethane (Aldrich) was dried on molecular sieves.

Initiators: 4,4'-azobis(4-cyanopentanoic acid) (ACP) from Aldrich and 4,4'-azobis(isobutyronitrile) (AIBN) from Fluka were purified by recrystallization from methanol. All reagents were used immediately after purification.

Carboxyl-terminated polystyrene P115-SCOOH (M_n=9700 g/mol, M_w=10476 g/mol), P2824-SCOOH (M_n=48000 g/mol, M_w=50400 g/mol), and poly(2-vinyl pyridine) (PVP-COOH; M_n = 39200 g/mol and M_w = 41500 g/mol) were purchased from Polymer Source, Inc (synthesized by anionic polymerization).

Silicon wafers obtained from Wacker Chemitronics (Germany) were cleaned with dichloromethane in an ultrasonic bath and then in a hot ammonia: hydrogen peroxide: water (1: 1: 1) by volume solution and rinsed several times in Millipore water.

We used different PA substrates to study each step of surface modification with ellipsometry, XPS, AFM and FTIR-ATR. Such experimental scheme was caused by different requirements for samples investigated by each method. We used PA samples of different cristalinity to study the effect of the substrate morphology on the grafting procedure. PA6 is partially crystalline material, while PA 6I is an amorphous polymer soluble in p-chlorophenol. PA 6I forms (by spin coating) smooth homogeneous films of the amorphous polymer on Si-wafers appropriate for ellipsometric experiments. PA6 is widely used for fiber productions

and we employ this substrate as a model sample representing large range of PA materials. Finally, we use different PA substrates to demonstrate that the key role for the grafting mechanism from the polymer surface is played by swollen polymer layer rather then by differences in chemical structure of different PA samples.

4.3. Surface Modification of PA Substrates.

A thin layer of PA-6I was spin coated from 1.5% p-chlorophenol solution onto the surface of cleaned silica wafers. The thickness of these PA films estimated with ellipsometry was in the range of 30 ± 5 nm. The plasma treatment was done in a computer controlled customized MICROSYS apparatus (Roth&Rau, Germany) supplied with a 2.46 GHz-electron cyclotron resonance plasma source. The distance between the sample and the excitation volume of the plasma source is about 200 mm. For the plasma treatment the following parameters were applied: NH_3 gas flow 15 sccm, pressure 3.8 $\times 10^{-3}$ mbar, effective microwave power 600 W. The time of the treatment was in the range from 10 to 180 sec.

In order to determine the amount of $–NH_2$ groups introduced by NH_3 plasma treatment we labeled amino-groups of the untreated, and 30, 60, 90, 120, 150 and 180 sec. treated samples via exposure to the vapor of 4-trifluoromethylbenzaldehyde (TFBA) for three hours as proposed by Favia et al. [Fav96]. Afterwards the samples were rinsed with ethanol and analyzed by XPS. The F_{1s} signal in the XPS spectrum is attributed to the presence of $–NH_2$ groups.

4.4. Preparation of the Binary Brushes via G*rafting From* Approach

4.4.1. Attachment of azo-initiator.

For the introduction of the azo-initiator onto PA surfaces treated with NH_3 plasma we used the reaction of surface amino-groups with the chloroanhydride derivative of azo-initiator [Bov90]. The chloroanhydride derivative of 4,4'-azobis-(4-cyanopentanic acid) was prepared by adding of the slurry of phosphorus pentachloride to a suspension of ACP in dichloromethane at 0^oC. The product (ACPC) after crystallization from hexane-dichloromethane mixture at 0^oC was washed and dried in vacuum. In the next step, ACPC was introduced on the surface of the NH_3 plasma treated PA substrate from 5% solution in dichloromethane with catalytic amount of triethylamine at room temperature for 4 hours. The resulting samples of PA on Si-wafers, PA plates and PA textile with chemically attached initiating groups were rinsed in ethanol in an ultrasonic bath. Each step of the surface

modification of PA on Si-wafers was controlled by ellipsometric measurements of the layer thickness.

4.4.2 Grafting Procedure.

Oxygen was removed from the solution of monomer (styrene or 2-vinylpyridine, 5 mol/l) and AIBN ($5 \div 9 \times 10^{-4}$ mol/l) in THF (AIBN was used as an additional initiator in the volume to control molecular weight of grafted chains [Min99a, Min99b, Sid99b]) using five freeze-pump-thaw cycles. The PA samples (also PA-6I on Si-wafers) with the chemically attached initiator were placed in monomer solution under argon atmosphere in the glass reactor. The reactor was immersed in a water bath (60 ± 0.1^{o}C) for different periods of time (6 - 24 h). The non-grafted polymer from the bulk was obtained and purified by precipitation in hexane. The PA surface modified samples were rinsed six times in THF.

In the next step, the same procedure was applied to graft the second polymer using the PA samples with the grafted first polymer. Afterward, the ungrafted polymers were removed by a Soxhlet extraction with THF for 4h (controlled by analysis of the film thickness). We assumed that the molecular weight of the grafted and non-grafted polymers was of the same order [Bov90, Min99a, Min99b, Sid99a]. Molecular weight of the non-grafted polymer was determined using gel permeation chromatography (GPC). In this paper we refer to number average values of molecular weight (M_n).

4.5. Preparation of the Binary Brushes via *Grafting To* Approach

In our route of synthesis we explore the method of grafting of end-terminated polymer from the melt recently proposed by I. Luzinov at. al. For grafting of PS and PVP onto PA substrates we used the reaction of carboxyl groups of the polymers and amino groups on the top of PA surfaces after ammonia plasma treatment. A thin film (50±5 nm as measured with ellipsometry) of PS-COOH was spin-coated on the top of the PA substrates after ammonia plasma from the 1% toluene solution. PA textiles were simply dipped in the PS solution for 5 min and dried with nitrogen flux. Then the film was heated at 170° C in vacuum oven for different periods of time to graft PS-COOH and to measure the kinetics of grafting. The non-grafted polymer was removed by Soxhlet extraction with toluene for 5-7 h. Then the second polymer PVP-COOH was spin-coated on top of the film, meanwhile, PA textiles were dipped in PVP solution for 5 min and dried. The heating procedure followed by subsequent Soxhlet extraction to remove any ungrafted polymer was performed.

4.6. Sample Characterization.

4.6.1 Ellipsometry

Layer thickness and the amount of the grafted substances are evaluated with Multiscope Optrel null-ellipsometer (Berlin, Germany) at an incidence angle of 70°. The measurements were performed for each sample after each step of the modification to use the measurement of the previous step as a reference for the simulation of ellipsometric data. Initially, the thickness of native SiO_2 layer (usually 1.4 ± 0.2 nm) was evaluated at the value of refractive index n = 3.858 – *i* 0.018 for Si and 1.4598 for SiO_2, respectively. Then the thickness of the PA-6I layer was evaluated using the two layer model: SiO_2/PA-6I for refractive index of PA-6I equal to 1.628. The thickness of grafted azo-initiator was evaluated with the three-layer model SiO_2/PA-6I/azo-initiator with n=1.551 for the layer of the azo-initiator. Finally, the thickness of the polymer film after grafting of each polymer was calculated using the tree layer model SiO_2/PA-6I/grafted polymer considering the thin polymer film as an effective optical medium with n=1.59. In reference experiments we found no influence of the surface roughness on the ellipsometric results for the prepared grafted films.

4.6.2 FTIR-ATR

FTIR-ATR spectra were taken with an IFS 66 (Bruker) spectrometer and variable angle ATR unit (HARRICK). We used three different internal reflection elements of a parallelogram geometry with different crystal end-face angles (θ_B) prepared from different crystals: Zn/Se θ_B = 45 ^{o}, and two different Ge crystals with θ_B equal to 45 and 60° to approach different penetration depths of IR irradiation into the sample of PA with grafted PS/PVP layers.

The internal angle of incident of IR-radiation can be calculated using equation (4.1):

$$\Theta = \theta_B - \frac{(\theta_B - \theta_R)}{n} \tag{4.1}$$

where θ_R is the angle of incidence of IR beam on the crystal (dial settings), *n* is refractive index equal to 2.4 and 4.0 for Zn/Se and Ge crystals, respectively. The penetration depth of IR-radiation d_p into the PA-samples at different incident angles can be calculated using equation (4.2)

$$d_p = \frac{\lambda_1}{2\pi(\sin^2\Theta - n_{21}{}^2)^{1/2}} \tag{4.2}$$

where $\lambda_1 = \lambda/n_1$, λ is the wavelength, $n_{21}=n_2/n_1$, n_2 and n_1 are the refractive indexes of PA and the material of ATR crystal, respectively, d_p is the depth, at which the electric field amplitude of the IR-radiation E_0 decays to a value $E=E_0\ exp(-1)$. Therefore E is not zero at d_p. The calculated depths of the penetration d_p at different incident angles and for different crystals are presented in Table 4.1. The range for penetration depth was from 0.35 to 2.33 μm.

Table4.1 Penetration Depth (d_p) of IR Radiation (at 1500 cm^{-1}) into PA Samples at Different Incident Angles and Different ATR Crystals

Crystal material	Θ_B, deg	Θ_R, deg	d_p, μm
Zn/Se	45	35	2.33
		45	1.33
		55	1.01
		65	0.88
Ge	45	25	0.51
		35	0.47
		45	0.44
		55	0.42
		65	0.40
Ge	60	60	0.34

4.6.3 XPS

XPS experiments were performed using an AXIS ULTRA spectrometer (Kratos Analytical, England) equipped with a monochromatized Al Kα X-ray source of 300W at 20mA. The kinetic energy of photoelectrons was determined with a hemispherical analyzer with a constant pass energy of 160 eV for survey spectra and 20 eV for high-resolution spectra. To eliminate sample charging an electron flood gun in combination with a magnetic immersion lens in the extraction optic was used during all measurements. The charge over-compensation required that all recorded spectra were adjusted to the C 1s reference peak of saturated hydrocarbons ($\underline{C}_xH_y$) at BE = 285.00 eV. The elemental compositions were quantified from the peak areas using experimentally determined sensitivity factors and taking the spectrometer transmission function into account. The inelastic spectrum background was subtracted according to Shirley's procedure. Peak fitting was carried out to obtain information about the chemical nature of functional groups. The parameters used for fitting were the peak

area, the position of the peak maximum, the peak full width at half maximum, and the Gaussian-Lorentzian ratio.

4.6.4 AFM

AFM studies were performed on a Dimension 3100 (Digital Instruments, Inc., Santa Barbara) microscope. The tapping and phase contrast modes were used to map the film morphology at ambient conditions. Silicon tips with a radius 20 $\pm$ 5 nm, a spring constant of 1.5-6.3 N/m and frequency 63-100 KHz were used. Root mean square roughness (RMS) was calculated from the images with the commercial software.

4.6.5 Contact Angle Measurements

Advancing *contact angles* of water were measured using DSA Krüss (Hamburg, Germany) equipment. Samples with mixed brushes were exposed to particular solvent for 10 minutes, then rapidly dried with Ar flux and afterwards water contact angle was rapidly (within first 30 seconds) measured.

4.6.6 Biological Tests of PA Materials With Grafted Binary Polymer Brushes[*].

The polyamide substrates with grafted binary PS/PVP brushes was examined for vitality of cell cultures by the norm of ISO 10993-5 which was establishes on the basis of the cytotoxicity of implanting materials. For the tests were used fibrolasts (L929) and endothel cells (bovine aorta endothel). The samples were placed in 24 well cell culture plates in which the samples are occupied with 500.000 cells, and incubated for 48 h. The vitality of the cells was estimated by means of an MTS-test. Test results of the vitality test of both the Polyamides and Polyamides with grafted polymer brushes were compared with a control sample (TCPS-Tissue Culture Polystyrene) and each with other.

[*] The Biological Tests were performed in the Institute of Textile Technology and Process Engineering Denkendorf.

4.7. Results and Discussion.

4.7.1 Plasma Treatment.

The PA samples were treated with NH_3 plasma for different periods of time as described above. Wettability of samples, obtained from contact angle measurements, was used to evaluate the efficiency of the plasma treatment. The untreated PA-6 sample has the highest values of advancing (71°) and receding (34°) contact angles, indicating the most hydrophobic surface. NH_3 plasma treatment reduces the advancing contact angle to the values of 61°, 57°, 62°, 63°, and 67° for the treatment time of 30, 60, 90, 120 and 150 s, respectively, thus resulting in less hydrophobic surfaces. The polar *N* and *O* containing groups introduced onto the surface by plasma treatment improve wettability [Chan96]. We used for grafting experiments samples treated with plasma for 60 s.

The ratio between number of atoms of oxygen and carbon ([O] : [C]) and nitrogen and carbon ([N] : [C]) in PA-6 calculated from the chemical composition equals 0.167.

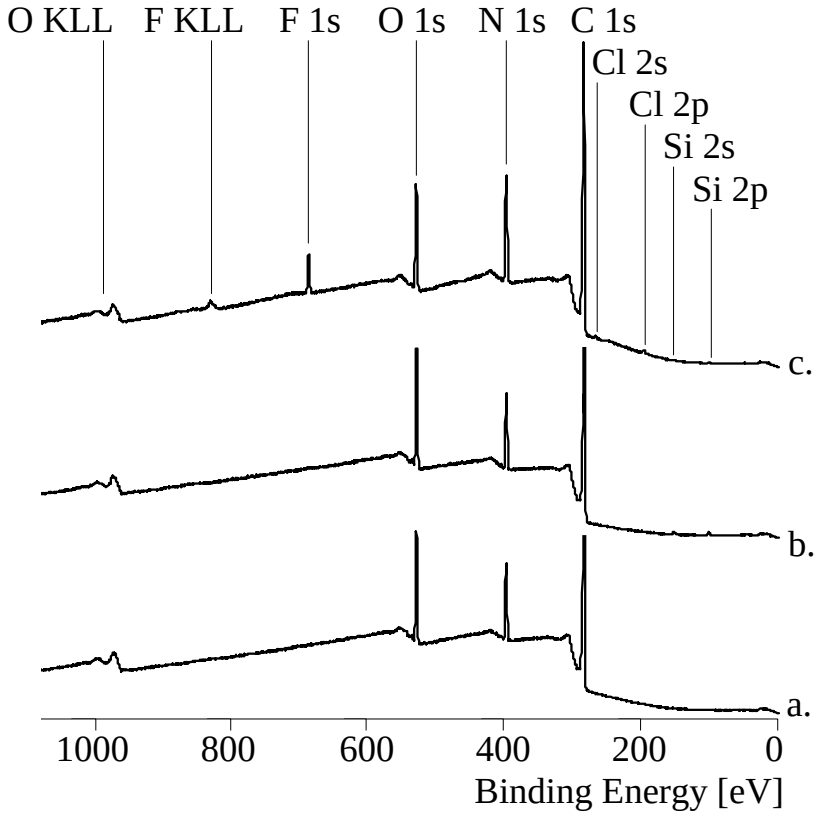

Figure 4.1. X-ray photoelectron spectra of PA-6I spin-coated on Si-substrate: the reference sample, no treatment, no label (a); the reference sample, no treatment, labeling with TBFA (b); NH_3 plasma treatment, labeling with TBFA (c).

The surface composition determined from the XPS spectra (Figure 4.1, 4.2) gives the ratios [O] : [C] = 0.15 and [N] : [C] = 0.14 which is in good agreement with the chemical composition of the substrate. The plasma treated samples of PA-6 show the increased ratios [N] : [C] = 0.19 which prove the introduction of the N- containing functionalities (Table 4.2). TBFA labels attached selectively to amino-groups indicate that more than 10% of N-containing functional groups are represented by amino groups. Similar results were obtained for the PA-6I samples.

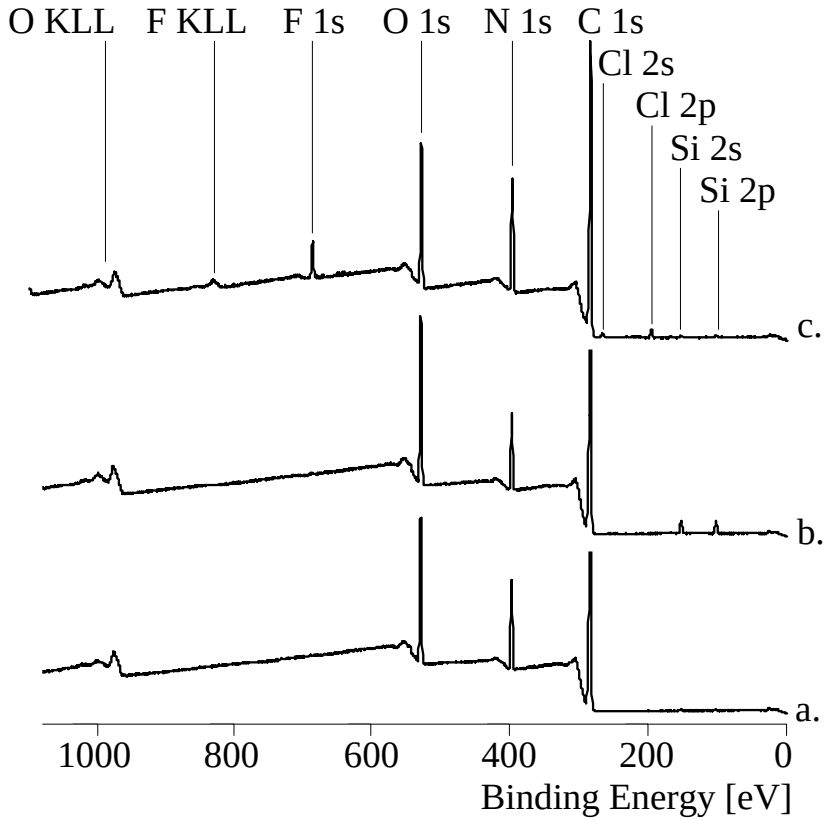

Figure 4.2. X-ray photoelectron spectra taken from the surface of PA-6 plates: the reference sample, no treatment, no label (a); the reference sample, no treatment, labeling with TBFA (b); NH_3 plasma treatment, labeling with TBFA (c).

The ammonia plasma treatment essentially enhances the roughness of the PA films as measured by AFM because of inhomogeneous etching (the RMS roughness increased from 2.5 to 9 nm), see Figure 4.3 (a and b). Therefore, using the plasma modification we obtained PA fictionalized substrates with well characterized structure and chemical composition.

Table 4.2. Quantitative surface composition of PA original samples, after NH_3 plasma treatment, and labeled with TBFA (F-labeling) determined employing XPS.

sample	atoms quantity of the surface, mass. concentration, %		
	[F]:[C]	**[O]:[C]**	**[N]:[C]**
PA-6, NH_3-plasma treatment, TFBA-labeling	0.033	0.16	0.19
PA-6, no treatment, TFBA-labeling	0.001	0.16	0.12
PA-6, no treatment, no labels		0.15	0.14
PA-6I on Si, NH_3-plasma treatment, TFBA-labeling	0.038	0.13	0.19
PA-6I on Si, no treatment, TFBA-labeling		0.12	0.13
PA-6I on Si, no treatment, no labels		0.11	0.13

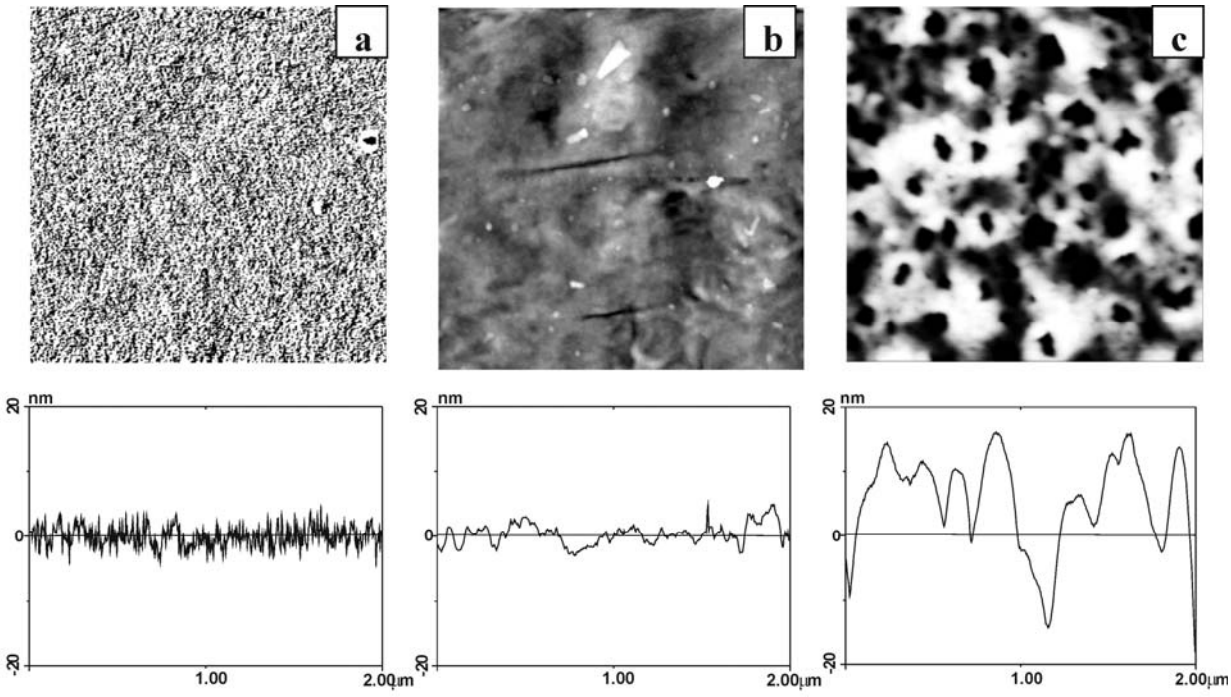

Figure 4.3. AFM topography images and corresponding cross sections of PA-6I on Si-wafers: original sample, RMS = 2.5 nm (a); after NH_3- plasma treatment, RMS = 9 nm (b), and after grafting of mixed brush (grafting from approach), RMS = 41 nm (c).

4.7.2 Synthesis of the Binary Brushes via *Grafting From* Approach

Grafting of azo-initiator. Our synthetic procedure (Scheme4.2) starts with the covalent grafting of the azo-initiator to the plasma modified PA surfaces. The azo-initiator was covalently bound to the surface via the reaction of the amino- and hydroxyl-groups with ACPC. This reaction is well reproducible. The resulting layer of the initiator is about 2.1 ± 0.3 nm thick as measured with ellipsometry on PA-6I surface. This value corresponds to 5.7 10^{-6} mol m^{-2} surface concentration of the initiator and to 0.5 nm average distances between grafted initiator molecules.

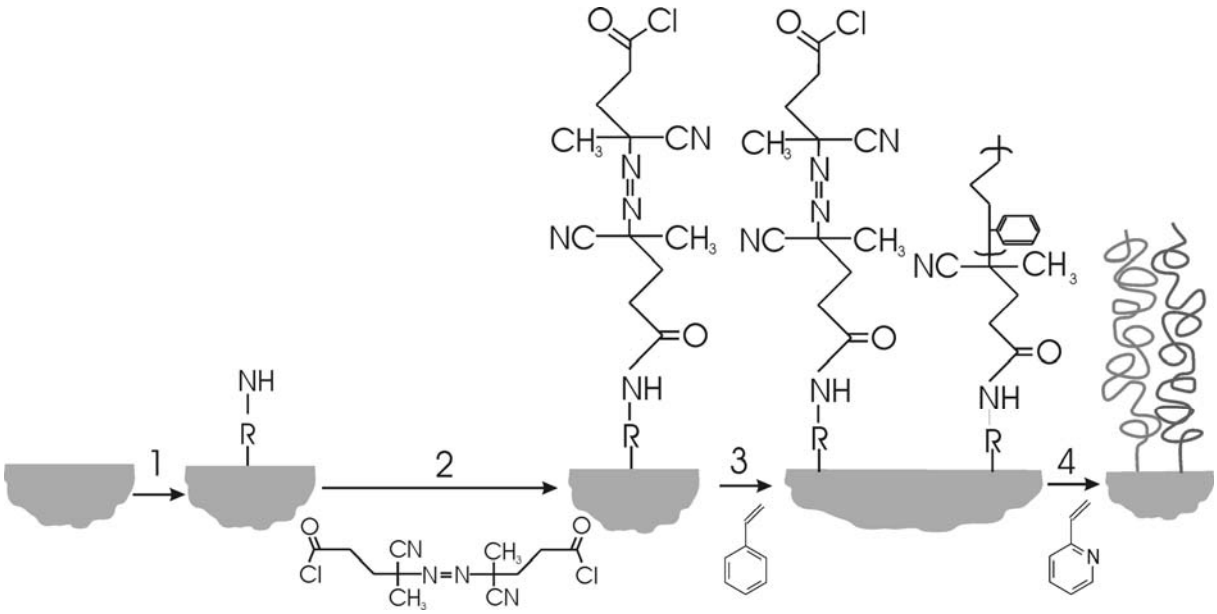

Scheme 4.2. Schematic Representation of Synthetic Rout To Fabricate Mixed Brushes on PA Surfaces:1-plasma treatment of the polymer substrate, 2-grafting of the azo-initiator, 3-free radical polymerization of styrene from the PA surface, 4- free radical polymerization of 2VP from the surface of PA.

4.7.3 Grafting of the Mixed Brushes.

Grafting of PS chains was performed by in situ radical polymerization initiated by thermal decomposition of the azo-initiator covalently attached to the PA surface. The amount of the grafted polymer and the residual initiator on the surface is regulated by polymerization time. Ungrafted polymer was washed out by a cold Soxhlet extraction. In the second polymerization step, the residual amount of the azo-initiator is used to carry out the graft

polymerization of 2-vinylpyridine. A representative example of the step-by-step grafting is shown in Table 4.3.

Table 4.3. Characteristics of the mixed polymer brushes grafted from PA-6I.

PA sample	M_n, kg/mol		grafted amount (mg/m^2)/grafting density (nm^{-2})		
	PS	PVP	PS	PVP	PS + PVP
No treatment	320	308	8/0.015	12/0.023	20/0.04
NH_3-plasma + azo-initiator	380	300	12/0.019	16/0.032	29/0.051

As a reference we performed the grafting polymerization according to the same procedure but using an untreated PA substrate. We investigated the reference PA sample expecting to graft polymers via chain transfer reaction of free macroradicals to the PA surface. In this reaction free radicals attack the hydrogen atoms of the main chain located near the carbon in the activated α-position to the amide group. The free radicals on the main chain of PA molecules, produced in the chain transfer reactions, initiate radical polymerization giving grafting of the polymer to the PA substrate. This is well known way to modify PA surfaces [Str91, Mei99].

4.7.4 Synthesis of the Binary Brushes via G*rafting To* Approach

Mixed brush (Scheme 4.3) consisting of two carboxyl-terminated incompatible polymers PS-COOH and PVP-COOH was synthesized by a two step “grafting to” procedure [Zhul96, Zha95, Wang00, Sed00, Zha00a]. In the first step, PS-COOH was spin coated on the surface of the PA sample (samples of PA textiles were simply immersed in the polymer solution and after that dried under nitrogen flux) and heated for a different period of time at $170^{O}C$ to graft the first polymer PS-COOH from the melt. Nongrafted polymer was removed with Soxhlet extraction. Then the second polymer PVP-COOH was grafted by the same procedure.

The thickness of the grafted polymer layers in terms of the ellipsometric thickness of the layer is presented in Table 4.4. As a reference we performed the grafting of polymer brushes according to the same procedure but using an untreated PA substrate. We did not found any grafted amount of the polymer.

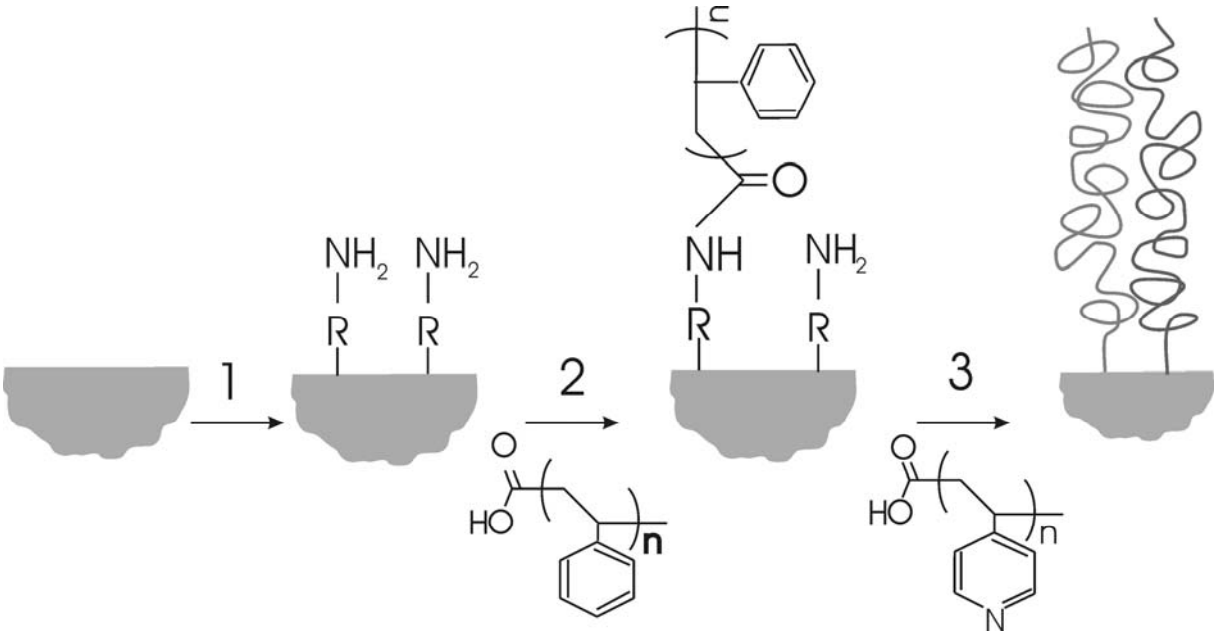

Scheme 4.3 Schematic Representation of Synthetic Rout To Fabricate Mixed Brushes on PA Surfaces via *grafting to* approach. 1- plasma treatment of the polymer substrate, 2- grafting of the first polymer (PS) from melt, 3-grafting of the second polymer (PVP) from melt.

Table 4.4 Ellipsometric thickness of polymer brushes after each step of grafting and surface treatment.

Thickness of PA 6I on Si wafer, nm	Grafted amount, mg/m^2				
	PS (M_n=9700g/mol)	PS (M_n=9700g/mol)	PVP	PS/PVP (M_n=9700g/mol)	PS/ PVP (M_n=9700g/mol)
39	2,8	3,3	3,4	5,7	6,2

4.7.5 Characterization of the Grafted Brushes

Additionally to the ellipsometric measurements the grafting of both polymers was proved with FTIR-ATR study performed with PA plates tightly pressed to the surface of ATR prisms (Figure 4.4b). The very well pronounced differences in the spectra of individual polymers (Figure 4.4 e and d) at 1400-1750 cm^{-1} and 2750-3200 cm^{-1} allowed us to analyze the layer composition at least qualitatively. The characteristic bands of aromatic and aliphatic groups observed for the mixed brushes (Figure 4.4 c, obtained by subtraction of the reference spectra of the PA substrate (a) from the spectra (b)) provide evidence for the grafting of PS and PVP. In the spectra we identify very pronounced PS bands at 1601 and at 1493 cm^{-1} and the characteristic bands of PVP at1568 and 1590 cm^{-1} .

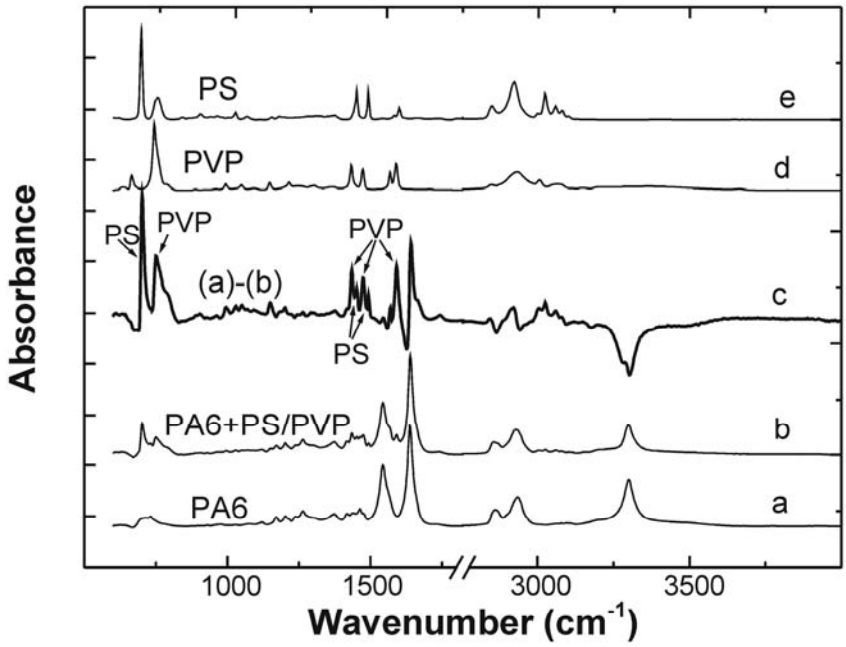

Figure 4.4. FTIR-ATR spectra: reference sample, PA-6 (a); PA-6 with grafted PS/PVP brush (b); spectra obtained by subtraction of (a) spectra from (b) spectra (c); reference PVP sample (d); reference PS sample (e).

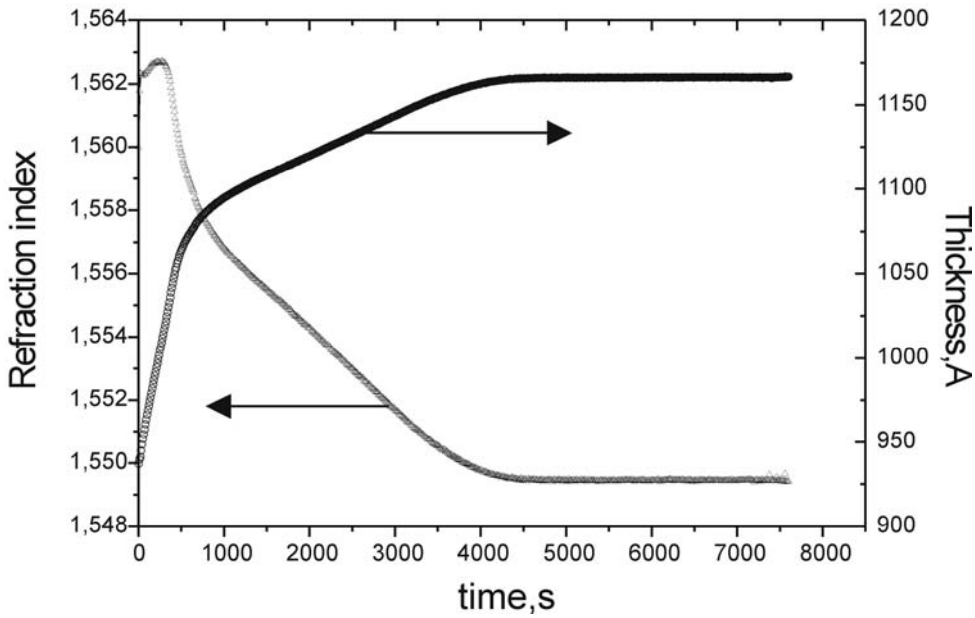

Figure 4.5. Swelling kinetics of PA-6I film (spin-coated on Si-wafer) in THF at room temperature

In contrast to the graft polymerization on a flat solid surface described elsewhere [Gon98, Sze96, Ale91, Pru98] we observed two quite pronounced specific effects in the case of “grafting from” method. Firstly, the grafted amount of both polymers on the unmodified PA surface was surprisingly large. The grafting via chain transfer reaction can be considered

as the "grafting to" approach where macroradicals penetrate the grafted layer to react with the substrate surface. For this approach, the grafted amount is usually kinetically limited and levels off at about 10 mg/m^2 of grafted polymers. In our case we received relatively thick 20 mg/m^2 mixed brush. Secondly, the roughness of the PA substrate dramatically increases during grafting polymerization (Figure 4.3 c).

These two facts can be explained if we take into account that the top layer of the PA substrate is swollen by solvent during the grafting procedure. We performed a model swelling experiment to demonstrate that. The swelling kinetics of the PA-6I film deposited on Si-wafer presented in Figure 4.5 shows that the PA film is more than 20% swollen by THF at room temperature, giving an increase of film thickness from 95 nm of the initial dry film to 117 nm of the swollen film. Therefore, PA is swollen by solvent and monomer when immersed into the reaction mixture. The latter may have two consequences. Firstly, swelling of polymers effects an decrease of glass transition temperature and, therefore, increase of mobility of segments. Secondly, the monomer is localized in the swollen PA layer. Penetration of free radicals in the swollen PA can induce polymerization and grafting to the PA somewhere inside the PA substrate. Consequently, we may expect different locations of the grafting process: on the top of the PA substrate, but also somewhere inside the swollen PA layer. Both these phenomena may effect the observed increase of the surface roughness of the PA substrate and enhance the grafted amount.

We used two different IR-spectroscopy experiments to study the depth of the penetration of the grafted polymers into the PA substrate. The first experiment using the FT-IR microscope (BRUKER) was performed with a microtome cut of the PA plate with grafted PS/PVP mixed brush in the direction perpendicular to the plane of the grafting. Figure 4.6.

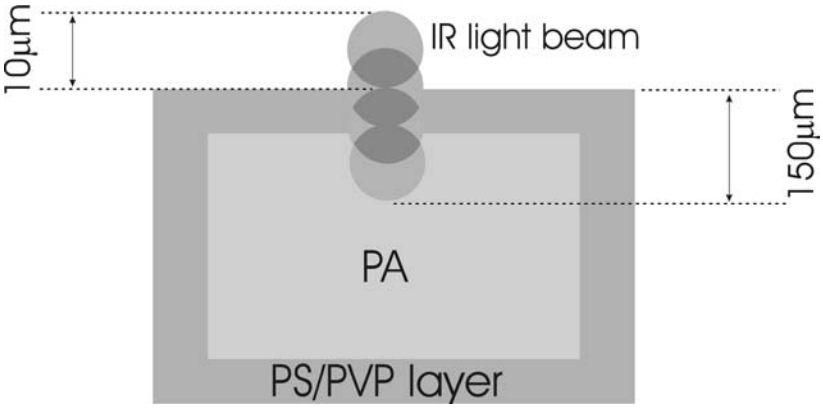

Figure 4.6. Scheme of IR investigation of PA microtom cut with grafted polymer layers.

We focused the IR-light beam (10 μm in diameter) step by step on the microtome cut starting from the edge with grafted polymer and moved the projection of the beam towards the middle of the cut with the step size of 10 μm until the 150 μm distance from the edge was approached. The transmission IR spectrum was recorded for each point (not shown in the

Chapter). We found characteristic bands of the grafted polymer only for the case when the beam was focused on the edge of the microtome cut proving that the depth of the penetration of grafted polymer is less than 10 μm from the edge.

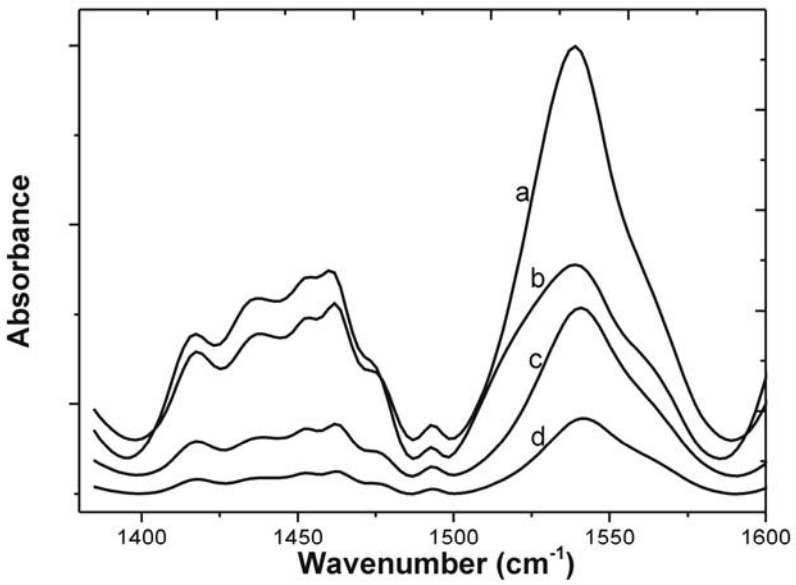

Figure 4.7. FTIR-ATR spectra of PA-6I with grafted PS/PVP layers at different d_p: 0.34 μm (a); 0.40 μm (b); 0.47 μm (c); 0.51 μm (d).

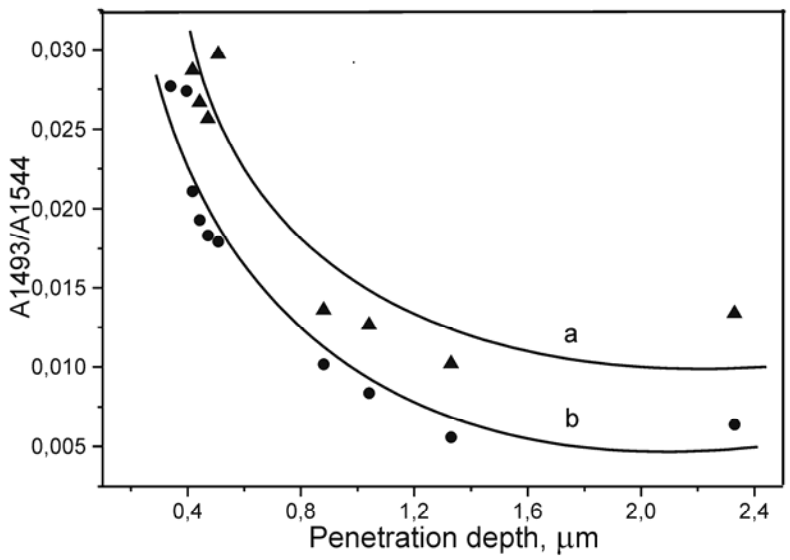

Figure 4.8. FTIR-ATR data for the penetration depth of PS into PA bulk: immediately after polymerization (no extraction) (a); after Soxhlet extraction in THF (b).

In the second experiment we applied FTIR-ATR mode described in the experimental section to study the penetration depth of the grafted PS into the PA-6 plates. The plate from

the side with grafted polymer was attached to ATR-prisms of different geometry (to change the incident angle) and prepared from different materials (to change the refractive index of the prism). Thus, the FTIR-ATR spectra were recorded for different penetration depths of IR-radiation inside the PA sample (Figure 4.7). For this investigation we used both the PA sample with grafted PS after a simple rinsing with THF and the similar sample after Soxhlet extraction of the ungrafted polymer in THF. In the spectra we compared integral absorbance for the bands of PA at 1544 cm^{-1} (1585–1500 cm^{-1} integration range) and grafted PS at 1493 cm^{-1} (1499-1487 cm^{-1} integration range). The intensity of both bands decreases with depth of the penetration reflecting the well known decreasing exponential law. The ratio between intensities of the bands reflects the change of the chemical composition with the depth of penetration (Figure 4.8).

We have made no attempts to resolve the intrinsic concentration profile of the grafted PS, because of the difficulty of quantitative interpretation. Nevertheless, the obtained results present a qualitative picture giving some information about the composition profile. Firstly, we have found that the Soxhlet extraction removes only relatively small amounts of nongrafted PS from the layer. Secondly, the depth of the PS location has been found to be up to 0.6 - 1 μm from the top of the sample. This value is of the same order as the roughness value RMS = 0.5 μm of the surface after grafting measured with AFM. With commercial AFM software we found that the increase of the surface roughness corresponds to about 10% increase of intrinsic surface of the PA substrates.

Therefore, we may suggest two possible scenarios to explain the obtained data. Firstly, the polymerization takes place on the surface and inside the swollen PA effecting the increase of roughness. Secondly, the grafted chains bend the swollen PA substrate due to the accumulated elastic energy of the deformed coils in the brush. Each of those mechanisms or both of them at the same time may cause the increased roughness of the substrate.

The larger as compared to usually observed for "grafting to" method amount of grafted polymers due to the chain transfer to PA substrate has the same reason as for grafting of end-functional polymers to the solid substrate modified with the anchoring layer of poly(glycidyl methacrylate) recently reported by Luzinov et.al. [Iyer02]. Mobility of the grafting points and their location on different levels (the interface becomes broader) due to the interpenetration of both the polymer of the substrate and the polymer of the brush substantially enhances the grafting amount. The interpenetration results in a complex interface with fractal characteristics. Consequently, the amount of polymer chains grafted to a swollen polymer substrate may be larger than just due to grafting to a flat solid substrate (Scheme 4.4).

It is noteworthy, that the grafting due to chain transfer reaction can be performed to any solid and polymer substrate and even to grafted polymer brush [Luz98, Luz96] depending on conditions of the polymerization. At the experimental conditions we used (styrene, P2VP, 60^0C) any grafting due to chain transfer to the brush layer was reported in literature [Pruc98]. However, PA is much more active in the chain transfer reaction and we may speculate that the grafting by chain transfer takes place mainly due to the interaction with the PA swollen substrate. We may speculate also that in the case of the surface-attached azo-initiator the most of polymers are grafted due to the surface-initiated radical polymerization because of high surface concentration of the azo-initiator when the rate of initiated polymerization is much higher than the rate of chain transfer reaction.

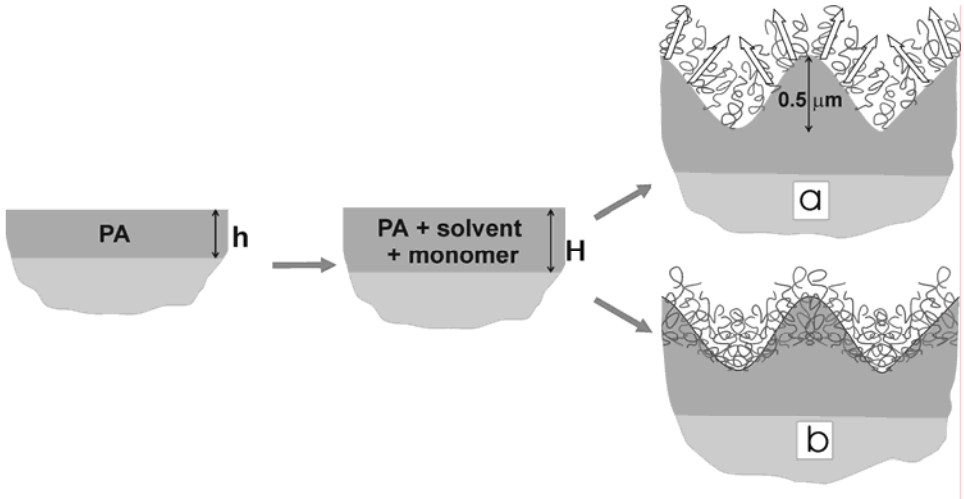

Scheme 4.4. Schematic representation of two possible mechanisms of the increase of the film roughness after grafting from PA surface: bending of swollen PA substrate due to the elastic energy of the brush (a); grafting inside the swollen PA film (b)

4.7.6. Switching/Adaptive Properties.

The same samples of PA on the Si wafer and on the PA plates both with the grafted PS/PVP mixed (via both “grafting from” and “grafting to” approaches) brushes were exposed for 5 minutes to solvents of different thermodynamic quality in respect to the polymers. After each treatment with a particular solvent the samples were dried in a flow of nitrogen and used for AFM and a rapid contact angle investigations. The experiments were repeated several times with each sample to prove the reversibility of the switching of surface properties. In these experiments we assume here that the morphology of the dry film is directly correlated with the structure of the swollen film. Time of the switching in a particular solvent is in the order of minutes (contact angle changes in 1-2 minutes and approaches to equilibrium in 5-10 minutes) that is much larger than time to dry the film under nitrogen flux (several seconds).

We may assume that we freeze the film morphology during solvent evaporation. At ambient conditions the polymers in the dry polymer film are in glassy state and the film morphology is stable for a long period of time.

The switching of morphologies upon exposure to different solvents was documented for similar mixed PS/PVP brushes grafted to the flat surface of highly polished Si-wafers [Sid99a]. This switching is affected by the phase segregation at nanoscopic scale and that results in regular patterns with average dimensions scaling with end-to-end distance of the grafted chains [Min02a]. For the grafted polymer with molecular weight of the order of 500 - 800 Kg/mol the characteristic size of clusters was measured to be in the range of 50-100 nm. In the case of the mixed brushes grafted to PA substrates the large roughness of the film introduced by grafting process decreases the lateral resolution of AFM images. We were not able to observe fine structure of grafted polymer layers on the surface caused by phase segregation, while contact angle measurements showed very pronounced switching of surface energetic state (Tables 4.5, 4.6).

Table 4.5. Wetting of the mixed brushes grafted from PA-6 and PA-6I substrates

sample	**treatment before polymerization**	**contact angles of water, deg**		
		toluene	**ethanol**	**water, pH=3**
PA-6I on Si-wafer	no treatment; grafting via chain transfer	92	61	75
	NH_3-plasma, azo-initiator	90	62	35
PA-6	no treatment; grafting via chain transfer	64	68	68
	NH_3-plasma, azo-initiator	90	61	39
Original PA-6I on Si-wafer (ref)	no grafting	64	62	64
Original PA-6 (ref)	no grafting	63	64	64

The data clearly show that a top layer of the binary brush switches from hydrophobic to hydrophilic energetic state and vice versa upon exposure to selective solvent for one of polymers. For example, if we expose the sample to toluene, the top of the layer is preferentially occupied by PS. In this case the contact angle approaches the value of 90°,

while in ethanol and water (pH=3.0) the surface is dominated by PVP with the contact angles 60° and 35°, respectively.

Table 4.6. Wetting of the mixed brushes grafted to PA-6 and PA-6I substrates

Sample	Contact angles of water, deg		
	Toluene	**Ethanol**	**Water, pH=3**
PA-6I on Si-wafer	88	72	49
PA-6	87	71	48
Original PA-6I on Si-wafer (reference)	64	62	64
Original PA-6 (reference)	63	64	64

The contact angles obtained on the mixed brush 90° and 60^0 after toluene and ethanol, respectively, correspond to the same values of the contact angles on the model PS and PVP single homopolymer brushes, respectively. This fact gives evidence that in a selective solvent the top layer of the mixed brush is formed due to the layered (perpendicular) segregation and the top is occupied by the favorite polymer. In acidic water PVP is protonated and charged. This layer is wetted by water much better as compared with neutral PVP. Wetting in this case is promoted by dissociation of the protonated PVP below water drop and at the same time the wetting behavior is complicated by diffusion of protons in bulk of the water drop deposited on the top of the brush [Sid99a]. Thus the contact angle is a function even of the drop size.

In the case of nonselective solvents after exposure to chloroform or THF both polymers are present on the top of the film (contact angle 80^0). Using the Cassie equation we calculated that this contact angle corresponded to the 65% PS fraction on the top of the brush when the surface of the brush is constructed from laterally segregated domains of PS and PVP. In a broad range of the binary brush compositions the range of switching between hydrophobic and hydrophilic states shows no strong influence of the composition (ratio between two polymers) [Min01].

Here we extend the study of switching behavior on substrates with a complicated texture and present the results of contact angle measurements on the PA textile with the grafted PS/PVP binary brushes as compared with the wetting behavior on the PA plates with

the same grafted brush. The fibers of about 200 μm in diameter forming the textile introduce an effect of a composite surface [Oen00] where the drop of water is in the contact partially with the surface of PA fibers and partially with air. In this case we observed the much more pronounced switching effect amplified by the surface texture of the PA textile (Figure 4.9)

The exposure of the textile sample to toluene results in highly hydrophobic properties of the material with advancing contact angle of 152°, while upon exposure to ethanol the advancing contact angle is 50°, and after treatment with acidic water the film is fully wetted and water soaks in the textile sample. These pictures demonstrate that, in contrast, the flat PA surface is less hydrophobic (90^0) and less hydrophilic (20^0) upon exposure to toluene and acidic water, respectively.

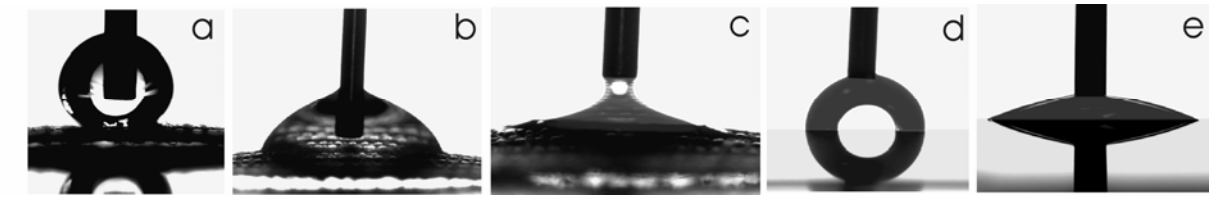

Figure 4.9. Video images of drops on the substrates with grafted PS-PVP brush from the PA-6 textile: after exposure to toluene, $\Theta = 150^0$ (a); ethanol, $\Theta = 50^0$ (b); water, pH=3, wicking regime (c), and from the PA-6 plates after exposure to toluene $\Theta = 90^0$ (d) and water, pH=3, $\Theta = 20^0$ (e)

Schematically this phenomenon is outlined in Scheme 4.5. The drop of water deposited on the textile is in contact with the textile fibers and air. Each fiber is a twist of single fibers forming a yarn with a rough surface. Thus, the textile surface has a complicated hierarchical texture. Depending on the bare contact angle on a flat surface, the liquid might fill all grooves of the rough substrate or might be in contact with the upper part of the relief and air can be trapped below a drop. The wicking criteria is determined as follows [Bic01]:

$$\cos\Theta_0 > (1-\phi_s)/(r-\phi_S)$$

where Θ_0 is the bare contact angle of water on a flat surface, ϕ_S is the solid surface fraction assigned with the upper part of the relief (in this case it is a fraction of the total area which is not in contact with the liquid), r is the ratio between the increased contact area of the rough surface and the corresponding projected area. An example of this regime is shown in Figure 4.9c.

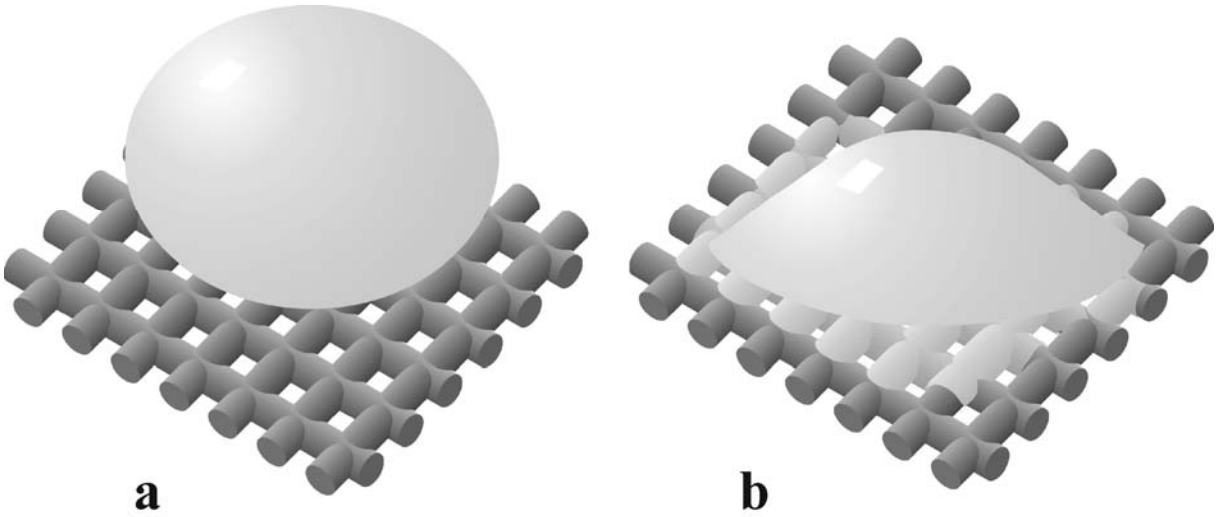

Scheme 4.5. Schematic representation of a drop of water on PA textile: $\Theta_0 > 90^o$, $\Theta \approx 150^o$, air is trapped below the drop giving the Cassie regime if the brush was switched in a hydrophobic state (a); $\Theta_0 << 90^o$, water soaks in the textile sample if the brush was switched in a hydrophilic state (b).

If the bare contact angle is smaller than 90^0 but the wicking criteria is not fulfilled the liquid fills the grooves of the rough surface only below a droplet contacting with fibers and the contact angle corresponds to Wenzel's regime [Wen36]

$$\cos\Theta = r(\gamma_{vs} - \gamma_{ls})/\gamma = r\cos\Theta_0$$

where Θ is the contact angle of water on a rough surface. An example of this regime is shown in Figure 4.9b.

If the bare contact angle is larger than 90^0, air can be trapped below a drop and the liquid is only in contact with the upper part of the relief of the rough surface of fibers resulting in the Cassie wetting regime given by: [Cas44, Bic99]

$$\cos\Theta = -1 + \phi_s(1 + \cos\Theta_0)$$

where ϕ_S is the fraction of the upper part of the relief (in this case that is the fraction of the total area contacting with liquid), which itself depends on Θ_0. An example of this regime is shown in Figure 4.9a.

Consequently, switching of the mixed brush on the surface of the textile material causes the transition between the Cassie regime (Scheme 4.5a, when the contact angle is larger than 90^0) and wicking regime (Scheme 4.5 b, when wetting is characterized by a small contact angle and the wicking criteria is fulfilled). Therefore, the textile material with the grafted mixed brush demonstrated the behavior effected by the combination of two possible approaches to regulate surface wetting: chemical composition and roughness.

Finally, we note that differences neither in surface modification and grafting process nor in switching behavior of the brushes were observed for different samples of PA substrates. The same for all PA samples specific grafting mechanism in a swollen top layer was observed. We speculate that this mechanism may be observed for various swollen polymer substrates.

4.7.7. The Estimation of Biological Efficiency of the Grafted Polymer Layers to PA Textiles.

The vitality tests of Fibrolasts (L929) for pure PA textiles, PA textiles with grafted monobrushes of PS and PVP, and PA textiles with grafted binary brushes with grafting to approach are presented in the Figure 4.10.

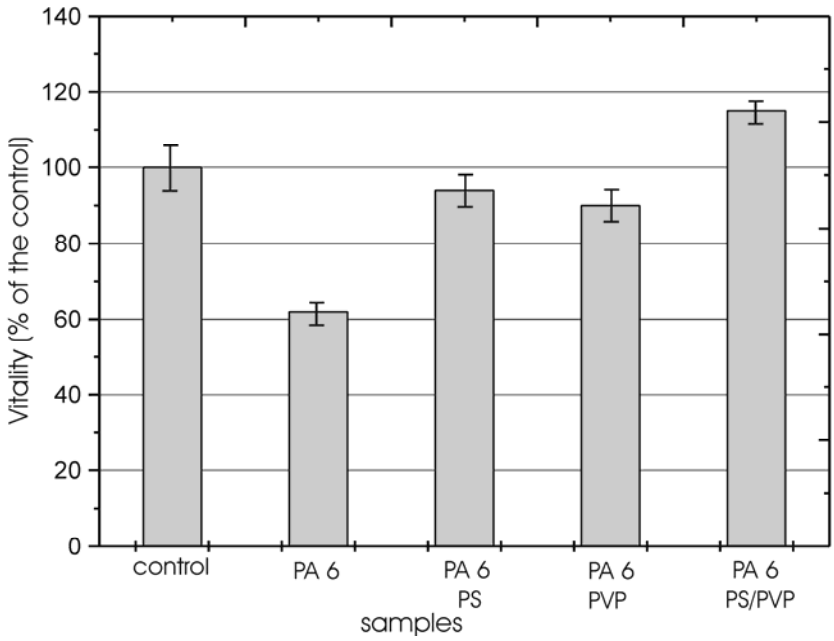

Figure 4.10. Vitality of Fibrolasts (L929) on different samples of PA.

In this test one can see a substantial difference between the original sample of the PA textile and the samples with grafted polymer layers. The vitality of the cells on original PA mounts only to 62%, for PA with grafted PVP brush the vitality mounts to 92% and up to 97%. In the case of PS brush, we might expect the longer vitality on PA with the hydrophilic PVP brush then on the hydrophobic PS, this result not in good agreement with the literature [Wac84] as well. The vitality on the sample of PA with grafted binary brush of PS/PVP mounts almost to 120% that might be explained, on the one hand, by adaptive behavior of the binary brush, and on the other hand, by the synergism of two components (hydrophobic/hydrophilic) of the brush. In general, preconditions for a high vitality are very complex and complicated. At the best, the cells can adhere to a material and then grow. If

cells have a weak adhesion to the material, they cannot properly propagate and pass away. The cell adhesion depends on many parameters of the material, *i.e.* hydrophilicity, roughness, crystallinity, zeta-potential, and also the type of cell and textile.

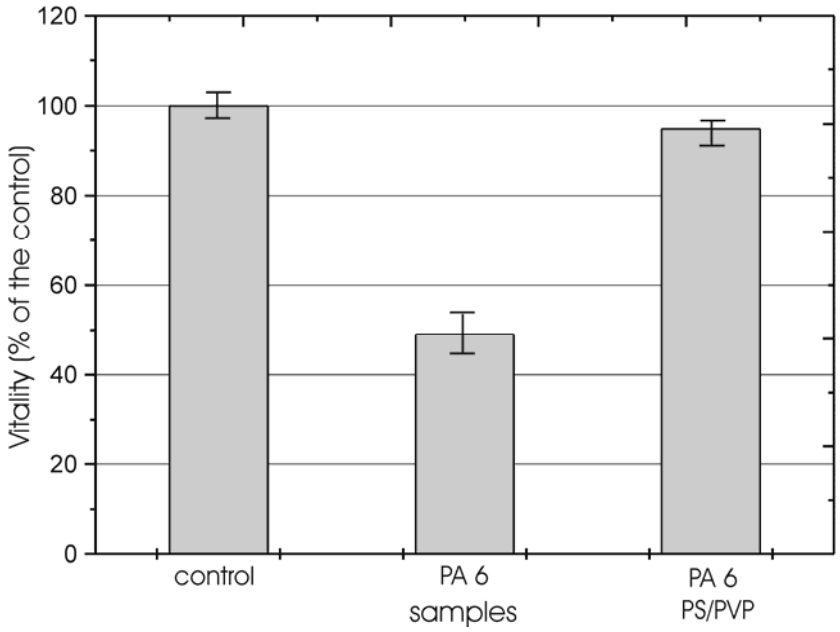

Figure 4.11 Vitality of endothel cells (RNE) on different samples of PA.

As the behavior of cells depends on the cell type the same test was performed on endothel cells (Figure 4.11).

It is known that endothel cells interact more sensible than fibrolasts cells with materials [Wac84]. The Figure 4.11 shows that for all materials tested the endothel cells have a significantly shorter vitality than the fibrolasts. But in this case also the binary polymer brush on PA textile improve the vitality.

4.8. Conclusions

In conclusion, we synthesized mixed PS/PVP polymer brushes via both step-by-step grafting of these two polymers from PA surfaces and the sequential grafting of a carboxyl terminated PS and PVP. We show that NH_3 plasma can be successfully used for the introduction of amino and OH functionalities on PA surfaces with the following attachment of azo-initiator for radical polymerization and for direct grafting of carboxyl terminated polymers. The covalent bonding of the initiator improves the grafting procedure, although the chain transfer mechanism introduces also, but less effective, the mixed brush on the untreated PA surface.

The “grafting from” procedure causes a substantial increase of the PA surface roughness, which we explain by banding of the swollen PA substrate during the grafting procedure. We found no deep penetration of the grafting process into the PA substrate and proved that surface roughness was driven by grafting events occurring on the very top layer of the swollen substrate.

The mixed brushes synthesized on PA substrates exhibited the same switching properties as it was recently shown for brushes grafted to Si-wafers. The mixed brushes prepared on the surface of PA textiles combined both the switching effect and effect of composite surface (Cassie regime) which substantially amplifies the switching range.

The vitality test shown that grafted binary polymer brushes improve the adhesion of fibrolasts and endothel cells to PA textiles. This effect can be used for further application of binary brush modified materials.

5 Chapter
Block Copolymer Responsive Brushes

5.0. Abstract

In this chapter we report on study of grafting of di- and triblock copolymers of highly incompatible polymers to both flat surface of silica wafers and to silica nanoparticles by means of the Minshutkin's quaternization reaction. For this goal the surfaces were modified with a bromoalkilsilane.

5.1 Introduction

Di- or triblock copolymers grafted to a solid substrate constitute a special class of block copolymer brushes. In general, thin films of block copolymers (BC) are the focus of intensive investigations due to their ability to self-assemble into well ordered, nanoscale periodic structures [Kra02]. BC demonstrate a variety of bulk and surface morphologies (spherical, cylindrical, gyroidal, and lamellar) depending on the ratio of block lengths and the segment-segment interaction parameter. The periodicity of these structures is determined by molecular weight and chemical composition in the BC and typically is in the range from 10 to 100 nm. This class of ordered materials is promising for sophisticated applications in many fields of nanoscience and nanotechnology such as surface patterning, lithography, and templating for the fabrication of information storage devices of terabits per cm^2 capacity, magnetic and optical materials, and nanowires and nanomembranes [Man95, Park97].

The grafted block copolymer surface layer strongly differs from physically adsorbed thin films of mobile block copolymer chains due to confinements introduced by tethering to a solid surface. However, even in the case of the immobilized polymer chains, a very rich phase behavior can be observed upon exposure to different media and external stimuli, which can be much more complicated then in the case of physisorbed films. The basis for the responsive behavior of BC brushes is the phase segregation mechanism, specifically if the solvent affinities to the different blocks are significantly different. The polymer-solvent interactions will govern the formation of the segregated phases even within the grafted layer.

A series of investigations of Zhao, Brittain et.al. on BC brushes of different structures [Zhao00, Zhao00a, Zhao00b] proved the mechanism of the phase segregation predicted by the theoretical investigations of Zhulina, Singh and Balazs. For example, in the case of the

tethered PS-*b*-PMMA and PS-*b*-PMA, CH_2Cl_2 is a good solvent for PS, PMMA, and PMA. When the sample is immersed in this solvent, the polymer chains are forced to stretch away from the interface to avoid contact with neighboring polymer chains. Removing the PS-*b*-PMMA brushes from CH_2Cl_2 condenses the polymer brushes and localizes PMMA blocks at the air interface. The T_g's of PS and PMMA in the bulk state are both around 100° C, and there is little difference in surface free energies of PS and PMMA. Therefore, the PMMA blocks remain at the air interface, which is supported by contact angle measurements and XPS results.

If the sample is immersed in cyclohexane, PMMA chains migrate from the solvent interface and form aggregates with the neighboring PMMA blocks to avoid contact with solvent. Although PS blocks have a low mobility because of the covalent bonding to the silicon wafer surface and to the PMMA block, they are miscible with cyclohexane and migrate to the solvent interface to form a shield around the PMMA aggregates.

Zhao and Brittain synthesized block copolymer brushes by sequential carbcationic polymerization and ATRP. They started with surface immobilization of functional trichlorosilane, which is an initiator for carbocationic polymerization. The silane layer was deposited on the silicate substrate. Treatment of the modified substrate with styrene under carbocationic polymerization conditions led to the formation of tethered PS layer. This PS film was immersed in a solution of MMA and polymerized using typical ATRP conditions resulting in the block copolymer brush.

In another development, K. Matyjaszewski et al. developed a two step ATRP routine for the fabrication of BC brushes [Mat99]. ATRP was successfully used for the fabrication of triblock copolymer brushes on planar surfaces and BC brushes directly on the surface of nanoparticles [Zhao03].

Recently, the reversible addition fragmentation chain transfer techniques was applied for synthesis of BC brush PS-*b*-PDMA (*N*,*N*-dimethylacrylamide), PDMA-*b*-PMMA on silicon wafers, and poly(3-[2-(*N*-methylacrylamido)-ethyldimethyl ammonio]propane sulfonate-*b*-PDMA on gold surface [Baum02, Sum03]. These brushes displayed reversible surface properties upon treatment with block-selective solvents. Finally, several research groups suggested and have developed living anionic polymerization for the synthesis of BC brushes [Qui02, Advi02].

All the above-mentioned synthetic methods are based on the approaches, which are very similar to that developed for synthesis of similar block copolymers in solution polymerization. The main challenges of the synthesis of chemically grafted layer on solid

substrates concern an appropriate choice to immobilize the initiator on the surface and, then, performing the process under conditions allowing to avoid side reactions, which can dramatically decrease quality of the brushes.

A specific case of BC brushes is represented by Y-shaped brushes when Y-shaped AB copolymers are grafted onto a flat surface. One "arm" of the Y-shaped brush is an A homopolymer, and the other arm is an incompatible B chain, and the short "stem" tethers the entire copolymer to the surface. This type of BC brush builds the bridge between end-tethered BC brushes and mixed binary polymer brushes [Kra02, Mat99, Sum03]. Here we develop an alternative approach for the fabrication of mixed polymer brushes on both flat and rough substrates.

5.2. Materials

Triblock copolymer of poly(styrene-b-2-vinypyridine-b-etyleneoxyde) P(S-b-2VP-b-EO) (M_n(PS-P2VP-PEO) 14100-12300-35000) was kindly offered by Prof. Gohy.

Poly(styrene-b-4-vinyl pyridine) P(S-b-4VP) (P105-S4VP; M_n(PS-P4VP)=2140-2070, M_w/M_n=1.13), was purchased from Polymer Source, Inc (synthesized by anionic polymerization)

Tetrahydrofurane (THF), nitromethane, 1,4-dioxane, hexane, toluene, ethanol (Aldrich) were used as received. Dichloromethane (Aldrich) was dried on molecular sieves. Highly polished silicon wafers (obtained from Wacker Chemitronics, Germany) were first cleaned in an ultrasonic bath for 30 min with dichloromethane, placed in cleaning solution (prepared from NH_4OH and H_2O_2) at 60^0C for 1 h and then rinsed several times in Millipore water (18 MΩ cm^{-1}). 11-bromoundodeciltrimethoxisilane (BUDTMS) ABCR (Karlsruhe, Germany) was used as received.

Silica nanoparticles (SiO_2-F-0.2; d=0.193 μm) were purchased from Microparticles GmbH, Berlin, Germany.

5.3. Preparation of the Mixed Brushes on Silica Wafers

In the route of synthesis of mixed polymer brushes on the surface, we explore the reaction of quaternization [Fuo48] of pyridine groups in vinylpyridine blocks of the block copolymers with Br-alkyl groups on the surface after modification with a ω-bromalkyl silane (BUDTMS).

BUDTMS was chemosorbed on the surface of the cleaned Si wafres from 1% toluene solution. In the next step, a thin films (50±5 nm as measured with ellipsometry) of the block

copolymers were spin-coated on the top of the BUDTMS layer from the 1% dichloromethan solution. Then the samples were heated at 160°C in a vacuum oven for different periods of time to graft the block copolymers and to measure the kinetics of grafting. The nongrafted polymer was removed by Soxhlet extraction with dichloromethane for 3-4 h. Each step was monitored with ellipsometry and atomic force microscopy (AFM). The same procedure was performed on the surface of a Silicone prism and monitored with Fourier transform infrared spectroscopy with attenuated total reflection (FTIR-ATR).

A control experiment showed that block copolymers deposited on the bare Si wafer were completely removed by Soxhlet extraction with dichloromethane.

5.4. Preparation of the Mixed Brushes on Silica Nanoparticles

To graft the block copolymers to the surface of silica nanoparticles the same approach of the quaternization reaction to the surface was used. BUDTMS was chemosorbed on the surface of the annealed at 110°C in a vacuum oven silica nanoparticles from 3% toluene solution. The concentration of nanoparticles in the solution was 5%. After adsorption of BUDTMS the nanoparticles were washed out from nonadsorbed silane several times in toluene using a centrefuge for the separation. The grafting of block copolymers was performed in 3% nitromethane polymer solution at 60°C for 68-72 h as proposed in [Fuo48]. The concentration of the particles in the solution was 3%. The nongrafted polymer was removed by washing out using the centrifuge for several times by chloroform.

5.5. Sample Characterization.

5.5.1 Ellipsometry

Layer thickness and the amount of the grafted substances was evaluated with Multiscope Optrel null-ellipsometer (Berlin, Germany) at incidence angle of 70°. The measurements were performed for each sample after each step of the modification to use the measurement of the previous step as a reference for the simulation of ellipsometric data. Initially, the thickness of native SiO_2 layer (usually 1.4 ± 0.2 nm) was evaluated at the value of refractive index n = 3.858 – *i* 0.018 for Si and 1.4598 for SiO_2, respectively. Then the thickness of the chemosorbed BUDTMS layer was evaluated using the two layer model: SiO_2/ BUDTMS for refractive index of BUDTMS equal to 1.4559 [ABCR]. Finally, the thickness of the polymer film after grafting was calculated using the tree layer model SiO_2/ BUDTMS /grafted polymer considering the thin polymer film as an effective optical medium

with n=1.59. In reference experiments we found no influence of the surface roughness on the ellipsometric results for the prepared grafted films.

5.5.2. FTIR

FTIR spectra were taken with an IFS 66 (Bruker) spectrometer for the chemosorbed BUDTMS layer, and grafted block copolymer layers to the silica nanoparticles using the diffuse reflection technique (the samples were mixed with the KBr powder. 500 mg of KBr powder was taken to 3mg of pure silica nanoparticles and the nanoparticles with grafted block copolymer brushes, and to 8 mg of the nanoparticles with the chemosorbed BUDTMS. As the background was used the pure KBr powder).

5.5.3. AFM

AFM studies were performed on a Dimension 3100 (Digital Instruments, Inc., Santa Barbara) microscope. The tapping and phase contrast modes were used to map the film morphology at ambient conditions. Silicon tips with a radius 20 $\pm$ 5 nm, a spring constant of 1.5-6.3 N/m and frequency 63-100 KHz were used. Root mean square roughness (RMS) was calculated from the images with the commercial software.

5.5.4. Scanning Electron Microscopy (SEM)

A DSM 982 Gemini, ZEISS instrument was used for SEM. Specimens were prepared by deposition of the silica nanoparticles from dichloromethane solution on Si wafers.

5.5.5 Contact Angles

Advancing contact angles of water were measured using DSA Krüss (Hamburg, Germany) equipment. Samples with mixed brushes were exposed to particular solvent for 10 minutes, then rapidly dried with Ar flux and afterwards water contact angle was rapidly (within first 30 seconds) measured.

5.6. Results and Discussion

5.6.1 Grafting of BUDTMS

The synthetic procedure (Scheme 5.1) starts with the covalent grafting of BUDTMS to the surface of Si wafer as mentioned in the experimental part.

For such conditions, it is possible to approach a reproducible preparation of covalently bonded thin layers of BUDTMS. AFM topographical images of the surface covered with BUDTMS (Figure 5.1) showed only few clusters of polymerized and precipitated BUDTMS, which do not have an influence on the following investigations.

The ellipsometric thickness of the film of about 16±3 Å corresponds to the 1-1.5 theoretical monolayers of the BUDTMS [Men97].

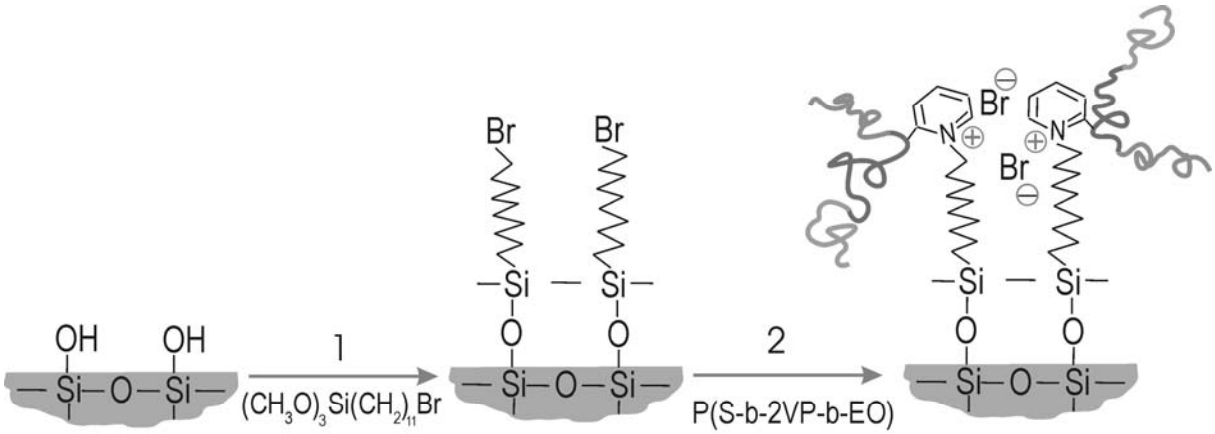

Scheme 5.1. Schematic representation of the grafting route to fabricate block copolymer brushes on Si wafers: 1-chemosorbtion of BUDTMS; 2-garfting of the triblock copolymer.

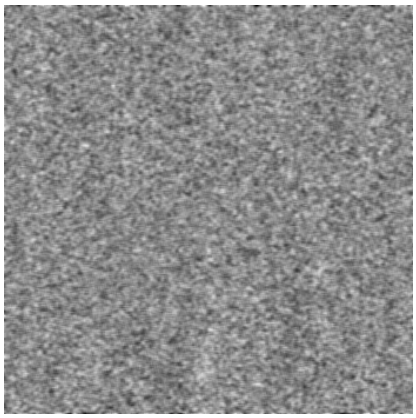

Figure 5.1. AFM topography image (1×1 μm^2, Z-range 5nm) of chemosorbed BUDTMS on a Si wafer.

5.6.2. Grafting of the Block Copolymers

The next step of the synthetic procedure comprises the grafting of the P(S-b-2VP-b-EO) or P(S-b-4VP) from the thin film deposited on the surface of the Si-wafer with chemosorbed BUDTMS. The kinetics of the grafting of P(S-b-2VP-b-EO) from 1% dichloromethane solution at 160° C in terms of the ellipsometric thickness of the layer is presented in (Figure 5.2).

With AFM we observe the phase segregation in the grafted block copolymer, which occurs at a nanoscopic scale with the apparent 30-40 nm average lateral size of domains. The size of the domains is overestimated because it is almost impossible for this morphology to perform the convolution procedure correctly for the tip curvature radius. Representive image of the 1×1 μm^2 scale of the laterally segregated phases is shown in Figure 5.3.

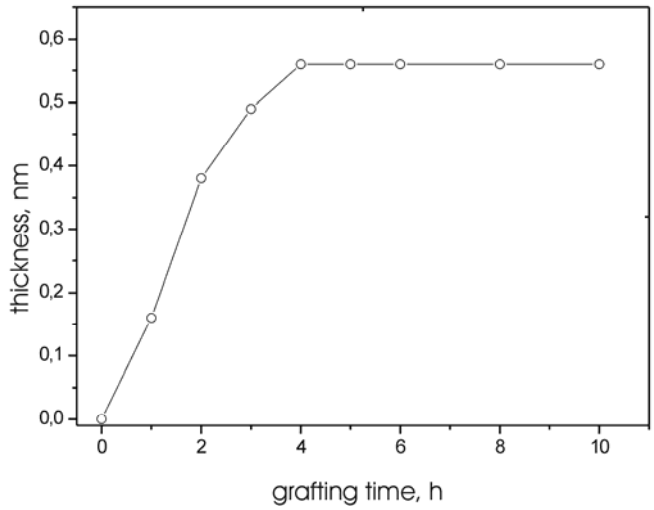

Figure5.2. Grafting kinetics of the P(S-b-2VP-b-EO) brush on the BUDTMS modified Si-wafer.

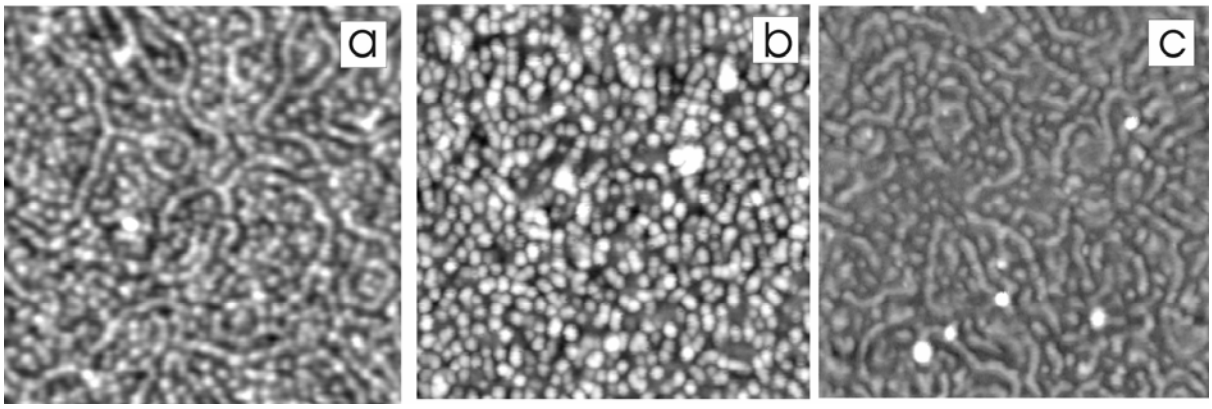

Figure 5.3. AFM topographical (1×1 μm^2, Z-range 5nm) images of the P(S-b-2VP-b-EO) brush after exposure to methanol (a), water with pH 3 (b), and THF (c).

5.6.3. Switching/Adaptive Properties

The block copolymer brush morphology and surface energetic state switch reversibly upon exposure to different solvents in the same way as it is observed for the binary brushes of PS/PVP prepared via “grafting from” and “grafting to” approaches. After exposure to different solvents, the silica wafers are taken from the solvent and rapidly dried under

nitrogen flux. Then the appropriate measurements of the film characteristics are performed. In these experiments we assume that the morphology of the dry film reflects the morphology of the swollen film as described above. At ambient conditions, the block copolymers in the dry film are in a glassy state and the film morphology is stable for a long period of time.

Contact angles of water were measured on the surface of the wafer immediately after the drop was set on the substrate. In these experiments we measured water contact angle on the surface of the frozen layer structure before it is changed under the water drop. Then the wafer was exposed to the next solvent and the same measurements were carried out. All changes of film properties observed experimentally were reversible and the switching experiments were repeated several times for each sample.

AFM images show the change of morphology and roughness of the polymer films upon exposure to methanol, THF and water pH 3 (Figure5.3). Two different morphology can be identified: dimples (round clusters) after water and so called mixed morphology (ripple-elongated domains and round clusters) after THF and methanol. These morphologies are caused by the lateral phase segregation of three incompatible blocks in the triblock copolymer.

The switching/Adaptive behavior of the block copolymer brushes can be observed from the contact angle data (Table 5.1). The data clearly show that a top layer of the brush switches from hydrophobic to hydrophilic energetic state upon exposure to selective solvents.

Table 5.1. Wetting of Block copolymer Brushes Grafted to Si Wafers

sample	**contact angles of water, deg**				
	toluene	CH_2Cl_2	ethanol	water, pH 7	water, pH 3
P(S-b-2VP-b-EO)	92	87	53	66	50
P(S-b-4VP)	90	83	65	71	53

When we expose the sample to toluene, the top of the layer is occupied by the block of PS, while in ethanol and water (pH 3) the surface is dominated by PVP and PEO blocks in P(S-b-2VP-b-EO) and P(S-b-4VP) respectively. The comparison of the switching behaviour of these di- and triblock copolymers after exposure to water with pH 7 allows to estimate the influence of the third block (PEO) of P(S-b-2VP-b-EO). In this case P2VP block has a negligible influence on the contact angle value because N atoms of the pyridine fragment are not protonated at pH 7 and the contact angle value depends preferentially on a fraction of

PEO on the top of the layer. Hence, we have a smaller contact angle for P(S-b-2VP-b-EO) after exposure to neutral water than for P(S-b-4VP).

Such a switching behavior of the block copolymer brush suggest both lateral and perpendicular phase segregation which is considered to be a second order transition resulting from the interplay between segment-segment and segment-solvent interaction [Min02a]

5.6.4. Block Copolymer Brushes on Silica Nanoparticles.

We used the same approach for the grafting of block copolymers to the surface of silica nanoparticles (Scheme 5.2). BUDTMS was grafted to the nanoparticles surface as mentioned in the experimental part.

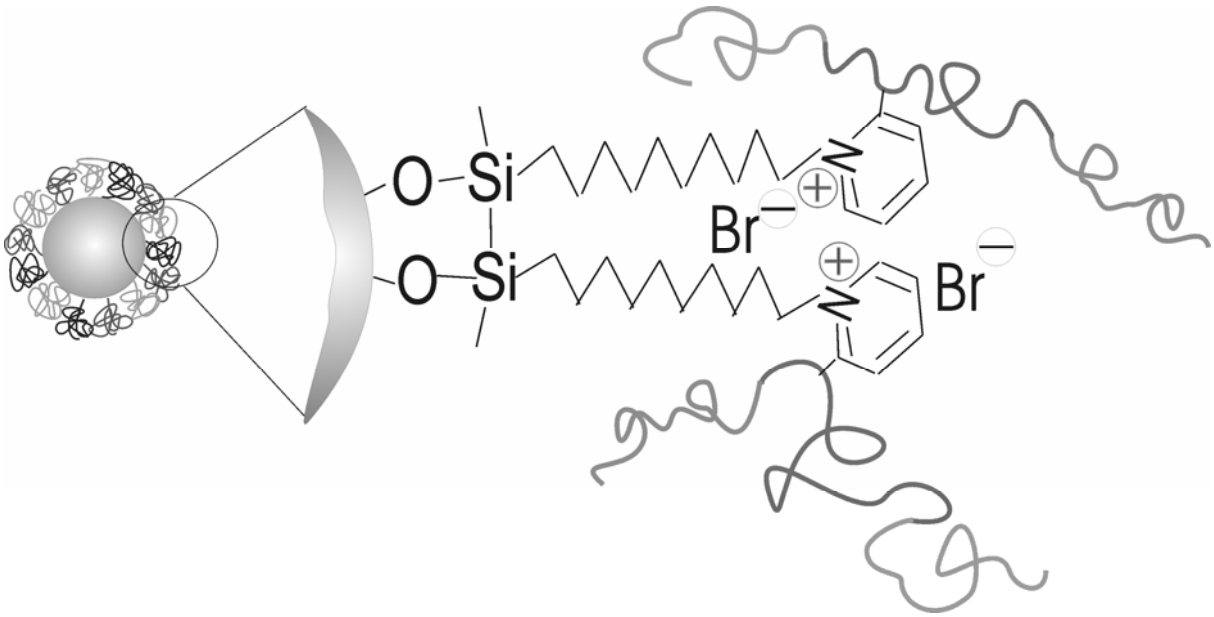

Scheme 5.2. Schematic representation of silica nanoparticle with grafted block copolymer via quaternization of the poly(2-vinypyridine) block

P(S-b-2VP-b-EO) and P(S-b-4VP) were grafted to the BUDTMS modified surface of the nanoparticles. To prove the fact of grafting of the block copolymers to the silica nanoparticles, we performed FTIR experiment using the diffuse reflection technique as described in the experimental section. The obtained spectra of silica nanoparticles with grafted P(S-b-2VP-b-EO) gave a very small absorbance of the characteristic band of quaternized N atoms (-C-N^{+}≡) at 1669 cm^{-1} due to only partial quaternization of vinylpyridine to the nanoparticle surface. This characteristic is poorly resolved and can not be considered as a sufficient evidence for the grafting. However, a multiple rinsing of the particles in THF results in the product with clearly identified bands of the block copolymer.

As a reference we used the spectrum of the pure P(S-b-2VP-b-EO) copolymer (Figure 5.4)

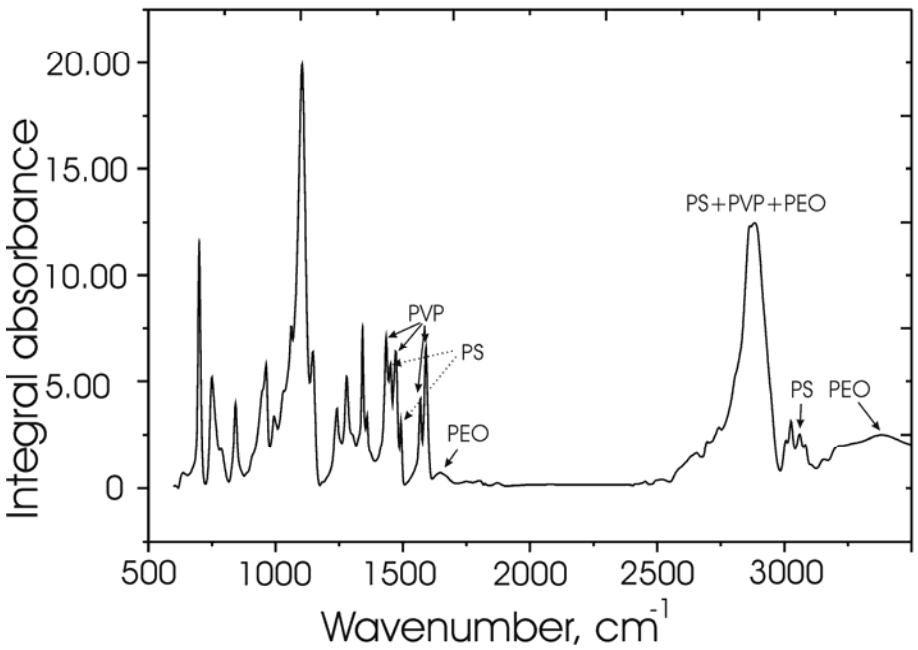

Figure 5.4. FTIR spectra of P(S-b-2VP-b-EO) thin film.

Very well pronounced differences in the spectra of individual blocks of the block copolymer (Figure 5.4, Figure 5.5) allowed us to analyse the chemical composition of the silica particles after grafting. The characteristic bands of aromatic and aliphatic groups observed for the block copolymer brushes (Figure 5.5d) were obtained by subtraction of the spectrum (a) of the silica nanoparticles with chemosorbed BUDTMS from spectrum of the silica nanoparticles with the chemosorbed BUDTMS and the grafted block copolymer (b). In the spectra we identify very pronounced PS block bands at 1601 and 1493 cm^{-1} , the characteristic bands of the PVP block at 1568 and 1590 cm^{-1}, and the characteristic bands of the PEO end block at 1648 and 3378 cm^{-1}, which provide evidence for the grafting of P(S-b-2VP-b-EO).

For the quantitative analysis of the particles we have prepared a calibration curve in terms of P(S-b-2VP-b-EO) fraction in mechanical mixtures of the block copolymer with the nanoparticles. For each mixture the intensity of FTIR spectraat 2926 cm^{-1} was measured. This characteristic band represents the C-H groups which can be found in all polymer blocks of the copolymer. Figure 5.6 presents the amount of the block copolymer in the mixture with silica nanoparticles vs. the integral absorbance at 2926 cm^{-1}.

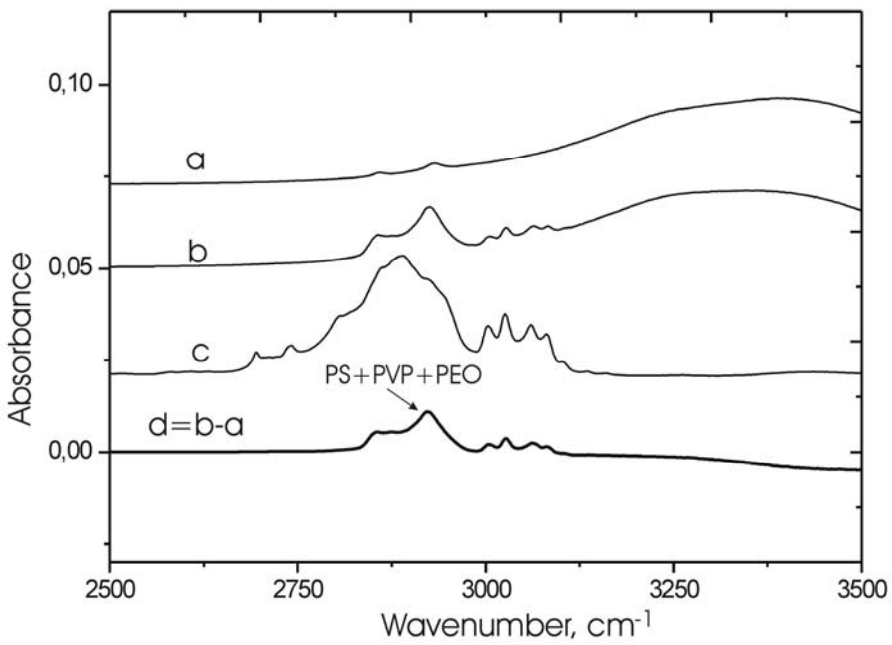

Figure 5.5. FTIR spectra: silica nanoparticles with chemosorbed BUDTMS (a); silica nanoparticles with chemosorbed BUDTMS and grafted P(S-b-2VP-b-EO), reference sample, P(S-b-2VP-b-EO) (c); spectra obtained by substraction of spectrum b from spectrum a (d).

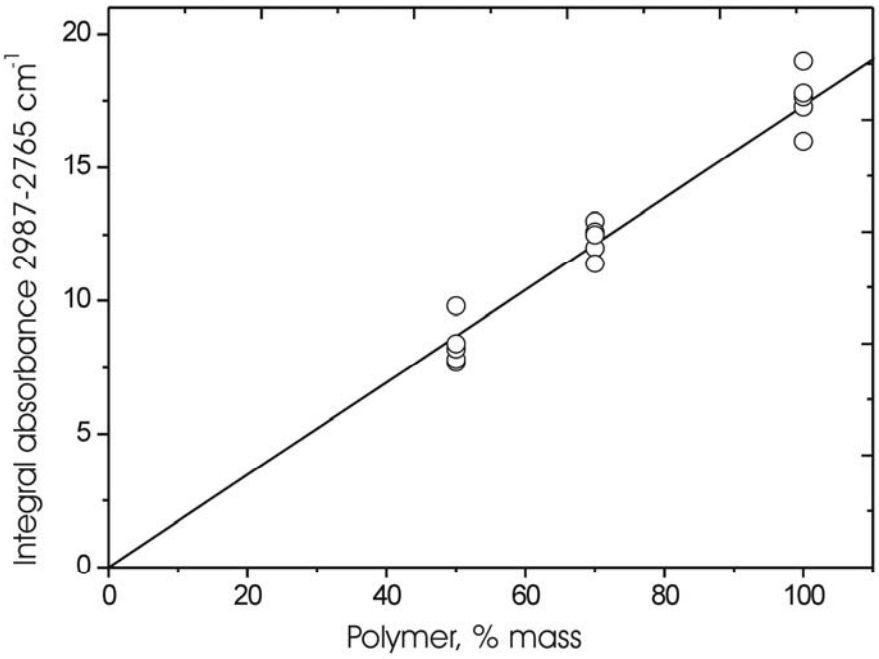

Figure 5.6 . The calibration plot for the P(S-b-2VP-b-EO) block copolymer in the mixture with silica nanoparticles in terms of the FTIR spectrum integral absorbance vs. mass fraction of the block copolymer.

For the analysis of FTIR spectra for the sample of copolymer coated nanoparticles we found that about 11% of the P(S-b-2VP-b-EO) (Figure 5.5d) was grafted. This value corresponds to the 6.7 mg/m^2 grafting amount and 0.066 nm^{-2} grafting density. These data are in good agreement with the thickness of the grafted layers to the silica wafers and with grafting of polymers via "grafting to" in general.

AFM images (Figure 5.7) obtained for the same nanoparticles with grafted block copolymer brushes deposited form dichloromethane on Si wafer give another evidence of the grafting to the nanoparticle surface.

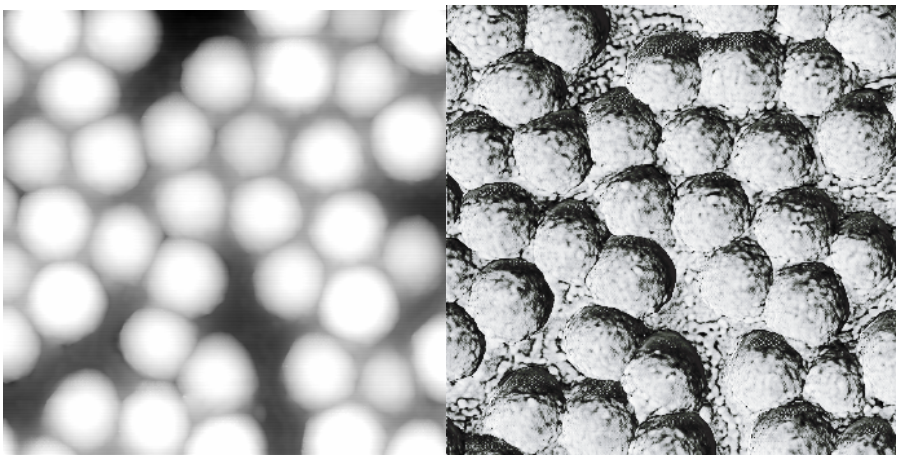

Figure 5.7. AFM topographical (left) and phase (right) ($1\times1\mu m^2$) images of the silica nanoparticles with grafted block copolymer brushes on the surface of silica wafers.

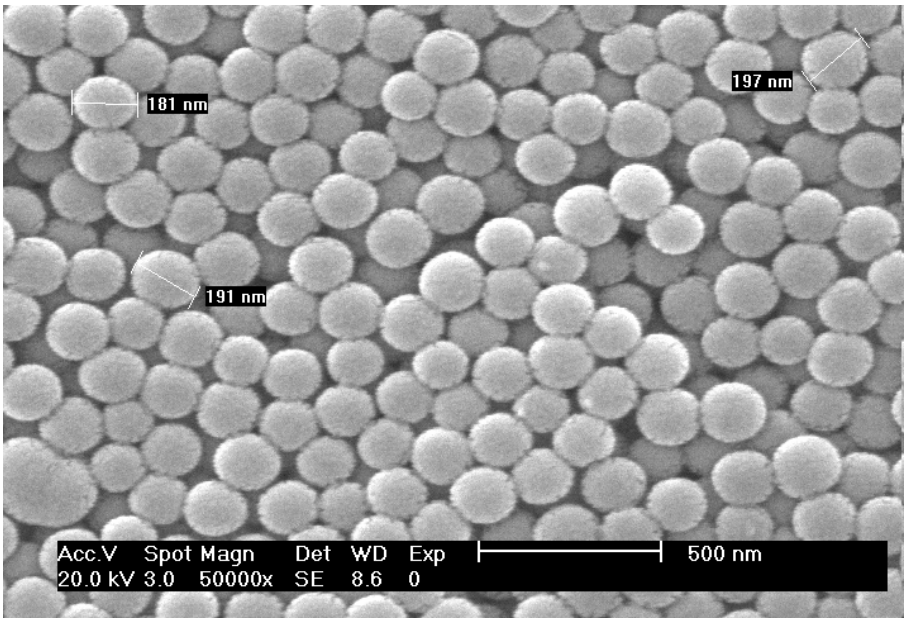

Figure 5.8. SEM image of silica nanoparticles with grafted block copolymer brushes.

The phase image allows to clearly see the prominent phase contrast which confirms the presence of the block copolymer on the particle surface and the phase separation of the block copolymer after exposure to dichloromethane. These data are in the good agreemnt with the AFM data obtained for the block copolymers grafted to the silica wafers.

The SEM micrograph, presented in Figure 5.8 also shows the surface of the nanoparticles with grafted brushes. The surface has a rough structure due to the block copolymer on the top.

5.6.5. Switching/Adaptive Properties of Block Copolymer Brushes on Silica Nanoparticles

For the investigations of switching/adaptive behaviour of block copolymer brushes on the silica nanoparticles we grafted the silica nanoparticles to silica wafers which were modified with the same BUDTMS. The Scheme 5.3 presents the grafting procedure of the nanoparticles to the silica wafer surface.

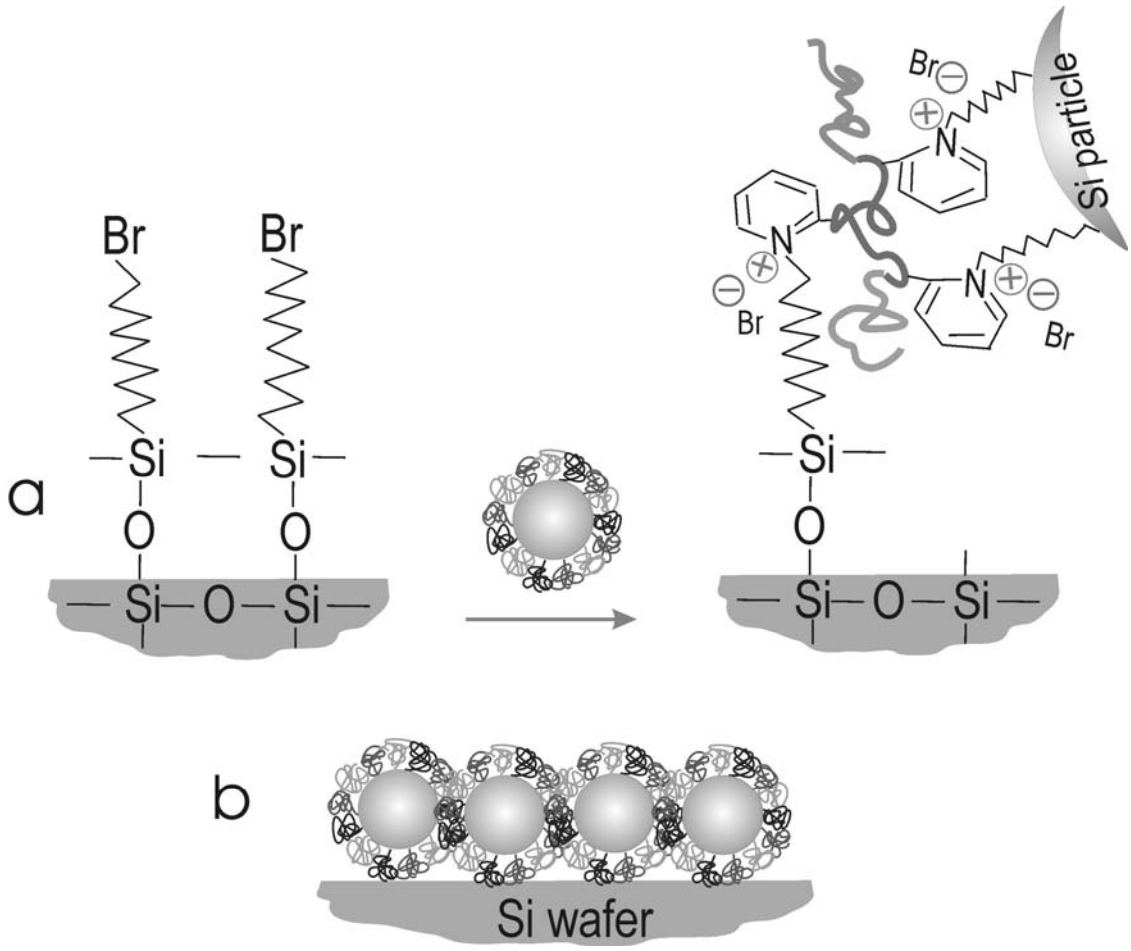

Scheme 5.3. Schematic representation of grafting silica nanoparticles with block copolymer brushes to the Si wafer surface (a); a layer of the nanoparticles on Si wafer (b)

The deposition of nanoparticles on silica wafers was performed using the vertical deposition approach. We prepared 3% suspension of the grafted particles in dichloromethane.

Then a silica wafer was immersed in the solution and the solvent was evaporated under low pressure. This approach can be used for the fabrication of coatings with well ordered structure [Kit03]. The AFM image (Figure 5.9) shows two dimensional ordering of a close dense hexagonal array of the particles with the grafted P(S-b-2VP-b-EO) block copolymer brush on the silica wafer.

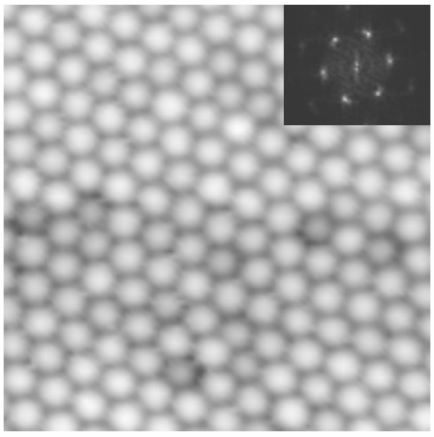

Figure 5.9. AFM topography image (2×2 μm^2) of the silica nanoparticles with grafted block copolymer brushe on the surface of the silica wafer.

The data of contact angle measurements on these surfaces demonstrate the well pronounced switching from hydrophobic to hydrophilic wetting behavior (Table 5.2) upon exposure to different solvents. This behavior is similar to the behavior of block copolymer brushes on a flat surface. However, the range of switching on the particle coated substrate is much larger than on the flat surface.

Table 5.2. Wetting of Block copolymer Brushes Grafted to Si particles on silica wafers.

sample	contact angles of water, deg				
	toluene	CH_2Cl_2	ethanol	water, pH=7	water, pH=3
P(S-b-2VP-b-EO)	131	117	57	69	29
P(S-b-4VP)	125	107	65	71	44

This fact may be considered as amplification effect of wetting by the surface roughness obtained on the silica wafer surface with grafted nanoparticles. The phenomena of amplification of wetting characteristics of the surface by the roughness was in detail discussed in the Secttion 4.1 for the case of textiles with grafted binary brushes and will be analyzed at issue in the following Chapter.

5.7. Conclusions

In conclusions, mixed polymer brushes prepared from P(S-b-2VP-b-EO) and P(S-b-4VP) block copolymers were grafted to both the flat surface (Si wafers) and to the surface of silica nanoparticles via quaternization reaction of the pyridine nitrogen. This one step grafting technique has a substantial advantage over the multistep grafting of mixed polymer brushes consisting of two incompatible polymers.

Nanoparticles with grafted mixed brushes may be used for the fabrication of coatings with switching behavior.

Chapter 6

Hierarchically Structured Self-Adaptive Surfaces on PTFE Substrates

6.0. Abstract.

In this chapter we report on a novel route to fabricate two level structured self-adaptive surfaces (SAS) of polymer materials. The first level of structure is built by a rough polymer film that consists of needlelike structures of micrometer size. The second level of structure is formed by the nanoscopic self assembled domains of a demixed polymer brush irreversibly grafted onto the micro needles. By exposing the surface to solvents that are selective to one of the components of the brush, we reversibly tune the surface properties. The large scale surface structure amplifies the response and enables the control of wettability, adhesion, and chemical composition of the surface over a wide range.

6.1. Introduction

Controlling the wettability of solid surfaces is of abiding importance for many processes in living organisms (e.g., ultra-water-repellent materials are found in self-cleaning surfaces of plants and insects [Bar97]) and for numerous industrial applications [Oga93, Tad97, Tsuj97, Nak99, Veer97, Youn99, Cou00, Cre99, Lai92, Sin97, Zhao95, Zhao00]. Advantages of ultra-hydrophobic surfaces, however, can turn into disadvantages: the self-cleaning properties of a surface may result in static electric charges, poor adhesion or dyeability. The ability to reversibly switch the properties of the *same material* from strongly water-repellent to hydrophilic would allow a diverse range of applications. In general, however, polymer surface has fixed properties and the design of switchable coatings is a formidable challenge [Cre99, Lai92].

Wettability can be regulated by chemical surface composition [Man97, Wen36, Bor95]. On a flat polymer film the contact angle of a liquid drop is determined by the balance of tensions at the contact line between the polymer film, the liquid and its vapor which results in Young's equation:

$$\cos\Theta_0 = (\gamma_{sv} - \gamma_{sl}) / \gamma$$

where Θ_0 is the bare contact angle of water (on a flat surface), γ is the surface tension of water, γ_{vs} and γ_{ls} are the surface tension of the solid-vapor and the solid-liquid (water) interface, respectively. Roughness of the surface can strongly amplify hydrophobicity or hydrophilicity [Wen36, Bor95, Bico99, Her00, Chen99, Cart00, Miwa00, Onda96, Bico01, Yos02, Muel02]. If the bare contact angle on a flat surface is very small, the liquid might fill the grooves of the rough surface and only the upper part of the relief, which comprises a fraction ϕ_s of the total area, is not in contact with the liquid. This occurs if the situation corresponds to wicking criteria [Bico01] (Figure 6.1). r denotes the ratio between the increased contact area of the rough surface and the corresponding projected area.

$$\cos\Theta_0 > (1-\phi_s)/(r-\phi_s)$$

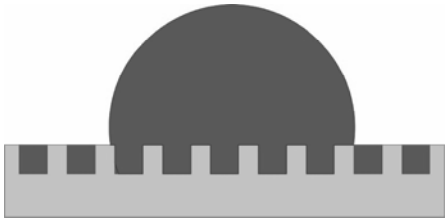

Figure 6.1 Wicking regime for a liquid drop on a rough solid surface.

If the bare contact angle is smaller than 90^0 but the wicking criteria is not fulfilled the liquid fills the grooves of the rough surface only below a droplet (Figure 6.2), and Wenzel's equation [Wen36] holds which takes into account the increased contact area between the liquid and the surface, where Θ is contact angle of water on a rough surface.

$$\cos\Theta = r(\gamma_{vs} - \gamma_{ls})/\gamma = r\cos\Theta_0$$

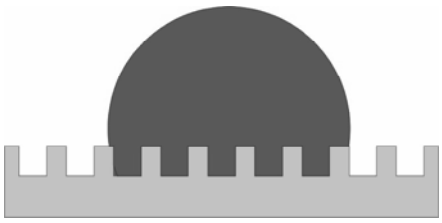

Figure 6.2. Wenzel's wetting regime for a liquid drop on a rough solid surface.

If the bare contact angle is larger than 90^0 (Figure 6.3), air can be trapped below a drop and the rough surface acts like a "fakir carpet" [Bico99] , i.e. the liquid is only in contact with the upper part of the relief of the rough surface. In this limit (Cassie regime [Cas44]) the contact angle is given by:

$$\cos\Theta = -1 + \phi_s(1+\cos\Theta_0)$$

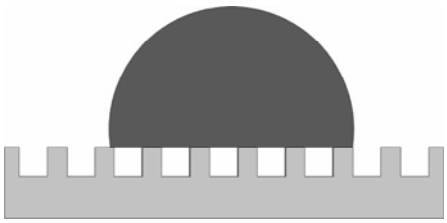

Figure 6.3 Cassie' regime: the suspended droplet sits on the crests of the rough pattern.

where ϕ_s is the fraction of the upper part of the relief, which itself depends on Θ_0. Superhydrophobic surfaces [Bico99, Her00, Chen99, Cart00, Miwa00, Onda96, Bico01, Yos02, Muel02] often possess surface textures which trap air between the liquid and the surface.

Thus, the ability of a surface to repel a liquid or to make it spread can be tuned by the surface design. For a fixed liquid (e.g., water), wettability may be regulated by an appropriate surface texture and/or by ($\gamma_{vs} - \gamma_{ls}$) value. Careful studies on model surfaces [Bico99, Her00, Chen99, Cart00, Miwa00, Onda96, Bico01, Yos02, Muel02], which consist of regular structures like spikes, pillars or stripes, reveal that if the contact angle on a flat surface is less than 90° the roughness amplifies hydrophilicity, while it enhances hydrophobicity otherwise. Very similar mechanism is also employed in biological systems (e.g., plant leaves [Bar97]). Details, however, depend on the geometrical properties of the surface as well as on the ability of the structures to pin the three-phase contact line between liquid, vapor and substrate[Bico99, Chen99, Miwa00, Yos02].

In the present chapter we take advantage of the amplification of hydrophilicity or hydrophobicity by the roughness of an etched substrate. It is shown that wettability is amplified by rather irregular structure of the plasma etched surface. The combination of controlling of the wetting properties of mixed polymer brushes and its strong amplification by the roughness enables to effectively fabricate surfaces with a wide span of reversibly tunable surface properties.

6.2. Materials

Polytetrafluoroethylene (PTFE) foils, 0.5mm thick, were purchased from PTFE Nünchritz GmbH, Germany. The material as recieved was cut into pieces of 2 x 2 cm^2 and subsequently cleaned in $CHCl_3$ for 10 min using an ultrasonic bath to remove any contaminants.

Highly polished silicon wafers (obtained from Wacker-Chemitronics) were first cleaned in an ultrasonic bath for 30 min with dichloromethane, placed in cleaning solution (prepared from NH_4OH and H_2O_2) at 60 ^{0}C for 1 h and then rinsed several times with Millipore water (18 $M\Omega\times cm^{-1}$).

Carboxyl-terminated poly(styrene-co-2,3,4,5,6-pentafluorostyrene) (PSF-COOH) (styrene units : pentafluorostyrene units = 0.75 : 0.25) (M_n=16000 g/mol, M_w=29500 g/mol) was synthesized by free radical polymerization in THF solution using 4-4′-azobis(4-cyanopentanoic acid) as initiator.

Carboxyl-terminated poly(2-vinyl pyridine) (PVP-COOH; M_n = 39200 g/mol and M_w = 41500 g/mol) was purchased from Polymer Source, Inc (synthesized by anionic polymerization).

Toluene and tetrahydrofuran (THF) were distilled after drying over sodium. Dichloromethane was dried on molecular sieves. 3-glycidoxypropyl trimethoxysilane (GPS) ABCR (Karlsruhe, Germany) was used as received.

Oxygen and ammonia for plasma treatment with purity of 99.95% and 99.999% respectively were purchased from Messer Griesheim, Germany.

6.3. Plasma treatment of PTFE substrates.

Plasma etching of PTFE was performed in a cylindrical vacuum chamber made of stainless steel with a diameter of 250 mm and a height of 250 mm. The base pressure obtained with a turbomolecular pump was kept at $<10^{-6}$ mbar. Oxygen was introduced into the chamber via a gas flow control system. The samples were introduced by a load-lock-system and placed on an aluminum holder near the center of the chamber which was coupled capacitively to a 13.56 MHz radio frequency (RF) generator Caesar 136 (Dressler, Germany) via an automatic matching network. The metallic wall of the whole chamber worked as a grounded electrode, i.e. the electrode configuration was higly asymmetric causing significant self bias voltages and ion energies at the RF electrode . The following parameters were used: oxygen flow 10 sccm, pressure 2 x 10^{-2} mbar, effective RF power 200 W. The resulting self bias voltage as displayed at the RF generator was approximately 1000 V. After plasma etching the samples were rinsed in an ultrasonic bath for 10 min in $CHCl_3$.

Ammonia plasma treatment of PTFE was carried out in a cylindrical vacuum chamber made of stainless steel with a diameter of 350 mm and a height of 350 mm. The base pressure obtained with a turbomolecular pump was $<10^{-7}$ mbar. On the top of the chamber a 2,46 GHz electron cyclotron resonance (ECR) plasma source RR160 (Roth&Rau, Germany) with a diameter of 160mm and a maximum power of 800 W was mounted. Ammonia was introduced into the active volume of the plasma source via a gas flow control system.

The samples were introduced by a load-lock-system and placed on a grounded aluminum holder near the center of the chamber. The distance between the sample and the excitation volume of the plasma source was of about 200 mm. The following parameters were used: ammonia flow 15 sccm, pressure 7 x 10^{-3} mbar, power 220 W, treament time varied from 20 s up to 120 s.

6.4. Preparation of the binary brushes.

Polymer chains of PSF-COOH and PVP-COOH were attached to the PTFE substrate by end functional groups (See also Scheme 4.3 in the Section 4.5). Hydroxyl and amino functional groups, introduced covalently by ammonia plasma treatment into the PTFE surface, were used to graft the mixed polymer brush. The brush was fabricated using a two-step "grafting to" procedure based on the "grafting to" approach suggested by Luzinov et al. [Luz00a, Luz00b]. In the first step, a thin film of PSF-COOH was spin-coated on the surface of the PTFE foil and heated for six hours at 150°C to graft the polymer from melt. Non-grafted polymer was removed with Soxhlet extraction and the second polymer PVP-COOH was grafted using the same procedure.

The amount of grafted polymer on the rough surface of PTFE substrate can not be determined. However, we performed control experiments on the surface of Si-wafers with covalently attached GPS. Epoxy groups of GPS were transformed to amino-groups by treatments with ethylenediamine. In this way we prepared a model surface modified with hydroxyl and amino gropus. The control experiments show that under these conditions about 3.5 mg/m^2 of each polymer can be grafted onto the Si-wafer which corresponds to the total thickness of 7 nm for the mixed polymer brush.

6.5. Sample Characterization.

6.5.1. Ellipsometry.

Layer thickness and grafted amount in the control experiments on Si-wafers were evaluated at λ=633 nm and an angle of incidence of 70° with Multiscope Optrel (Berlin, Germany). The measurements were performed for each sample and after each step of the modification. The measurements of the previous steps were used as a reference for the simulation of the ellipsometric data as it is described elsewhere [Luz00a, Luz00c].

6.5.2. SEM

The surface topography was investigated using scanning electron microscopy (SEM) and scanning force microscopy (SFM). SEM micrographs were obtained without

metallization of the sample at a beam voltage of 1 kV with a low voltage scanning electron microscope Gemini LEO/ DSM 982.

6.5.3. AFM

SFM experiments were carried out under ambient conditions using a Dimension 3100 of Veeco/ Digital Instruments, Inc., Santa Barbara, USA. The SFM was used in tapping mode to reduce tip induced surface degradation and to avoid sample damages. Standard and ultra sharp silicon tips were used with a resonance frequency of 300 kHz and 60 kHz, respectively. The surface root mean square (rms) roughness values S_q were determined using a scan size area of 20 x 20 μm^2 and a commercial software. According to the definition of the standard deviation of the elevation, z values, within the given area and is calculated from

$$S_q = \sqrt{\frac{1}{MN} * \sum_{j=1}^{N}\sum_{i=1}^{M}\left|Z^2(x_i; y_j)\right|} \qquad (6.1)$$

The rms roughness describes only structures vertical to the surface. However, the surface topography consists of both, vertical and lateral structures. To include also the lateral distribution of the height features, the power spectral density function (PSD) was determined from radially integrated 2d FFT images. The PSD is interpreted as a spatial frequency analysis of the surface topography. The PSD intensity describes the probability of a spatial frequency q. Thus, a peak on the PSD plot corresponds to a most prominent frequency which is related to a dominant in-plane length λ using the relationship

$$\lambda = 2\pi/q \qquad (6.2)$$

In addition, a roughness coefficient r_s was calculated

$$r_S = \frac{\text{actual surface area}}{\text{geometric surface area}} \qquad (6.3)$$

characterizing the ratio of the actual surface area and the geometric surface area. The r_s parameter implies both vertical and lateral changes of the roughness features.

Images of the PTFE surfaces were obtained at three different locations and the average rms and r_s roughness was determined for a particular surface-treated PTFE sample based on these images from three different locations. The surface roughness was also quantified using

section analysis. We obtain vertical distance (depth), horizontal distance, angle between two or more points, and roughness along a section line.

6.5.4. XPS

Changes of the elemental surface composition of the treated samples were examined using X- ray photoelectron spectroscopy (XPS). An Axis Ultra spectrometer (Kratos Analytical, UK) equipped with a monochromatized Al K_α X-ray source of 300 W at 15 kV was used. The kinetic energy of photoelectrons was determined using a hemispherical analyzer with a constant pass energy of 160 eV for survey spectra and 20 eV for high-resolution spectra. The take-off angle, here defined as the angle between normal of the sample surface and the electronoptical axis of the spectrometer, was 0°. Hence, the information depth of XPS was limited by 5 nm. An effective charge compensation unit over-compensating charging effects was used during all measurements. Spectra were referenced to the C 1s peak of the $–CF_2–$ structure in PTFE at binding energy BE=292.48 eV. Quantitative elemental compositions were determined from peak areas using experimentally determined sensitivity factors and the spectrometer transmission function.

6.5.5. Contact Angle Measurements

The modified surface wettability was characterized by contact angle measurements using sessile water droplets. Two techniques were applied, a goniometer technique and axisymmetric drop shape analysis-profile (ADSA-P). Using Krüss goniometer DSA10 advancing (θ_a) and receding (θ_r) contact angles from 6 individual drops placed on 6 new surface areas were measured by adding or withdrawing a small volume of water through a syringe. The needle was maintained in contact with the drop during the experiments. All readings were then averaged to give a mean advancing and receding contact angle for each sample. The accuracy of this technique is in the order of ± 2°. ADSA-P is a technique to determine liquid-fluid interfacial tensions and contact angles from the shape of axisymmetric menisci, i.e., from sessile as well as pendant drops. Details of the methodology and experimental set-up can be found in the Section 3.4.4. and elsewhere [Kwo97].

Low-rate dynamic contact angle measurements were carried out supplying liquid to the sessile drop from below the solid surface using a motorized syringe device. It is a good strategy first to deposit a drop of liquid on a given solid surface covering a small hole, which is needed to supply liquid from below. This experimental procedure is necessary since ADSA

determines the contact angles based on a complete and undisturbed drop profile. Compared to the goniometer technique, the accuracy of the contact angle measurement is distinctly higher (± 0.5°). While the drop is growing at very slow motion of the three-phase contact line, a sequence of images is recorded by the computer (typically 1 image every 2-5 seconds). Since ADSA-P determines the contact angle and the three-phase contact radius simultaneously for each image, the advancing dynamic contact angles as a function of the three-phase contact radius (i.e., location on the surface) can be obtained. Furthermore, the drop volume and the liquid surface tension are determined for each image, and can also be recorded. If the polymer surface is not very smooth or other complexities due to swelling, stick/slip, etc. occur, irregular and inconsistent contact angle or liquid surface tension values, respectively, will be seen as a function of the three-phase contact radius. Details of the procedure and the experimental set-up for low-rate dynamic contact angle measurements are given elsewhere [Kwo97, Aug98]. During the experiments the temperature and relative humidity were maintained, respectively, at (23 ± 0.5)°C and about 40%.

6.5.6. FTIR-ATR

Fourier transform infrared spectroscopic measurements in the attenuated total reflection mode spectra were taken with IFS 55 (Bruker) spectrometer.

6.6. Results and Discussion

The approach for the design and the fabrication of two-level structured surfaces, which are capable of reversibly switching from hydrophilic to ultra-hydrophobic states upon external stimuli (solvent selectivity, acidity, or temperature), is outlined in Figure 6.4.

PTFE film with roughness on the micrometer scale was produced using plasma etching. Then, the "grafting to" technique was employed to synthesize a mixed polymer brush [Luz00a, Luz00c] onto this rough surface. The mixed brush forms domains of nanometer size and its (average) surface composition stems from an intricate interplay between lateral and perpendicular segregation [Min02a, Min01, Sid99a]. Exposing this mixed brush to different environments, we can reversibly modify its surface properties, and the range of switching is substantially amplified by the needle-like, micrometer-roughness of the etched PTFE substrate.

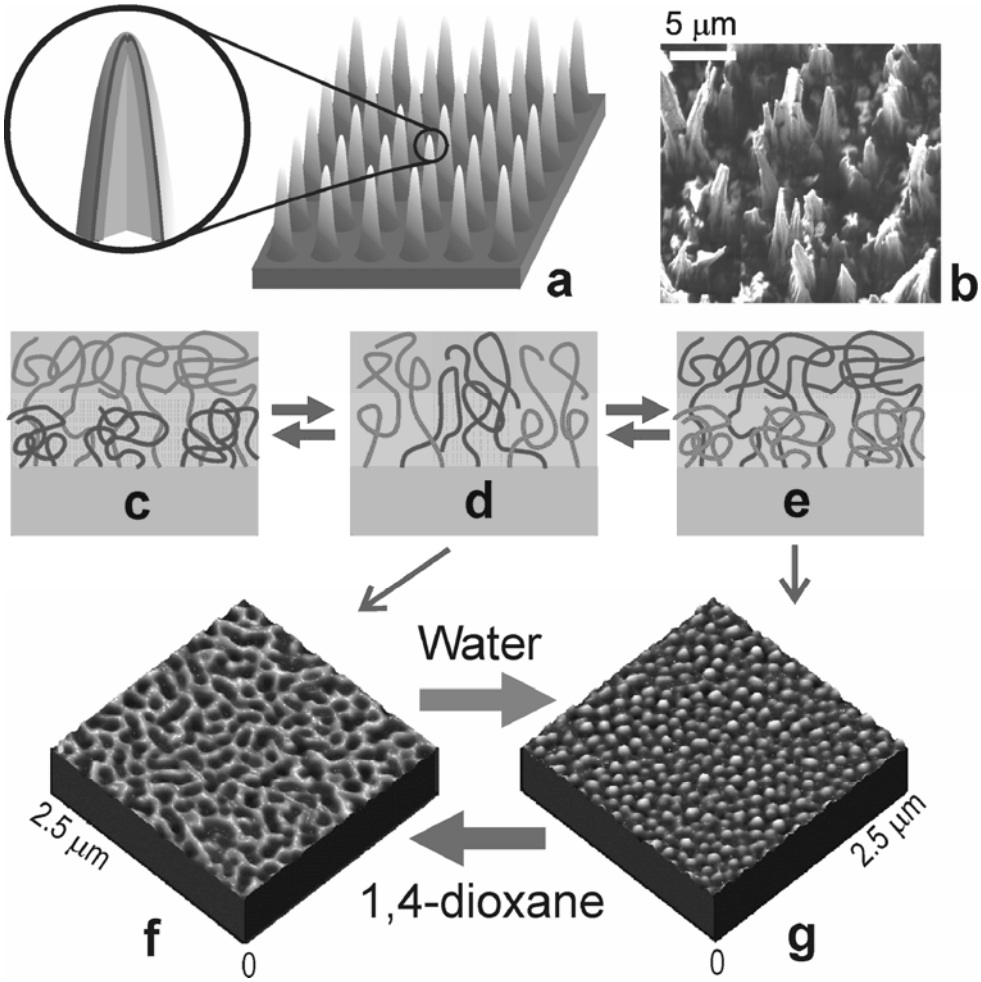

Figure 6.4. Two-level structure of self-adaptive surfaces (SAS): Schematic representation of needle-like surface morphology of the PTFE surface (first level) (a) and SEM image of the PTFE film after 600 s of plasma etching (b). Each needle is covered by a covalently grafted mixed brush which consists of hydrophobic and hydrophilic polymers (second level) depicted schematically in panel (c-e). Its morphology results from an interplay between lateral and vertical phase segregation of the polymers which switches the morphology and surface properties upon exposure to different solvents. In selective solvents the preferred polymers preferentially occupies a top of the surface (c and e), while in non-selective solvents, both of polymers are present in the top layer (d). The lower panels (f and g) show AFM images (model smooth substrate) of the different morphologies after exposition to different solvents.

The first step of the procedure comprises the fabrication of the composite surface with functional groups required for further modification steps. The radio-frequency oxygen plasma etching is used to create a rough PTFE surface with large scale features of 1-2 µm both in lateral as well as vertical dimensions.

The morphology of an untreated virgin PTFE surface and of O_2 plasma treated samples after different treatment times obtained by SEM is shown in Figure 6.5. All scanning electron micrographs have the same magnification. The untreated PTFE foil has a rough and to some extent porous surface. With increasing treatment time in oxygen plasma, the original morphology of the PTFE surface is changed and a pin-like surface structure is observed. For longer treatment times, the spires become gradually coarser and taller while the general appearence of the features is preserved. After 10 minutes treatment time, a widely spaced spire or cone-like structure of the PTFE surface is observed.

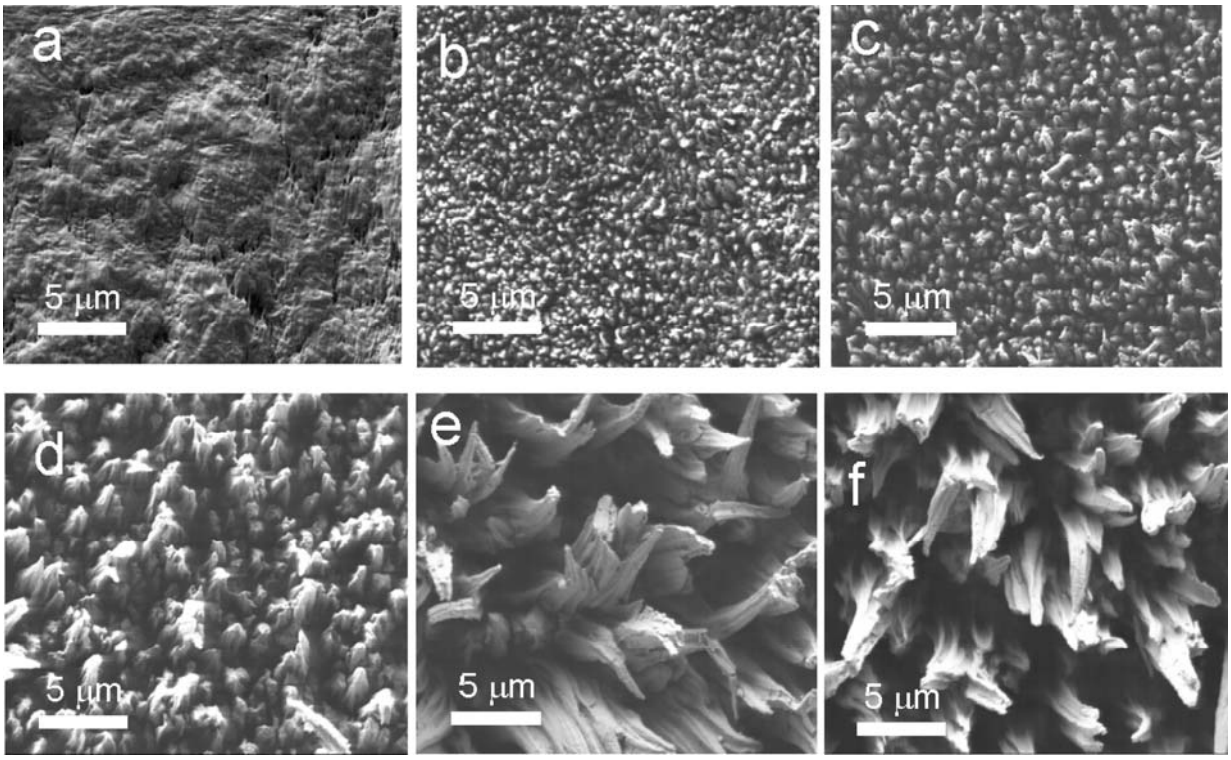

Figure 6.5 Scanning electron micrographs of PTFE foils: untreated (a), treated with oxygen plasma 60 s (b), 120 s (c), 5 min (d), 10 min (e), 10 min oxygen plasma + 1 min NH_3 (f).

The etched PTFE surfaces were additionally treated in ammonia plasma in order to functionalize these surfaces with reactive groups for a subsequent grafting procedure. As it is seen from the electron micrographs, no change in the surface morphology was observed.

The prolongation of etching time from 60 s to 300 s yields an increase of the surface roughness from 150 nm to 1 μm as measured by AFM (Figure 6.6) rms roughness values of the treated PTFE surfaces increase with increasing treatment time.

These values describe only roughness features vertical to the surface. To take into acount lateral distribution, we calculated the ratio between the actual surface area and the geometric surface area r_s. The dynamics of r_s value development is ploted in Figure 6.7.

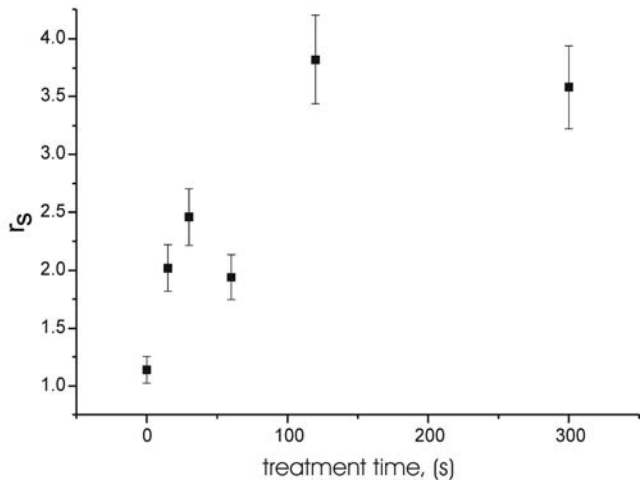

Figure 6.6. Plot of rms roughness of PTFE surfaces over the treatment time in oxygen plasma. Longer treatment time's results in even more gradually increase of roughness. After 10 minutes treatment time a widely spaced cone-like structure of the PTFE surface is observed

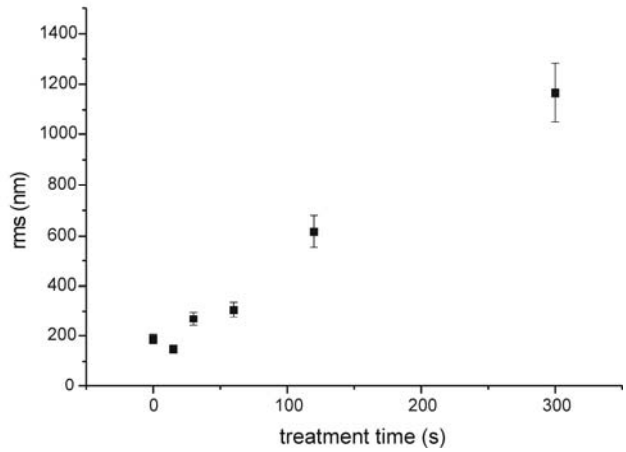

Figure 6.7 A plot of r_s roughness values of PTFE surfaces development with the treatment in oxygen plasma.

Based on the roughness development dynamics, we concluded that the actual surface area of the PTFE surface increases distinctly after very short treatment (15 sec). Up to a treatment time of 60 sec, the actual surface area does not change remarkably. During120 sec of treatment it increases again to distinctly higher values. From the fact that at longer treatment times (300 sec) the rms roughness values are strongly increasing while the r_s roughness is nearly constant we can conclude that the roughness features became coarser and widely spaced. This conclusion was also supported by an estimation of the dominant in-plane length λ, calculated from the power spectral density curves (PSD).

From the λ values shown in Table 6.1 it is apparent that the lateral distances between the roughness features increase up to a treatment time of 60 sec. A considerable increase is observed when the etching duration was increases from 60 sec to 120 sec and from 120 sec to 300 sec. A comparison between the different quantitative roughness values (rms, r_s, and λ) shows that all values start to increase considerably at a certain treatment time (60 sec → 120

sec). In other words, at this point the vertical height of the roughness features, their lateral distances and the actual surface area start to change considerably.

Table 6.1 Dominant in-plane length λ, calculated from the power spectral density curves (PSD) of SFM topography images obtained from PTFE surfaces after different treatment times in oxygen plasma

Treatment time (sec)	λ (q) (nm)	Δλ (nm)
15	806	
		324
30	1130	
		357
60	1487	
		1161
120	2648	
		2613
300	5261	

With regard to the general appearence of the morphology, SEM results indicates qualitatively a change in the roughness features from the original morphology to a more pin-like structure when the treatment time was increased from 30 sec to 60 sec (cf. Figure 6.5). However, the size of the needle-like features do not change remarkably from 30 sec to 60 sec as was shown by AFM.

XPS investigations of the oxygen plasma treated surfaces revealed only minor changes in the F/C ratio and only traces of oxygen as can be seen from Figures 6.8. 6.9. In accordance with results obtained by Garbassi et al. [Mor89], some increase in the oxygen content together with a fluorine depletion was only observed at short treatment times (Figure 6.9). The F/C ratio shows a minimum at a treatment time of 10 sec and develops to the expected value of F/C = 2 for longer treatment times. It is known that oxygen plasma promotes etching via preferential attack of the carbon-carbon bonds [Kim00].

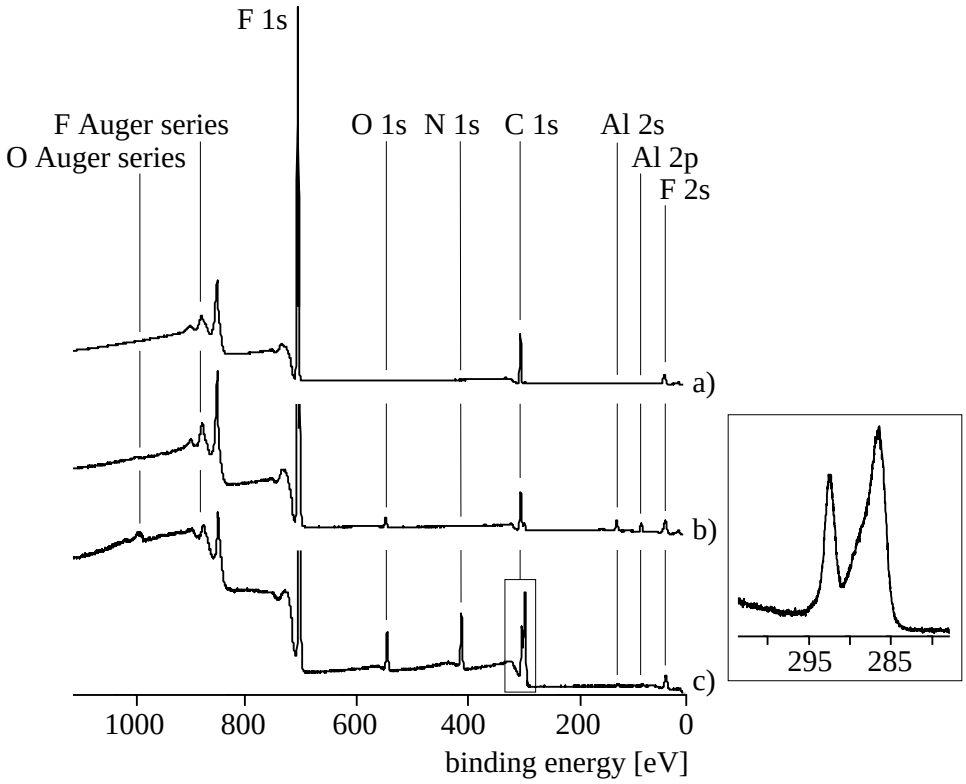

Figure 6.8. XPS survey spectra of PTFE: untreated (a), 600 sec oxygen plasma treated PTFE (b), plus 60 sec ammonia plasma treatment (the inset shows the high-resolution C 1s spectrum of sample) (c).

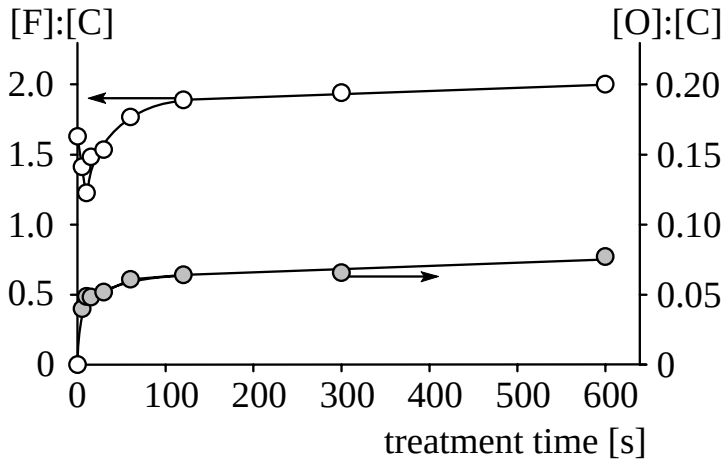

Figure 6.9. Elemental surface composition of the untreated and oxygen plasma treated PTFE samples with the treatment time; [F]:[C] (○), [O]:[C] (●).

High resolution C1s spectra of the oxygen plasma treated samples (Figure 6.10) show these structural changes. In addition to the characteristic CF_2 peak at 292.48 eV, an increased amount of CF_3 and CF groups is found at 294.3 eV and 290.6 eV, respectively, at the surface of the etched PTFE samples compared to the untreated surface. Hence, we concluded that the

oxygen plasma induces some chemical modification. But at longer treatment times, fast etching process predominates chemical surface modification resulting in morphology changes which was confirmed by SEM and SFM measurements. Due to the difference in plasma susceptibility of crystalline and amorphous polymer regions, crystalline regions etch more slowly than amorphous regions [Yas90, Dwi84, Dwi77].

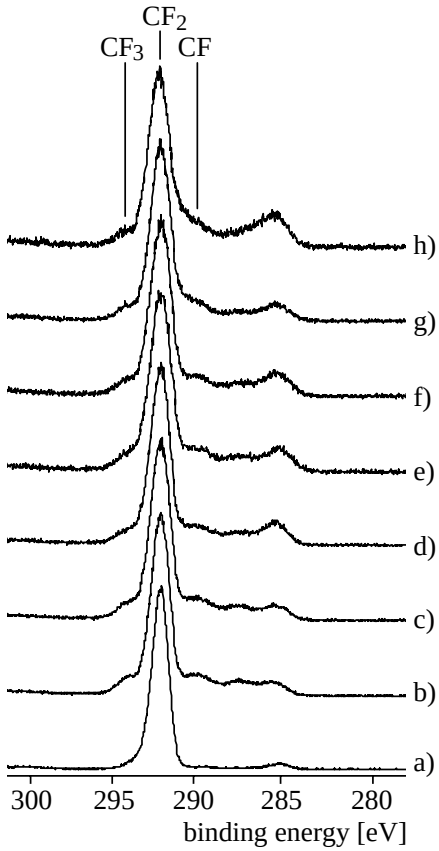

Figure 6.10 High-resolution C 1s spectra of untreated (a) and oxygen plasma treated PTFE; duration: 5 s (b), 15 s (c), 30 s (d), 60 s (e), 120 s (f), 300 s (g), and 600 s (h).

The survey spectrum together with the high-resolution C1s spectrum of a PTFE sample treated for 10 min by oxygen plasma and subsequently by ammonia plasma for 60 sec is shown in Figure 6.8c. Based on the quantitative analysis of O1s, N1s and C1s peaks of XPS spectrum, it can be concluded that amino groups and hydroxyl groups were incorporated covalently into the PTFE surface after ammonia plasma etching. Thus, we obtained rough functionalized PTFE surface.

To characterize the wetting behavior of the PTFE surfaces with water we carried out contact angle measurements using two sessile drop techniques, as described in Section 4.3.5

We obtained a composite surface with ultra-hydrophobic properties using plasma treatment. The large structures (at the micrometer scale) of the surface trap air below a drop of liquid. The drop sitting on the surface is in the contact with both solid surface and air.

Figure 6.11 shows a typical ADSA contact angle plot obtained for untreated and after 600 s O_2 plasma treated PTFE foils. When the drop volume V is increased (Figure 6.11a) the three-phase contact line starts to move and the contact radius R increases with a velocity of 0.19 mm/min while the advancing contact angle θ_a is nearly constant. The mean θ_a is calculated to be of 133° ± 0.1°. Then the volume of the drop is decreased constantly while the contact radius of the drop remains constant and the contact angle decreases. At a certain point, the contact line starts to recede and the contact angle becomes constant. A value of 98.7° was determined at that point. Obviously, the roughness of the untreated PTFE foil (rms ≈ 200 nm) causes this high contact angle.

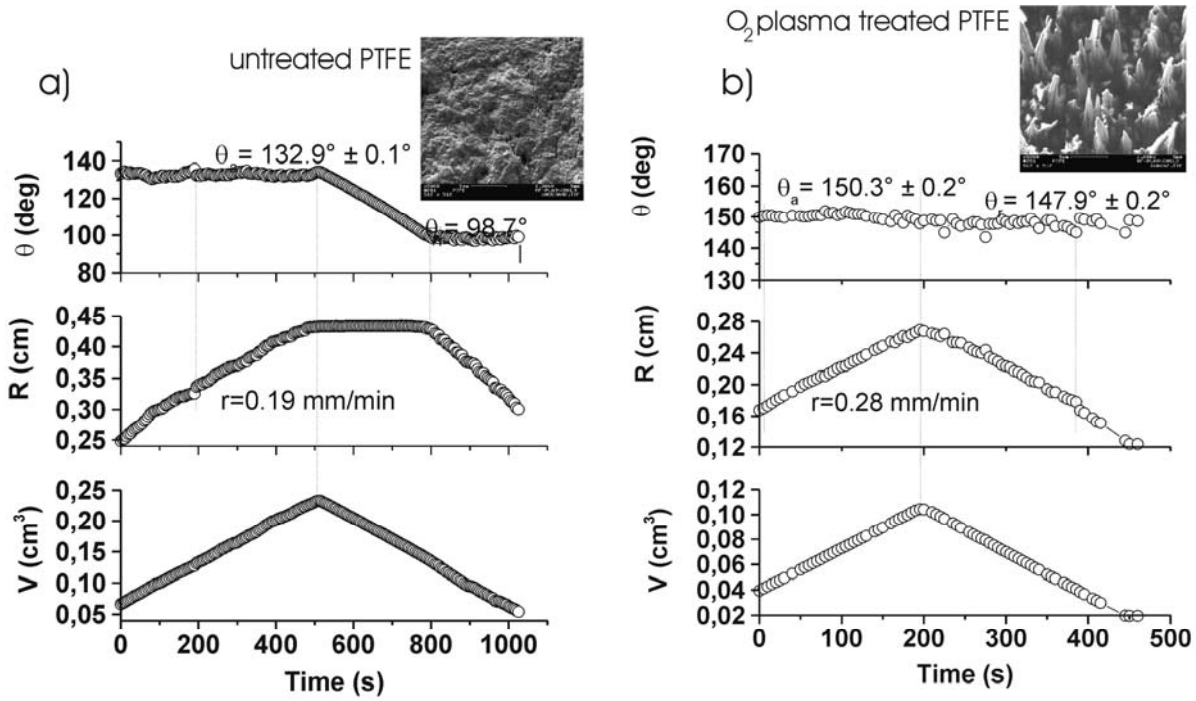

Figure 6.11 ADSA contact angle measurements of water on untreated (a) and oxygen plasma treated (600 sec) PTFE surfaces (b). θ is the contact angle, R is the contact radius of the sessile drop and V is the drop volume. Contrary to untreated surface, the contact radius starts to decrease immediately when the volume of the drop is decreasing indicating nearly no contact angle hysteresis for oxidized surface.

Longer treatment times cause an increase in the receding contact angle, while the advancing angle does not change significantly. After 600 sec very high advancing and

receding contact angles of about 150° up to 160° are found indicating nearly no contact angle hysteresis. From Figure 6.11b it can be seen that in this case the contact radius starts to decrease immediately when the volume of the drop is decreasing.

Afterwards, the PTFE samples were treated by micro-wave ammonium plasma for a short period of time (20 s). It was observed a some additional increase of the film roughness after this treatment. XPS spectra indicate the incorporation of amine groups into the surface (16% of nitrogen) (Figure 6.8c). Advancing and receding contact angles decrease substantially to 100° and 45°, respectively, showing large hysteresis (Figure 6.12).

The hydroxyl and amino functional groups, which have been introduced by the plasma treatment, are subsequently used to create the second level of surface structure: a mixed brush consisting of two carboxyl terminated incompatible polymers PSF-COOH and P2VP-COOH. The brush was fabricated using two-step "grafting to" procedure. In the first step, PSF-COOH was spin-coated on the surface of the PTFE film and heated for 6 hours at 150° C to graft the first polymer PSF-COOH from the melt. Non-grafted polymer was removed with Soxhlet extraction. Then, the second polymer P2VP-COOH was grafted using the same procedure. FTIR ATR spectra give evidence for the grafting of both polymers: characteristic bands of PSF-COOH (1601, 2923, and 3027 cm^{-1}) and PVP-COOH (1586 and 1590 cm^{-1}) are identified in the spectra. Quantitative evaluation using XPS and FTIR-ATR spectra gives the composition of the mixed brush 50:50 ± 10 %.

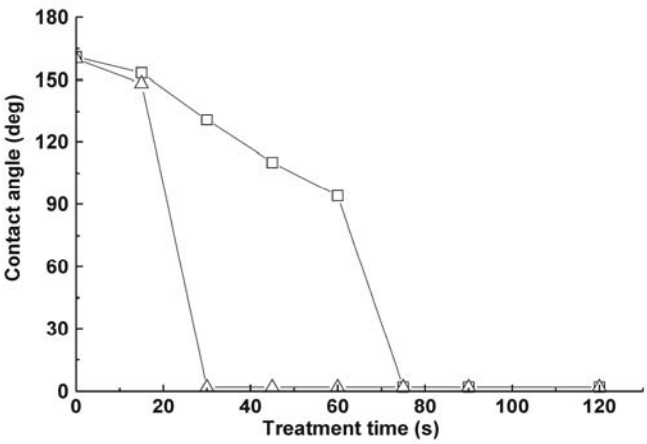

Figure 6.12. Advancing and receding water contact angles measured on surface treated PTFE foils as a function of the treatment time in ammonia plasma. The PTFE surfaces were etched in oxygen plasma for 600 sec and then treated with ammonia plasma.

A reference sample was also prepared using the same protocol except for a much shorter treatment (60s) in oxygen plasma which resulted in a surface roughness of less than 100 nm.

Covalent binding to the substrate surface prevents macrophase separation in the mixed brush and the chains self-assemble laterally into domains which are of the molecule (50 nm)

size[Muel02]. Simultaneously, the chains segregate perpendicular to the grafting surface. There is a subtle interplay between lateral and perpendicular segregation which affects the film morphology and its surface properties. This switching of morphology has been recently proved based on X-ray photoemission electron microscopy experiments [Min02b, Min01, Sid99a]. Exposure to a selective solvent results in enrichment of the favored component at the top of the polymer film, while the other component collapses into dense dimples in the interior of the polymer film (Figure 6.4c-e). On the other hand, P2VP builds round domains in the matrix of PSF (Figure 6.4g) upon exposure to toluene. The inverse situation is observed upon exposure to acid water (pH 3). In the latter case PSF forms clusters buried in the P2VP matrix. We observe lamellar-like domains of both polymers on the surface (Figure 6.4 f) upon exposure to 1,4-dioxane. Contact angle measurements confirm the switching of surface composition.

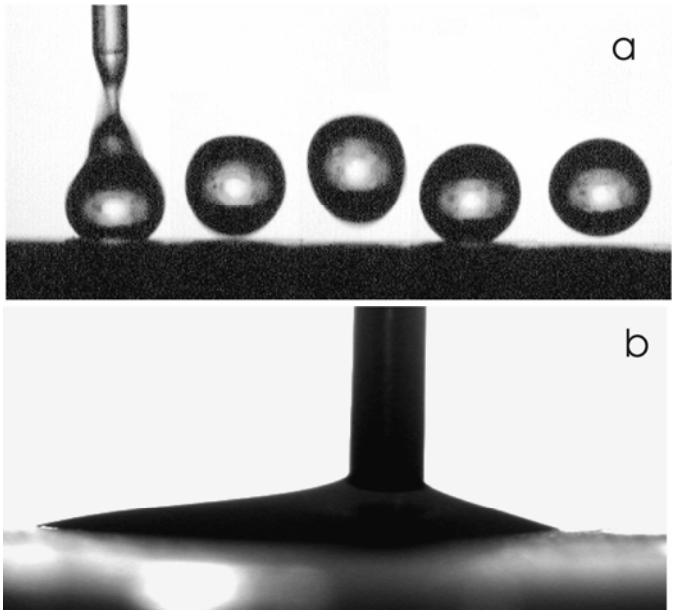

Figure 6.13. Photograph of a water drop deposited onto the SAS: the stroboscopic image shows that a water drop jumps and rolls on the ultra-hydrophobic surface obtained after exposure of the sample to toluene (a). In contrast, exposure to acidic water switches the sample to a hydrophilic state and the water drop spreads on the substrate (b).

The advancing contact angle of water on the control sample was measured to be 118° after exposure to toluene, 25° after exposure to water (pH 3), and 75° after exposure to 1,4-dioxane. In contrast, a much more pronounced modification of surface properties was observed for the two-level structured surface. An advancing contact angle of 160° was measured after exposure to toluene. A drop of water rolls easily on the surface, a fact that indicates also a very small hysteresis of the contact angle (Figure 6.13a). Afterwards, the same sample was immersed in acid water (pH 3) bath for several minutes and dried. However, a drop of water spreads on the surface because of the wicking effect (Figure 6.13b). These observations demonstrate the usefulness of combining large scale roughness (scale of micrometers) with the self-assembled structure of a binary polymer brush in the range of nanometers, and it reflects the "smart" properties of the self-adaptive surface (SAS). From Figure 6.14 it can be seen that switching

of wettability between θ_a=150°/θ_r=150° and θ=0° is completely reversible by dipping the sample in toluene and water (at pH=3), respectively.

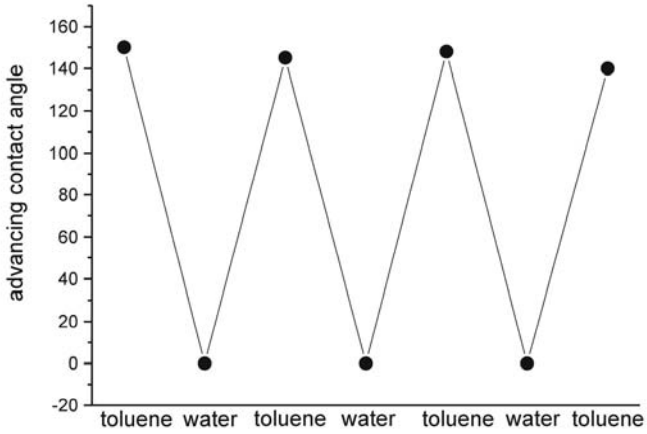

Figure 6.14 Reversible switching between ultra-hydrophobic and hydrophilic surface properties by dipping the PTFE sample with grafted PSF/P2VP binary brush in toluene and water (pH=3), respectively. The hydrophobicity/hydrophilicity is measured by water contact angles.

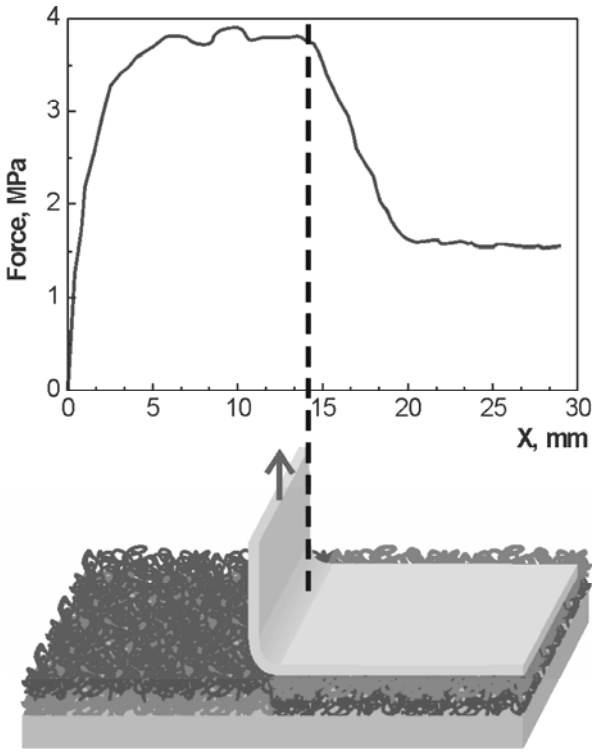

Figure 6.15. Switching adhesion with SAS: the plot presents the change of the force applied to the Tesa® band defoliated from SAS vs. distance (X) from the starting point. The dashed line marks the border between ultra-hydrophobic (black) and hydrophilic (gray) areas on SAS.

It is noteworthy that after the treatment with toluene the wetting hysteresis depends on the time of the water drop contact with the substrate. The difference between advancing and receding contact angles is within the error of the measurement (± 2°) after 30 sec while in several minutes the difference increases dramatically due to the slow switching of the surface composition to more hydrophilic state.

SAS can be employed for constructing sophisticated functional materials. Switching of SAS results in tuning of various kinds of interaction mechanisms with its surroundings. An

example of practical importance are van der Waals interactions which can be used to regulate adhesion.

As an illustration, a simple adhesion test was performed in which the Tesa®-tape was glued to the plate with SAS. Half the plate is in the hydrophilic state and the other half is in the hydrophobic state. A sharp decrease of adhesion was observed, when we cross the border between the ultra-hydrophobic and hydrophilic areas on the sample (Figure 6.15).

6.7. Conclusions.

Plasma etching is a suitable technique to fabricate ultrahydrophobic polymer surfaces. To produce ultrahydrophobic PTFE surfaces with specifically designed surface roughness an interplay of the size scale of the roughness features, their morphology and the surface free energy are important. Contact angle hysteresis strongly depends on the geometrical nature of the roughness: a certain type of roughness rather than its absolute size is the determining factor to reach ultrahydrophobicity. “Composite” (air trapped) surfaces, with pin- or spire-like features and open spaces between them are necessary. To preserve ultrahydrophobicity, the size scale of the features regarding their vertical heights and lateral distances can vary from submicrometer to micron-scale roughness. The transition to ultrahydrophobicity can be shifted to a lower size scale of roughness by lowering the surface free energy.

We reversibly tuned the surface properties of PTFE by grafting demixed polymer brushes of PSF-COOH and PVP-COOH onto the structured surfaces. It results in a sharp transition of wettability from ultrahydrophobic to hydrophilic wetting behavior upon exposure to different solvents.

Summary and Outlook

Surfaces and interfaces play an important role in controlling the properties of a broad range of modern materials. Recent advances in the analytical techniques for surfaces have led to improved knowledge of material surfaces and interfaces. At the same time, synthetic and processing tools have been proved for a better control of surfaces and interfacial characteristics for specific applications.

The framework of this thesis aims to fabricate materials, which change surface characteristics in response to environmental conditions. This response may be employed to improve such material characteristics as adhesion, wettability, interaction with cells etc. One of the possible routes to approach this goal comprises the grafting of *mixed polymer brushes* onto the solid surface. The mixed brushes introduce adaptive and switching behavior in different surrounding media.

Mixed polymer brushes are an remarkable representative of the class of responsive materials and may find diverse applications for the development of smart materials, devices, sensors, imaging technologies, adaptive biomaterials, molecular lubricants etc. If a mixed brush of hydrophilic and hydrophobic homopolymers is exposed to a hydrophilic solvent the hydrophilic component preferentially segregates to the top of the film and the surface becomes hydrophilic. Exposing the same brush to a hydrophobic solvent reversibly switches the surface from hydrophilic to hydrophobic state. The phase behavior of mixed brushes is determined by competition of the mixing entropy and elastic behavior of polymer chains. Anchoring of the polymer chains prevents macroscopic segregation of incompatible species. By this mean, two main approaches were employed to fabricate mixed polymer brushes: *"grafting to"* and *"grafting from"*.

The main difference between the fabrication of mono and mixed (binary) brushes is introduced by two times repeating grafting procedure, when the grafting of the first polymer is followed by the grafting of the second polymer. Block copolymers with anchoring groups were also grafted to fabricate mixed polymer brushes with similar switchable behavior.

Applying different surface modification approaches mixed PS/PVP polymer brushes were synthesized via step-by-step grafting of these two polymers from polyamide (PA) surfaces. The surface of PA should be functionalized to anchor the initiator of radical polymerization or to graft end functionalized polymer chains. We show that NH_3 plasma can be successfully used for the introduction of amino and OH functionalities on PA surfaces with following attachment of azo initiator of radical polymerizaton. The covalent bonding of the initiator improves the grafting procedure, although the chain transfer mechanism introduces also, but less effective, the mixed brush on the untreated PA surface.

The grafting procedure causes a substantial increase of the PA surface roughness, which we explain by banding of the swollen PA substrate during grafting procedure. We found no deep penetration of the grafting process into the PA substarte and proved that the surface roughness is driven by grafting events occurring on the very top layer of the substrate.

The mixed brushes prepared on the surface of PA textiles combine both the switching effect and effect of composite surface (i.e. micrometer scale roughness) which substantially amplifies the switching range.

The vitality tests have shown that the grafted binary polymer brushes improve the adhesion of fibrolasts and endothel cells to the modified PA textiles. This effect can be used for the further application of the binary brush modified materials.

We used also another approach for fabrication of mixed polymer brushes on silica surfaces. Mixed polymer brushes prepared from P(S-b-2VP-b-EO) and P(S-b-4VP) block copolymers were grafted to both the flat surface (Si wafers) and to the surface of silica nanoparticles via quaternization reaction of the pyridine nitrogen. This one step grafting technique has a substantial advantage over the multistep grafting of mixed polymer brushes consisting of two incompatible polymers.

Nanoparticles with grafted mixed brushes may be used for the fabrication of coatings with switching behavior.

Reversibly tuning of the surface wetting behavior can be performed with mixed brushes in a broad range of contact angle values. Surface texture may strongly amplify the switching effect between wetting and non-wetting states. We have demonstrated that combination of the two level hierarchical organization of polymer films at macroscopic and nanoscopic levels resulted in the formation of self adaptive surfaces switchable in controlled

environment from ultra-hydrophobic to hydrophilic energetic states. The PFS/PVP mixed brush was grafted onto the pre-treated PTFE surface (plasma etching) with the needle like topography. The size of vertical needles was at micron scale. If the brush was switched to the hydrophobic state upon exposure to toluene the layer has shown a unique ultra-hydrophobic behavior (complete non-wetting) with the contact angle approaching value of 160°. If the mixed brush was switched into the hydrophilic state upon exposure to acidic water, the surface became completely wetted due to the capillary forces in the pores formed by the needle like structure. Thus, the surface can be either highly wettable or completely non-wettable with the self cleaning properties.

In conclusion, we obtained a series of results related to reversible changes in structural organization and surface morphology of polymeric systems composed of grafted polymer brushes of different types. We demonstrated how the changes of structural organization results in dramatic alterations of surface properties. These properties can be controlled by external stimuli and, therefore, these surfaces can be used as both sensing and active elements responsive to environmental conditions.

References

[ABCR] ABCR, Gelest 2000. *Silanes, Silicones and Metal-Organics Catalog*. Copyright Gelest, Inc.**1998**

[Advi02] Advincula, R.; Zhou, Q.; Park, M.; Wang, S.; Mays, J.; Sakellariou, G.; Pispas, S.; Hadjichristidis, N.; *Langmuir,* **2002**; *18,* 8672-8684

[Aks96] Aksay, A.; Trau, M.; Manne, S.; Honma, I.; Yao, N.; Zhou, L.; Fenter, P.; Eisenberger, P. M.; Gruner, S. M. *Science* **1996**, *273*, 892-894.

[Ale77] Alexander, S. J. *J. Phys (Paris),* **1977**, *38*, 977

[Ale91] Alexander S. J. *J. Phys (Paris)* **1977**, *38*, 983-987. (b) Milner, S. T. *Science* **1991**, *251*, 905-914

[All81] Allain, C.; Ausserr, D.; Rondelez, F. . *Phys Rev Lett,* **1981**, *49*, 1694

[Ami93] Amiji, M.; Park, K. J. *Biomater. Sci. Polym. Ed.* **1993**, *4*, 217

[Aug98] A. Augsburg, K. Grundke, K. Pöschel, H.-J. Jacobasch, A. W. Neumann, *Acta Polymerica* **49**, 417-426 (1998).

[Aur91] Auroy, P.; Auvray, L.; Leger, L. *Phys Rev Lett,* **1991**, *66*, 719

[Azz77] Azzam, R. M. A.; Bashara, N. M. *Ellipsometry and Polarized Light*, 1st edition, North-Holland Publishing Company: Amsterdam, New York, Oxford, 1977

[Bar97] Barthlott, W.; Neinhuis, C. *Planta* **1997**, *202*, 1-8

[Baum02] Baum, M.; Brittain, W. J.; *Macromolecules;* **2002**; *35,* 610-615

[Bea98] Beamson, G.; Briggs, D. *Surf. Interface Anal*. **1998** 26, 343

[Ber91] Bergbreiter, David E.; Kabza, Konrad. Journal of the American Chemical Society (1991), 113(4), 1447

[Ber94] Bergbreiter, D. E. Prog. Polym. Sci. 1994, 19, 529

[Ber98] Bergbreiter, D. E.; Walchuk, B.; Holtzman, B.; Gray, H. N.; Macromolecules; 1998; 31(11); 3417

[Berm98] Berman, A.; Steinberg, S.; Campbell, S.; Ulman, A.; Israelachvili, J. N. *Tribol. Lett*. **1998**, *4*, 43-48

[Bhu97] *Micro/Nanotribology and Its Applications* Eds: B. Bhushan, Kluwer Press, **1997**

[Bhu98] *Tribology Issues and Opportunities in MEMS* (Eds: B. Bhushan), Kluwer Academic Publ., Dordrecht, **1998**

[Bic01] Bico, J.; Rordeux C.; Quéré, D. *Europhys. Lett.* **2001,** *47*, 220

[Bic99] Bico, J.; Marzolin, C.; Quéré, D. *Europhys. Lett.* **1999,** *47*, 220

[Bir00] Birstein, T. M.; Amoskov, V. M. *Polym. Sci.* **2000**, *C42*, 172

[Bli98] V. N. Bliznyuk, M. P. Everson, V. V. Tsukruk *J. Tribology, 120,* 489, 1998

[Bor95] Borgs, C.; Conninck, J.D.; Kotecky, R.; Zinque, M. *Phys. Rev. Lett.* **1995**, *74*, 2292

[Bov90] Boven, G; Oosterling, M; Challa, G.; Shouten, A. J. *Polymer*, **1990**, *31*, 2377-2382

[Bri77] D.Briggs. ed., "Handbook of X-ray and Ultraviolet Photoelectron Spectroscopy", **1977**, Lheyden, London

[Bri82] Briggs, in., „Surface Analysis and Pretreatment of Plastics and Metals", D. M. Brewis ed., **1982**, Macmillan, New York, 73

[Bri98] Briggs, D. *Surface Analysis of Polymers by XPS and SIMS*, Cambridge University Press: Cambridge, 1998

[Can81] Cantor, R. *Macromolecules,* **1981**, *11*, 1186(a32)

[Car00] Carey, Deborah H.; Grunzinger, Stephen J.; Ferguson, Gregory S. Macromolecules (2000), 33(23), 8802

[Cart00] McCarthy, T. J., Oner, D.; *Langmuir* **2000**, *16*, 7777 -7782

[Car96] Carey, Deborah H.; Ferguson, Gregory S. Journal of the American Chemical Society (1996), 118(40), 9780

[Cas44] Cassie, A B.D.; Baxter, S. *Trans Farad Soc* **1944,** *40*, 546-551.

[Chan93] Chan C-M, Polymer surface modification and characterization, Hanser, Munich-Vienna-New York 1993

[Chan96] Chan, C. M.; Ko, T. M.; Hiraoka, H. *Surface Sci. Reports* **1996**, *24*, 1-54

[Chen99] Chen, W.; Fadeev, A. Y.; Hsieh, C.; Oner, D.; Youngblood, J.; McCarthy, T. J. *Langmuir* **1999**, *15*, 3395-3999

[Cla66] Clayfield, E. J.; Lumb, E. C. *J. Colloid. Sci.,* **1966**, *22*, 269

[Cos87] Cosgrove, T.; Heath, T. G.; Ryan, K.; Crowley, T. L. *Macromolecules,* **1987**, *20*, 1361

[Cos90] Cosgrove, T.; Ryan, K.; . *Langmuir,* **1990**, *6*, 136178

[Cou00] Coulson, S.; Woodward, I.; Badyal, J.P.S.; Brewer, S. A.; Willis, C. *J. Phys. Chem.* **2000**, *104*, 8836-8840.

[Cre03] C. Creton, MRS Bull., 28, 434, 2003

[Cre99] de Crevoisier, G.; Fabre, P.;. Corpart, J.-M.; Leibler, L. *Science* **1999**, *285*, 1246

[DI99] Digital Instruments, Veeco Metrology Group, *Training Notebook*, rev. 3.0, 1999

[Dwi77] D. W. Dwight in: Characterization of Metal and Polymer Surfaces (Ed. L. H. Lee), Vol. 2, Academic Press, p. 313 (1977).

[Dwi84] D. W. Dwight, S. R. F. McCartney, Org. Coat., Appl. Polym. Sci. (Am. Chem. Soc.) **50**, 459 (1984)

[Eja03] M. Ejaz, K. Ohno, Y. Tsujii, T. Fukuda Polymer Preprints, 2003, 44, 532-533.

[Fav96] Favia, P.; Stendardo, M. V.; d'Agostino, R. *Plasmas and Polymers*, **1996**,*1*, 91-105

[Flo81] Flory, P. J. Principles of polymer chemistry. Ithaka, NY: Cornell university Press, 1981

[Fri81] U.P. Fringeli and Hs.H. Günthard, in ´*Membrane Spectroscopy*´, E. Grell (ed), 270-332, Springer, Berlin (1981) & U.P. Fringeli, in ´*Encyclopedia of Spectroscopy and Spectrometry*´, J.C. Lindon, G.E. Tranter, J.L. Holmes (eds), Academic Press (2000)

[Fuo48] Fuoss, R. M.; Strass, U. P. *Journal of Polymer Scienece,* **1948,** *2*, 247-263

[Gen00] Genzer, Jan; Efimenko, Kirill. Science (Washington, D. C.) (2000), 290(5499), 2130

[Gen76] de Gennes. *J. Phys (Paris),* **1976**, *37*, 1443

[Gen80] de Gennes. *Macromolecules,* **1980**, *13*, 1069

[Gon98] Gong, L.; Friend, A. D.; Wool, R. P. *Macromolecules* **1998**, *31*, 3706-3714

[Goo92] Good, R. J.; van Oss, C. J. in *Modern Approaches to Wettabillity*, Schrader, M. E., Loeb, G. I., Eds.; Plenum Press, New York, 1992

[Gra00] Graighead, H. G. *Science* **2000**, *290*, 1532

[Gra93] Graham, R. L.; Bain, C. D.; Biebuyck, H. A.; Laibinis, P. E.; Whitesides, G. M. *J. Phys. Chem.* **1993**, 97, 9456.

[Guo99] Guo, X.; Weiss, A.; Ballauff, M. *Macromolecules* **1999**, *32*, 6043-6046.

[Hab99] Habicht, J.; Schmidt, M.; Ru¨ he, J.; Johannsmann, D. *Langmuir* **1999**, *15*, 2460-2465.

[Hal88] Halperin, A. *J. Phys (Paris),* **1988**, *49*, 547

[Hal92] Halperin, A.; Tirrell, M.; Lodge, T. P. *Adv. Polym. Sci.* **1992**, *100*,31-71

[Han88] Hansma, P. K.; Elings, V. B.; Marti, O.; Bracker, C. E. *Science* **1988**, *242*, 209

[Har67] N. J. Harrick, *Internal Reflection Spectroscopy*, Wiley, New York (1967)

[Her00] Herminghaus, S. *Europhys. Lett.* **2000**, *52*, 165

[Hol87] Holmes-Farley, Stephen Randall; Reamey, Robert H.; Nuzzo, Ralph; McCarthy, Thomas J.; Whitesides, George M.. Dep. Chem., Harvard Univ., Cambridge, MA, USA. *Langmuir* (1987), 3(5), 799

[Hol88] Holmes-Farley, Stephen Randall; Bain, Colin D.; Whitesides, George M.. *Langmuir* (1988), 4(4), 921

[Hon02] Honigfort, M. E.; Brittain, W. J.; Bosanac, T.; Wilcox, C. S. *Macromolecules* **2002**, *35*, 4849-4851

[Hus00] Husseman, M.; Benoit, D. G.; Frommer, J.; Mate, M.;Hinsberg, W. D.; Hendrick, J. L.; Hawker, C. J. *J. Am. Chem. Soc.* **2000**,*122*, 1844-1845

[Ito97] Ito, J.; Ociai, Y.; Park, Y. S.; Imanishi, Y. *J. Am. Chem. Soc.* **1997**, *119*, 1619

[Iyer02] Iyer, K. S.; Klep, V.; Luzinov, I. *Polymer Preprint* **2002**, *43(1)*, 455

[Jih93] Ji, H.; de Gennes, P. G. *Macromolecules* **1993**, *26*, 520

[Jul03a] D. Julthongpiput, M. C. LeMieux, K. N. Bergman, V. V. Tsukruk Polymeric Materials: Science & Engineering 2003, 89, 342

[Jul03b] D. Julthongpiput, Y-H. Lin, J. Teng, E. R. Zubarev, V. V. Tsukruk*, Macromolecules,* submitted

[Kaw88] Kawaguchi, M.M Kawarabayashi, M.M Nagata, N.; Yoshioka, A.; Tagahashi, A. *. Macromolecules,* **1988**, *21*, 1059

[Kho01] Khongtong, Sureurg; Ferguson, Gregory S Journal of the American Chemical Society (2001), 123(15), 3588

[Kho02] Khongtong, Sureurg; Ferguson, Gregory S. Journal of the American Chemical Society (2002), 124(25), 7254

[Kim00] S. R. Kim, J. Appl. Polym. Sci. **77**, 1913-1920 (2000).

[Kit03] Kitaev, V.; Ozin, G. A. *Adv. Mater.***2003**, *15*, 75-78

[Kle03] V. Klep, S. Minko, I. Luzinov *Polym. Mater. Sci. Eng,* 2003, in press

[Kle94] Klein, J.; Kumacheva, E.; Mahalu, D.; Perahia, D.; Fetters, L. J. *Nature***1994**, *370*, 634-636.

[Kra02] Krausch, G.; Magerle, R. *Adv. Mater.* **2002**, *14*, 1579–1583

[Kwo97] D. Y. Kwok, T. Gietzelt, K. Grundke, H.-J. Jacobasch, A. W. Neumann, *Langmuir* **13**, 2880-2894 (1997) and references therein

[Kwo99] Kwok, D. Y.; Neumann, A. W. *Adv. Colloid Interface Sci*. **1999**, 81, 167

[Laf03] Lafuma, A.; Quere, D. *Nat. Mater.* **2003**, *2*, 457.

[Lai92] Laibinis, P. E.; Whitesides, G. M. *J. Am. Chem. Soc.* **1992**, *114*, 1990-1995

[Lam00] Lampitt, R. A.; Crowther, J. M.; Badyal, J. P. S.; J. Phys. Chem. B. ; 2000; 104(44); 10329

[Lem03a] Lemieux, M.; Usov, D.; Minko, S.; Stamm, M.; Shulha, H.; Tsukruk, V. V.;*Macromolecules;* **2003**; ASAP

[Lem03b] M. Lemieux, S. Minko, D. Usov, M. Stamm, V. V. Tsukruk *Langmuir*, 2003, *19*, 6126

[Lem03c] M. Lemieux, D. Usov, S. Minko, M. Stamm, V. V. Tsukruk, *Polymer Brushes*, Ed. W. Brittain, in press

[Luz00c] I. Luzinov, D. Julthongpiput, A. Liebmann-Vinson, T. Cregger, M. D. Foster, V. V. Tsukruk, *Langmuir*, *16*, 504, 2000

[Luz00b] Luzinov, I.; Julthongpiput, D.; Malz, H.; Pionteck, J.; Tsukruk, V. V. *Macromolecules* **2000**, *33*, 1043-1048

[Luz00a] Luzinov, I.; Julthongpiput, Liebmann-Vinson, A.; Cregger, T.; Foster, M. D.; Tsukruk, V. . *Langmuir*, **2000**, *16*, 504-516

[Luz03] I. Luzinov, K. Swaminatha Iyer, V. Klep, B. Zdyrko, J. Draper, Y. Liu Polymer Preprints 2003, 44, 437-438

[Luz96] Luzinov, I., Voronov, A., Minko, S., Kraus, R., Wilke, W., Zhuk, A. *J. Appl. Polym. Sci*. **1996**, *61*, 1101-1109

[Luz98] Luzinov, I., Minko, S., Senkovsky, V., Voronov, A., Hild, S., Marti, O, Wilke, W. *Macromolecules* **1998**, *31*, 3945-3952

[Mac51] Mackor, E. L. *. Colloid. Sci.,* **1951**, *6*, 492

[Mac52] Mackor, E. L.; Van der Waals, J. H. *Colloid. Sci.,* **1952**, *7*, 535

[Man95] Mansky, P.; Chaikin, P.; Thomas, E. L. *J. Mater. Sci.* **1995**, *30*, 1987–1992

[Man97] Mansky, P.; Liu, Y.; Huang, E.; Russell, T. P.; Hawker, C. J. *Science* **1997**, *275*, 1458-1460

[Mar91] F. Marko, T. A. Witten, *Phys. Rev. Lett*. **1991**, *66*, 1541

[Mat94] M. W. Matsen, M. Schick, *Phys. Rev. Lett*. **1994**, *72*, 2660

[Mat99] Matyjaszewski, K.; Miller, P. J.; Shukla, N.; Immaraporn, B.; Gelman, A.; Luokala, B. B.; Siclovan, T. M.; Kickelbick, G.; Vallant, T.; Hoffmann, H.; Pakula, T.; *Macromolecules;* **1999**; *32,*8716-8724

[Mei99] Meiert, P.; Schebden, R. A.; Caseri, W. R.; Suter, U. W. *Macromolecules* **1999**, 32, 3590-3596

[Mel03] Melburne C. Lemieux, Minko S, Usov D, Stamm M, and Vladimir V. Polymeric Materials: Science & Engineering **2003**, 89

[Men97] H. Menzel et al, Gummi, Fasern, Kunsts., *50*, 288, **1997**

[Mil88] Milner, S. T.; Whitten, T. A. *J. Phys (Paris),* **1988**, *49*, 1951

[Mil89] Milner, S. T.; Whitten, T. A.; Cates, M. E. *Macromolecules,* **1989**, *22*, 1951

[Mil91] Milner, S. T. *Science,* **1991**, *251*, 905

[Min00] Minko, S.; Stamm, M ; Goreshnik, E.; Usov, D.; Sidorenko, A. *Polym. Mater. Sci. Eng,* 2000, **83**, 533-534

[Min01] Minko, S., Usov, D., Goreshnik, E., Stamm, M. *Macromol. Rapid. Commun*., **2001**, *22*, 206-211

[Min02a] Minko, S.; Müller, M.; Usov, D.; Scholl, A.; Froeck, C.; Stamm, M. *Phys. Rev. Lett.* **2002**, *88*, 035502

[Min02b] Minko, S.; Patil, S.; Datsyik, V.; Simon, F.; Eichhorn, K.-J.; Motornov, M.; Usov, D.; Tokarev, I.; Stamm, M. . *Langmuir* **2002**, *18*, 289-296

[Min03a] Minko, S.; Müller, M.; Motornov, M.; Nitschke, M.; Grundke, K.; Stamm, M. *J. Am. Chem. Soc.* **2003**, *125*, 3896-3900

[Min 03b] Minko, S.; Usov, D.; Luchnikov, V.; Müller, M.; Ionov, L.; Scholl, A.; Pfütze, G.; Stamm, M. "Responsive Mixed Polymer Brushes for Patterning of Surfaces", *Polymer Preprints* **2003**, *44*(1), 478

[Min99a] Minko, S., Gafiychuk, G., Sidorenko, A., Voronov, S. *Macromolecules* **1999**, *32*, 4525-4531

[Min99b] Minko, S., Sidorenko, A., Stamm, M., Gafijchuk, G., Senkovsky, V., Voronov, S. *Macromolecules* **1999**, *32*, 4532-4538

[Miw00] Miwa, M.; Nakajima, A.; Fujishima, A.; Hashimoto, K.; Watanabe, T. *Langmuir* **2000**, *16*, 5754 - 5760.

[Mor89] M. Morra, E. Occhiello, F. Garbassi, *Langmuir* **5**, 872-876 (1989).

[Mots91] Motschmann, H.; Stamm, M.; Toprakcioglu, C. *Macromolecules* **1991**, *24*, 3681-3688. –ins

[Mots91a] Motschmann, H. *Aufbau eines Ellipsometers zum Studium von Monoschichten an der Wasser-Luft-Grenzfläche und Adsorptionsprozesse aus Lösung von Blockcopolymeren,* Ph. D. thesis, Universität Mainz, 1991. –ins

[Muel02] M. Müller, Phys. Rev. **2002**, *E65*, 030802

[Mun90a] Munch, M. R.; Gast, A. P.; *J Chem Soc Faraday Trans,* **1990**, *86*, 1341

[Mun90b] Munch, M. R.; Gast, A. P.; *Macromolecules,* **1990**, *23*, 2313

[Nak99] Nakajima, A.; Fujishima, A.; Hashimoto, K.; Watanabe, T. *Adv. Mater.* **1999,** *11*, 1365-1368

[Nie95] Niemantsverdriet, J. W. *Spectroscopy in Catalysis*, VCH Verlagsgesellschaft: Weinheim, 1995

[Niu98] Niu, Q. J.; Frechet, J. M. *Angew. Chem., Int. Ed. Engl.* **1998**, *37*,667-670.

[Oen00] Öner, D., McCarthy, T. J. *Langmuir* **2000**, *16*, 7777-7782

[Oga93] Ogawa, K.; Soga, M.; Takada, Y.;Nakayamy, I. *Jpn. J. Appl. Phys.* **1993**, 32, L614-L615.

[Oli77] Oliver J. F., Huh C. and Mason S. G., *J. Colloid Interface Sci*., **1977**, *59*, 568

[Onda96] Onda, T.; Shibuichi, S.; Satoh, N.; Tsujii, K. *Langmuir* **1996**, *12*, 2125 -2127

[Oss88] Van Oss, C. J.; Chaudhury, M. K.; Good, R. J. *Chem. Rev*. **1988**, 88, 927.

[Owe69] Owens, D. K.; Wendt, R. C. *J. Appl. Polym. Sci*. **1969**, 13, 1741. b) Kaelble, D. H. *J.Adhesion* **1970**, 2, 50

[Park97] Park, M.; Harrison, C.; Chaikin, P. M.; Register, R. A.; Adamson, D. H. *Science* **1997**, *276*, 1401–1404

[Pat87] Patel, S.; Hadziioannon, G.; Tirrell, M. *Proc Natl Acad Sci USA,* **1987**, *84*, 4725

[Per87] Personage, E.; Tirrell, M.; Watanabe, H.; Nuzzo, R. *Macromolecules,* **1987**, *24*, 1987

[Phe98] McPherson, T.; Kidane, A.; Szleifer, I.; Park, K. *Langmuir* **1998**, *14*, 176-186

[Pin91] Pincus, P. *Macromolecules* **1991**, *24*, 2912-2919

[Pok02] A. V. Pokius, Adhesion and Adhesion Technology, Hansen Gardner, Munich, 2002

[Pol96] Polymeric Materials Encyclopedia, Ed. J. C. Salamone. B. Ranton: CRC Press 1996, Vol. 10, P. 7303-8237. Vol. 7, P 5409-5418

[Pow90] Powell, C. J.; Seah, M. P. *J. Vac. Sci. Technol*. **1990**, A8, 735

[Pru98] Prucker, O.; Ruhe, J. *Macromolecules* **1998**, *31*, 602-613

[Qui02] Quirk, R. P.; Mathers, R. T.; Cregger, T.; Foster, M. D.; *Macromolecules,* **2002**; *35,* 9964-9974

[Qui94] Quist, A. P.; Ahlbom, J.; Reimann, C. T.; Sundqvist, B. U. R. *Nucl. Instrum. Methods B* **1994**, *88*, 164

[Rap92] Raphael, E.; de Gennes, P. G. *J. Phys. Chem.* **1992**, *96*, 4002-4007.

[Rut00] Ruths, M.; Johannsmann, D.; Ru¨ he, J.; Knoll, W. *Macromolecules*, **2000**, *33*, 3860-3870

[San93] *Physics of Polymer Surfaces and Interfaces*, (Ed.: I. Sanchez), Manning:NY, **1993**

[Sau89] Sauer, D. B.; Yu, H.; Kim, M. W. . *Langmuir,* **1989**, *5*, 278

[Sed00] Sedjo, R. A.; Mirous, B. K.; Brittain, W. J. . *Macromolecules* **2000**, *33*, 1492-1493

[Sem75] Semenov, A. N. *Sov Phys JETP,* **1975**, *61*, 733

[Sid99a] Sidorenko A.; Minko S.; Schenk-Meuser K.; Duschner H.; Stamm M. *Langmuir* **1999**, *15*, 8349-8355.

[Sid99b] Sidorenko, A., Minko, S., Gafiychuk, G., Voronov, S. *Macromolecules*, **1999**, *32*, 4539-4543

[Sin97] Singh, C.; Pickett, G. T.; Zhulina, E. and Balazs, A. C. *J. Phys.Chem. B.* **1997**, *101*, 10614-10624

[Sog96] Soga, K.; Zuckermann, M. J.; Guo, H. *Macromolecules* **1996**, *29*, 1998

[Str91] Strobel, J. M.; Strobel, M.; Lyons, C. S.; Dunatov, C.; Perron, S. J. *J. Adhes. Sci. Technol.* **1991**, *5*, 119-130.

[Sum03] Sumerlin, B. S.; Lowe, A. B.; Stroud, P. A.; Zhang, P.; Urban, M. W.; McCormick, C. L.; *Langmui,* **2003**; *19,* 5559-5562.

[Swa03] K. Swaminatha Iyer, B. Zdyrko, H. Malz, J. Pionteck, I. Luzinov *Macromolecules*, 2003, in press

[Sze96] Szeleofer, I.; Carigano, M. A. *Adv. Chem. Phys.* **1996**, *94*, 165-259

[Tad97] Tadanaga, K.; Katata, N.; Minami, T. *J. Am. Ceram. Soc.* **1997,** *80*, 1040-1042

[Tam96] Tamayo, J.; García, R. *Langmuir* **1996**, *12*, 4430-4435

[Tan94] Tanuma, S.; Powell, C.J.; Penn, D.R. *Surf. Interface Anal.* **1994**, 21, 165

[Tha00] Thao, B.; Brittain, W. J. *Prog. Polym. Sci.* **2000***, 25*, 677-710 and references therein

[Tke94] Tkey, Y. G.; Aoki, T.; Sanui, K.; Ogata, N.; Sukari, J.; Okano, T. *Macromolecules* **1994**, *27*, 6163

[Tsu00] V. V. Tsukruk, K. Wahl, Eds. *Microstructure and Microtribology of Polymer Surfaces,* ACS Symposium Series, v. 741, 2000

[Tsu01] V. V. Tsukruk, *Adv. Materials, 13,* 95, 2001.

[Tsu90] Tsubokawa, N.; Kogure, A.;Maruyama,K.; Sone, Y.; Shimomura, M. *Polym. J.* **1990**, *22*, 827.

[Tsu97] V. V. Tsukruk, *Progress in Polymer Science*, *22*, 247, **1997**

[Tsu98] V. V. Tsukruk, V. N. Bliznyuk, *Langmuir* **1998,** *14,* 446

[Tsu99] V. V. Tsukruk, I. Luzinov, D. Julthongpiput, *Langmuir,* 1999, *15*, 3029

[Tsuj97] Tsujii, K.; Yamamoto, T.; Onda, T.; Shibuichi, S. *Angew. Chem.* **1997**, *109*, 1042-1044

[Uso02] D. Usov, M. Stamm, S. Minko, C. Froeck, A. Scholl, and M. Müller Nanostructured Polymer Brushes With Reversibly Changing Properties Nanostructured Interfaces, R2.5., Editors: G. Duscher, J.M. Plitzko, Y. Zhu, H. Ichinose. MRS Proceedings,v. 727, 2002

[Vee97] Veeramasuneni, S.; Drelich, J.; Miller, J. D.; Yamauchi, J. *Prog. Org.*

Coatings. **1997**, *31*, 265.
[Waa50] Van der Waarden, M. *J. Colloid. Sci.,* **1950**, *5*, 317
[Waa51] Van der Waarden, M. *J. Colloid. Sci.,* **1951**, *6*, 443
[Wac84] van Wachem, P. B.; Beugeling, R.; Feijen, J.; Bantjes, A.; Detmers, J. P; van Aken, W. G. The Interaction of Cultured Human Vascular Endothelial Cells and Biomaterials Life Support Systems. **1** (1984), 98-102
[Wang00] Wang, J.; Kara, S.; Long, T. E.; Ward, T. C. *J. Polym. Sci.: Part A: Polym. Chem.* **2000**, *38*, 3742-3750
[Wen36] Wenzel, R. *Ind. Eng. Chem.* **1936**, *28*, 988.
[Wen49] Wenzel R. N., Ind. Eng. Chem., 28 **1936** 988; *J. Phys. Colloid Chem*., *53* **1949** 1466
[Whi90] Whitesides, George M.; Laibinis, Paul E. Langmuir (1990), 6(1), 87.
[Wil88] Wilson, Mark D.; Whitesides, George M.. Journal of the American Chemical Society (1988), 110(26), 8718
[Wus82] Wu, S. *Polymer Interface and Adhesion* Marcel Dekker: New York, 1982; Chapter 5.
[Yas90] T. Yasuda, H. Yasuda, T. Okuno, M. Miyama, Pol. Mater. Sci. Eng. (Am. Chem. Soc.) **62**, 457 (1990).
[Yos02] Yoshimitsu, Z.; Nakajima, A.; Watanabe, T.; Hashimoto, K. *Langmuir* **2002**, *18*, 5818-5822
[Yos02] Yoshimitsu, Z.; Nakajima, A.; Watanabe, T.; Hashimoto, K. *Langmuir* **2002**, *18*, 5818-5822.
[You99] Youngblood, J.; McCarthy, T. J. *J. Macromolecules* **1999**, *32*, 6800-6806.
[Zan88] Zangwill, A. *Physics at Surfaces* Cambridge University Press: Cambridge, 1988; Chapter 1.
[Zan92] Joanny, J.-F. *Langmuir,* **1992**, *8*, 989
[Zan94b] Van Zanten, J. H. *Macromolecules* **1994**, *27*, 6796(a13)
[Zer94] Zerushalmi-Royen, R.; Klein, J.; Fetters, L. *Science* **1994**, *263*, 793-795
[Zha00c] Zhao, B.; Brittain, W. J. . *Macromolecules* **2000**, *33*, 8813-8820
[Zha00a] Zhao, B.; Brittain, W. J.; Zhou, W.; Cheng, S. Z. D. *J. Am. Chem. Soc.* **2000**, *122*, 2407-2408.
[Zha00b] Zhao, B.; Brittain, W. J. *Prog. Polym. Sci,* **2000**, *25*, 677-710
[Zha03] B. Zhao Polymer, 2003, 44, 4079-4083.
[Zha99] Zhao, B.; Brittain, W. J. *J. Am. Chem. Soc.* **1999**, *121*, 3557
[Zhan96] Zhang, Y.; Tirrell, M. *Macromolecules* **1996**, *29*, 7299-7301. –Ins
[Zhul96] E. B. Zhulina, C. Singh, A. C. Balazs, *Macromolecules* **1996**, *29*, 6338
[Zhu96] Zhuang, H.; Marra, K. G.; Ho, T.; Chapman, T. M.; Gardella, Jr., J. A. *Macromolecules* **1996**, 29, 1660.
[Zis64] Zisman, W. A. in *Contact Angle, Wettability and Adhesion*, Ed. F. W. Fowkes, ACS Symp. Series, Vol. 43, Washington, DC, 1964

LIST OF ABBREVIATIONS AND SIMBOLS

N	polymerization index.
R_E	wavelength of the ripples
α	absorption coefficient
φ	concentration of statistical segments
Θ	contact angle
Θ^*	contact angle on rough surface
Λ	coupling constant
λ	dominant inplane length
χ	Flori Huggins interaction parameter;
Θ	internal angle of incident of IR radiation
ζ	solvent selectivity
Ω	surface of the layer.
γ	surface tension
χ	the Flory-Huggins parameter
λ	wavelength of light
ν	dimensionless volume parameter
μ	chemical potential
χ'	repulsion (attraction) parameter for two unlike monomer units
φ_b	ratio of the surfaces of the spike bases over the total solid surface
γ_{lv},	interfacial tension of the liquidvapor
θ_R	angle of incidence of IR beam on the crystal
φ_s	solid fraction of the surface
γ_{sl}	solidliquid interfacial tension
γ_{sv},	solidvapor interfacial tension
1,4PBD	1,4polybutadiene
a –	diameter
A	surface area
A_0	amplitude of free oscillations
ACPA	4,4´azobis(4cyanopentanoic acid);
ADSAP	Axisymmetric Drop Shape Analysis Profile
AFM	Atomic Force Microscopy
A_i	peak area for element *I*

AIBN	4,4'azobis(isobutyronitrile)
ATR	Attinuated Total Reflection
ATRP	Atom Transfer Radical Polymerization
BC	Block Copolymers
BUDTMS	11bromoundodeciltrimethoxisilane
c	speed of light in vacuum
CHA	Concentric Hemispherical Analyzer
Ci	background the atomic concentration
ClACPA	chloroanhydride of ACPA;
d	average distance between the tethering points
d_p	penetration depth of IRradiation
DSA	Drop Shape Analysis
E	mixing free energy per chain
e.g.	for example;
E_b	binding energy of the photoelectron in the excited electron shell
ECR	electron cyclotron resonance
E_k	kinetic energy of the photoelectron
ESCA	Electron Spectroscopy for Chemical Analysis
et al.	Latin abbreviation meaning *and others*;
eV	electronvolt, an energy unit which equals $1.60218 \cdot 10^{19}$ J;
F	free chain energy
F_{el}	price of a high elastic free energy
F_{int}	interaction energy per polymer chain
FTIR	Fourier Transform Infrared Reflectometry
G	the Gibbs energy
GPC	Gel Permeation Chromatography
GPS	(3glycidoxypropyl)trimethoxysilane;
h	the Planck's constant
IR	Infrared Spectroscopy
I_r	reflected ratio of the light intensity
IRE	Internal Reflection Element
I_t	transmitted ratio of the light intensity
k	(1)imaginary part (extinction coefficient); (2) the Boltzmann constant, $1.38065 \cdot 10^{23}$ J/K

L	layer thickness
Mn	chain number averaged molecular mass;
Mw	weight averaged molecular mass;
ń	complex refractive index
n	number of moles
N	number of statical segments
n	(1) real part or index of refraction; (2) refractive index; (3) total number of molecules in the layer
N_A	the Avogadro constant which is the number of particles in one mole of matter, $N_A = 6.02214 \cdot 10^{23}$ mol^{1};
NMR	Nuclear Magnetic Resonance
NMRP	NitroxideMediated Radical Polymerization
p	pressure
P(Sb2VPbEO)	Poly(styreneb2vinypyridinebetyleneoxyde)
P(Sb4VP)	Poly(styreneb4vinyl pyridine)
PA	polyamide
PA6	polyamide Durethan® B
PA6I	polyamide Durethan® T
PAA	polyacrylic acid
PBA	polybutylacrylate
PBD	1,2polybutadiene
PDMS	polydimethylsiloxane;
PE	polyethylene
PEO	polyethyleneoxide
PGMA	poly(glycidylmethacrylate)
PMA	polymethylacrylate;
PMMA	polymethylmethacrylate
PS	polystyrene
PS*b*PDMA	polystyrenebpoly(dimethylsiloxane)
PS*b*PMA	polystyrenebpoly(methylacrylate)
PS*b*PMMA	polystyrenebpoly(methylmetacrylate)
PS*b*PVP	polystyrene*b*poly(4vinylpyridine)
PSF	poly(styreneco2,3,4,5,6pentafluorostyrene);
PtBA	polytetrabutylacrylate

PTFE	polytetrafluoroethylene
R	reflection intensity ratio
r	surface roughness
R_0	radius of an unperturbed ideal coil
RMS	Root Mean Square
r_s	roughness coefficient
S	entropy
SAS	Self Adaptive Surface
SCF	Self Consisted Field
SEM	Scanning Electron Microscopy
S_i	relative sensitivity factor for element
S_q	surface root mean square roughness value
SSL	Strong Stretching Limit
T	(1) temperature; (2) transmission intensity ratio
TEM	Transmission Electron Microscopy
T_g	glass transition temperature
THF	tetrahydrofurane
U	internal energy
UHV	Ultra High Vacuum
UVO	Ultraviolet/Ozone
v	speed of light in the material
V	volume
XPEEM	X ray Photoemission Electron Microscopy
XPS	X ray Photoelectron Spectroscopy
XRD	X ray Diffraction
Δ	(1) difference (e.g. Δx = x2 – x1); (2) ellipsometric angle;
´	inverse stretching parameter
λ	wavelength,
	frequency of the X ray
	work function of the spectrometer
Ψ	ellipsometric angle;

PUBLICATIONS

Patent DE 1022 06 481 C1 (EP 1 350 575 A2) *Oberflächen mit schaltbarer Ultrahydrophobie und Verfahren zur Realisierung*: Nitschke, M.; Minko, S.; Motornov, M.; Grundke, K.; Stamm, M. **10.02.2003**

Minko, S.; Usov, D.; Motornov, M.; Ionov, I.; Stamm, M. Smart responsive interface. *Polym. Mater. Sci. Eng*. **2003**, *89*, 156

Motornov, M.; Minko, S.; Eichhorn, K.-J.; Nitschke, M.; Simon, F.; Stamm, M.; Reversible Tuning of Wetting Behavior of Polymer Surface with Responsive Polymer Brushes, *Langmuir*; **2003**; *19(19)*; 8077-8085

Motornov, M.; Minko, S.; Nitschke, M.; Grundke, K.; Stamm, M. Mixed polymer brushes on polyamide substrates. *Polym. Mater. Sci. Eng*. **2003**, *88*, 264-265.

Minko, S.; Müller, M.; Motornov, M.; Nitschke, M.; Grundke, K.; Stamm, M. Two-level structured self-adaptive surfaces with reversibly tunable properties, *J. Am. Chem. Soc*. **2003**, *125 (13)*; 3896-3900

Motornov, M.; Minko, S.; Nitscke, M.; Grundke, K.; Stamm, M. Hierarchically structured self-adaptive surfaces. *Polym. Mater. Sci. Eng*, **2002**, *43*, 379 – 380

Minko, S., Patil, S., Datsyuk, V., Simon, F., K.-J. Eichhorn, Motornov, M., Usov, D., Tokarev, I., Stamm, M. Synthesis of adaptive polymer brushes via grafting to approach from melt. *Langmuir*, **2002**, *18*, 289-296.

Contributions to conferences

Synthesis of binary polymer brushes on the polyamide surface *M. Motornov, S. Minko, E. Goreshnik, D. Usov and M. Stamm* (poster), **, EPF Meeting, Eindhoven, 15.07-20.07 2001**

Switching of polymer brushes on polymer surfaces *M. Motornov, S. Minko, K.-J. Eichhorn, E. Goreshnik, D. Usov and M. Stamm,* (poster), "**Interfaces and Colloidal Systems", Aqwa-Freda (Italy) 8.09-13.09.2001**

Mixed polymer brushes on polymer surfaces, *M. Motornov, S. Minko, M. Nitschke,K. Grundke, K-J. Eichhorn, and M. Stamm* (poster) **"Crossing lenghtscales and disciplines; from macromolecular structures to functional polymer systems", Netherlands, Rolduc Polymer Meeting 5.05-8.05, 2002**

Self Adaptive Polymer Brushes on Polymer Substrates *M. Motornov, S. Minko, M. Nitschke,K. Grundke, K-J. Eichhorn, and M. Stamm,* (poster) **Discussion Meeting on Multi-Level Ordering "Molecular Organization for Nanosystems", Kloster Banz, Germany, 15.02-20.02, 2003**

Self-adaptive Polymer Brushes on Polyamide Substrates, *Mikhail Motornov, Sergij Minko, Mirko Nitschke, Karina Grundke and Manfred Stamm,* (poster), **DPG Meeting, Dresden 24.03 - 28.03 2003**

Danksagung (acknowledgement).

Ich bedanke mich bei Herrn Prof. Dr. Manfred Stamm für die Ermöglichung dieser Arbeit und Herrn Prof. Dr. Sergiy Minko für die wissenschaftliche Führung.

Für die wichtigen wissenschaftlichen Beratungen und Diskussionen möchte ich Herrn Dr. Alexander Sydorenko danken.

Herrn Igor Tokarev, Frau Anna Gorodyska, Frau Alla Synytska, Herrn Dr. Denys Usov, Herrn Nikolay Houbenov, Herrn Leonid Ionov, Herrn Dr. Jevgeny Goreshnik, danke ich für die gute freundliche Atmosphäre, Beratungen und praktische Hilfe bei experimentellen Versuchen.

Für die Durchführung der Plasmaätzung von Polymerschichten möchte ich Herrn Dr. Mirko Nitschke danken.

Für die Ermöglichung von Randwinkelmessungen möchte ich mich bei Frau Dr. Karina Grundke und Frau Kathrin Pöschel bedanken.

Für die Durchführung der Röntgenshotoelektronenspektroskopie (XPS) bedanke ich mich bei Herrn Dr. Frank Simon und Herrn Dieter Pleul.

Herrn Prof. Dr. J.-F. Gohy danke ich für die Bereitstellung verschiedener Block Copolymere.

Bei Herrn Dr. Klaus-Jochen Eichhorn und Frau Gudrun Adam bedanke ich mich für die Beratungen und infrarotspektroskopische Messungen.

Mein besonderer Dank gilt meinen Eltern und Freunden, deren Unterstützung mein Studium und somit diese Arbeit erst ermöglichte.

Versicherung (insurance).

Hiermit versichere ich, dass ich die vorliegende Arbeit ohne unzulässige Hilfe Dritter und ohne Benutzung anderer als der angegebenen Hilfsmittel angefertigt habe; die aus fremden Quellen direkt oder indirekt übernommenen Gedanken sind als solche kenntlich gemacht. Die Arbeit wurde bisher weder im Inland noch im Ausland in gleicher oder ähnlicher Form einer anderen Prüfungsbehörde vorgelegt.

Die vorliegende Arbeit wurde unter der wissenschaftlichen Betreuung von Prof. Dr. Manfred Stamm und Prof. Dr. Sergiy Minko am Institut für Polymerforschung Dresden e. V. angefertigt.

Die Promotionsordnung der Technischen Universität Dresden der Fakultät Mathematik und Naturwissenschaften erkenne ich an.

M. I. Motornov